Optical parameters Determination for absolute luminosity and total cross section measurements in ATLAS

Sophie Cavalier

LAL 13-168
Juin 2013

THÈSE

Présentée le 12 juin 2013

par

Sophie CAVALIER

Discipline : Physique des particules et accélerateurs

pour obtenir le grade de

Docteur ès Sciences
de l'Université Paris Sud, Orsay

Détermination des paramètres optiques nécessaires pour la mesure de la luminosité absolue et de la section efficace totale dans ATLAS

Soutenue devant la commission d'examen composée de :

Mme.	A.	Faus-Golfe	Rapporteur
M.	A.	Nadji	Rapporteur
M.	A.	Stocchi	Président
M.	J.	Payet	Examinateur
M.	P.	Puzo	Directeur de thèse

Point n'est besoin d'espérer pour entreprendre,
ni de réussir pour persévérer.
Charles le Téméraire - Guillaume d'Orange

A mes grands-parents

Remerciements

Après un certain nombre d'années passées au laboratoire, je me suis lancée dans l'expérience d'une thèse de doctorat. Mais étant de nature partageuse, un grand nombre de personnes du laboratoire ont aussi profité de mon expérience y compris (et surtout) de mes sautes d'humeur. Les remerciements vont donc être un exercice difficile car je l'espère, je ne vais oublier personne et je demande à celles et ceux que j'aurais oublié de bien vouloir m'en excuser.

Je tiens tout d'abord à remercier Patrick Puzo, sans qui je n'aurais jamais soutenu cette thèse, et qui malgré mon grand âge et surtout en plus de la somme de travail qui lui est déjà imputée, m'a tout d'abord proposé cette thèse et ensuite a généreusement accepté d'en prendre la direction. Je le remercie de m'avoir fait confiance. Je remercie aussi Alessandro Variola de m'avoir permis de me lancer dans l'aventure de la thèse et d'avoir accepté de me laisser du temps pour l'accomplir et la terminer malgré les nombreux projets en cours au département accélérateurs.

Je remercie aussi Achille Stocchi et Fabien Cavalier d'avoir validé ma décision de m'inscrire en thèse, ainsi que mes rapporteurs Amor Nadji et Angeles Faus Golfe pour avoir accepté la lourde tâche de relecture du manuscrit, leurs commentaires très instructifs en ayant permis l'achèvement. Merci beaucoup aussi à Jacques Payet d'avoir accepté de faire partie de mon jury. Je remercie aussi Bruno Espagnon, qui s'est occupé avec gentillesse des papiers concernant la soutenance de thèse afin que je sois dans les temps.

Merci à Helmut Burkhardt, pour avoir travaillé avec moi au CERN et m'avoir encouragée. Son expertise a été très précieuse pour moi, elle m'a permis d'apprendre énormément à son contact et j'espére que nous serons encore amenés à collaborer.

Merci à ceux (toutes et tous) avec qui j'ai pu interagir au CERN que ce soit pour les mesures ou pour l'opération machine. Merci à Glenn et Yngve qui ont toujours répondu à mes questions avec enthousiasme.

Je remercie aussi Catherine, pour sa patience et pour ses efforts pour la mise en place de la soutenance. Les emplois du temps divers et variés de chacun rendant l'entreprise quelquefois difficile. Merci aussi à Geneviève qui m'a toujours guidée efficacement lors de mes différentes démarches et m'a souvent aidée à retrouver Patrick. Merci à Isabelle, Sabine, Cristelle et Annie, qui m'ont dépannée de nombreuses fois lors de mes "ratages" de train ou d'avion et qui ont toujours été très efficaces malgré les aléas. Merci à tous le personnel administratif et au service informatique du LAL qui se sont toujours montrés efficaces et m'ont aidée dans mes différentes démarches.

Merci aussi à Daniel Fournier et RD Schaffer pour m'avoir intégrée dans le groupe ATLAS et permis de mener mon activité sur ALFA à bien. Merci au groupe ATLAS de m'avoir encouragée durant cette période. Un grand merci à Karlheinz, Sune, Hasko, Patrick et Per pour leur aide précieuse lors des MDs ou pour les simulations et analyses de physique ainsi

qu'à tout le groupe ALFA avec qui j'ai toujours eu plaisir à interagir lors des meetings et avec qui j'ai toujours passé de bons moments notamment lors des barbecues au CERN.

Un remerciement plus spécial pour Matthieu, pour toute ton aide que ce soit pendant ta thèse ainsi qu'une fois au CERN. Ton aide a toujours été précieuse et tu n'as jamais refusé de me l'apporter. La collaboration avec toi a toujours été un plaisir pour moi et j'espère qu'elle pourra continuer.

Merci aussi à Samah qui m'a de nombreuses fois dépannée en urgence surtout avec cet outil périlleux qu'est Root. :-) Travailler avec toi a aussi été très agréable et peut-être cela continuera-t'il après ta thèse. Je te souhaite quoi qu'il en soit une bonne fin de thèse et une bonne continuation.

Un grand merci aux membres du département accélérateurs, Agnès, Christelle, Raphaël, Cécile, Nicolas, Thomas V., Melissa, Joanna, Olivier, Wallid, Irina, Pierre, Theo, Jean-Luc, Jean-Noël, Vincent, Robert, Noureddine, Hugues, Leïla, Illya, Viktor, Jianfeng, Samy, Mohamed, Thomas C. ainsi qu'aux ex-membres, Julien, Bernard M., Bernard L., Francis et Emilienne qui ont tous participé activement à cette thèse, que ce soit en m'aidant techniquement, scientifiquement ou moralement.

Merci aux collègues du SDTM qui m'ont supportée durant les repas de midi et qui ont eu à subir quelquefois mes complaintes de fatigue de fin de thèse. Un remerciement plus particulier à Alice, qui m'a appris l'art du loisir créatif et qui a su me remotiver pendant les pauses cafés.

Merci aussi à Gisèle, Nathalie, Julien, Stéphane et Christophe pour m'avoir initiée au footing ce qui m'a permis d'évacuer le stress et de me défouler. Merci aussi à Selma, Pierre, Fred, Ludo, Salleh et Damien pour leur gentillesse et leur soutien.
Merci aux nombreuses personnes du laboratoire qui se sont intéressés de près ou de loin à mon travail et aussi à celles qui m'ont souvent apporté des encouragements et dont je ne peux malheureusement citer tous les noms.

Merci à mes amies qui m'ont toujours soutenue: Claire, Lydie, Cécile, Angelina, Marie-Jo et Minh Chau. Nos fous rires durant nos soirées ont toujours été un vrai bol d'air frais et un échappatoire des plus agréables. Merci à ma belle-famille, qui a aussi subi les affres de mon stress malgré mes tentatives quelques peu avortées de ne pas trop le montrer. Merci à Nanie et Hélène pour leur présence à la soutenance. Merci à mes parents pour leur soutien et leurs encouragements qui m'ont permis d'arriver là où je suis maintenant. Ainsi que d'avoir peut être aussi joué le rôle de "punching ball"à distance parfois :-) mais sans casse toutefois. Merci à ma sœur Mélanie, qui s'est déplacée pour la soutenance malgré son gros "bidon" (temporaire) :-) et à John.

Et merci à toi, Antoine, pour ton soutien sans faille, ton stoïcisme et ta grande capacité d'écoute. Merci d'avoir accepté mes horaires quelque peu compliqués. Tu as toujours été présent même dans les moments difficiles et le réconfort que tu m'as apporté a plus

que compté pour moi, il m'a aussi permis de mener mon travail jusqu'au bout. Tu m'as redonné confiance au moment où j'en avais le plus besoin. Merci pour tout!! Et place à nos nouveaux projets maintenant. :-)

Contents

Introduction

The **L**arge **H**adron **C**ollider (LHC) [1] located at CERN close to Geneva is the largest accelerator in the world with 27 km circumference. It has been installed in the former tunnel of LEP [2]. LHC provides proton – proton collisions for high energy physics with a planned ultimate energy of 14 TeV in the center of mass. This should be achieved after a shutdown period which started in february 2013. Nevertheless, in 2011, LHC has already achieved 7 TeV energy in the center of mass. The major goal of this accelerator was to discover and study the Higgs boson predicted in 1964. The ATLAS [3] and CMS [4] experiments have been built at two opposite collision points in the LHC ring for this purpose. The LHC has run with a very high luminosity of $\mathcal{L} = 7.7 \times 10^{33}$ cm^{-2} s^{-1}.

Each physic process has a specific signature in the detector. The experiments count the number of events linked to each process. To know the likelihood of occurrence, i.e. the total cross section, one need to know the luminosity. This quantity depends only on the beam parameters but using them will allow a precision of only 5 to 6 %. In this case, the luminosity will be the dominant parameter for the systematic uncertainties. To go over this, detectors dedicated to absolute luminosity measurements have been installed on the LHC.

These ALFA detectors [5] complement the ATLAS detector in the very forward region and are dedicated to abolute luminosity and total cross section measurements. The basic idea is to measure the elastic scattering at very small angle at the ATLAS Interaction Point, small enough to reach the Coulomb regime which could be exactly calculated. This allows to determine both the absolute luminosity and the proton – proton total cross section.

To do this, the ALFA detectors are located in the LHC tunnel at 240 m from the Interaction Point on both sides of ATLAS. For data taking, the detectors have to be set at about 2 mm from the beam axis. This is done using the so-called "Roman Pot"technique. This technique was also used by the UA4 experiment [6] and by the TOTEM experiment [7] close to CMS in the LHC.

Being able to detect very small scattering angles requires a dedicated optics, different from the nominal LHC optics. For the ultimate LHC running parameters, the main characteristic of this optics is $\beta^* = 2625$ m. This optics is called "high β^* optics".

Firstly, the context where ALFA detectors measurement takes place (ATLAS and LHC) will be described in chapter 1. Then, in order to better understand the high β^* optics,

a summary of transverse dynamics notions is given in chapter 2. In chapter 3, after the description of the various luminosity measurement methods used in ATLAS, the one used to measure with ALFA detectors is given. Also, the Roman Pots mechanical and electronic description is briefly shown. After these introducting chapters, the first high β^* optics design with $\beta^* = 2625$ m is explained in chapter 4. The PhD work starts with this optics which was studied in more details than before by including it in the overall ALFA simulation package. The experimental acceptance was determined with the simulation. The study has been completed by applying misalignement errors.

For hardware reasons, the nominal $\beta^* = 2625$ m optics could not be used during the first years of LHC operation. The work, then, has been focussed on an intermediate $\beta^* = 90$ m optics described in details in chapters 5 and 6. Finally, in response to the request for higher β^*, new optics up to $\beta^* = 500$ m and 1000 m have been developped and commissionned as shown in chapter 7 but particle physics analysis of these runs is not yet performed.

Chapter 1

The LHC accelerator complex and ATLAS

Contents

This chapter describes the accelerator complex with its operation scheme and instrumentation goals and then describes the ATLAS experiment.

1.1 The LHC ring

1.1.1 LHC accelerator chain description

The LHC (**L**arge **H**adron **C**ollider), described in a TDR (**T**echnical **D**esign **R**eport) [1], has been able to reach in 2012 the highest luminosity ever achieved for hadron colliders with $\mathcal{L} = 7.7 \times 10^{33}$ cm^{-2} s^{-1}. This proton – proton facility, based at CERN between Switzerland and France, close to Geneva, is approximately 100 m underground in the same tunnel as the former collider of CERN, LEP (**L**arge **E**lectron **P**ositron). Its circumference is 27 km and to be able to reach the ultimate energy of 7 TeV, it relies on an injector chain which consists of a LINAC and the Booster, the PS (**P**roton **S**ynchrotron) and the SPS (**S**uper **P**roton **S**ynchrotron) as shown in Fig. 1.1. The LHC also accelerates and collides lead ions.

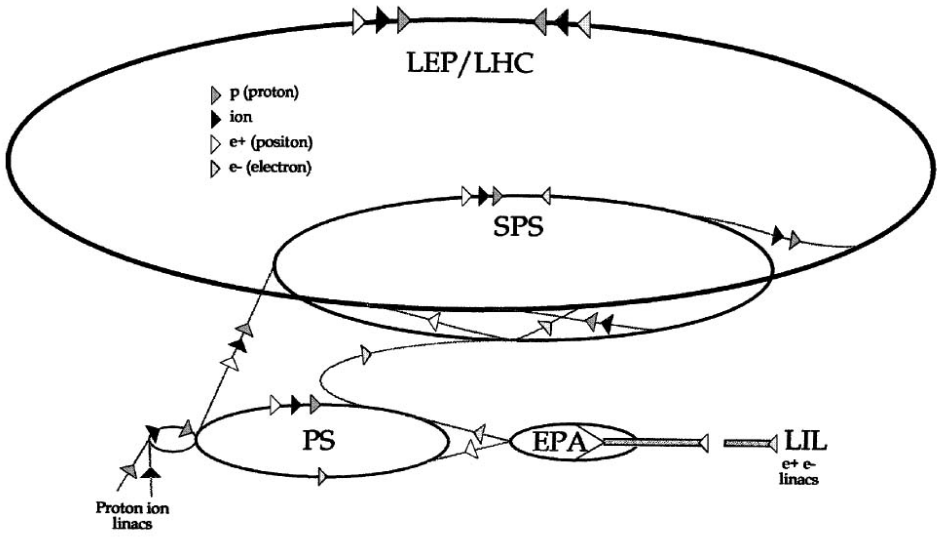

Figure 1.1: LHC accelerator chain including the LINAC, the booster, the PS, the SPS and finally the LHC.

The LINAC, 80 m long, accelerates the proton beam up to 50 MeV. The booster with 157 m circumference, takes over to 1.4 GeV. It's followed by a 628 m ring (PS) to bring the beam up to 26 GeV. Then the SPS ring, 6.9 km long, allows to reach 450 GeV and finally the beam is transferred to the LHC to reach the highest energy. The LHC energy was 3.5 TeV per beam in 2011 and 4 TeV per beam in 2012. Nominal energy of 7 TeV per beam will not be reached before 2015.

As seen on Fig. 1.2, two beams are circulating in the ring, beam 1 is circulating clockwise whereas beam 2 is circulating counter-clockwise. These two proton beams cross at four different IPs (**I**nteraction **P**oints) where the collisions occur. The four IPs correspond to four LHC experiments: ATLAS (**A** **T**oroidal **L**hc **A**pparatuS) [3] located at IP1, CMS (**C**ompact **M**uon **S**olenoid) [4] located at IP5, LHCb (**L**arge **H**adron **C**ollider **b**eauty) [8] located at IP2 and ALICE (**A** **L**arge **I**on **C**ollider **E**xperiment) [9] located at IP8. AT-

LAS and CMS aim at very high luminosity up to 10^{34} cm^{-2} s^{-1}. Their primary goal is the search and study of the Higgs boson. A more detailed description of the ATLAS detector will be given in § 1.4. LHCb studies the B – Physics whereas ALICE uses the heavy ions to study quark – gluon plasma.

Two other experiments complete the LHC foreground: TOTEM (**TOT**al **E**lastic and diffractive cross section **M**easurement) [7] and LHCf (**LHC f**orward) [10]. The former studies diffractive and elastic physics to determine in particular proton – proton total cross section and the later focuses on forward neutral particles.

1.1.2 LHC ring description

The LHC is divided in **I**nsertion **R**egion**s** (IRs) and arcs as shown in Fig. 1.2. There are 8 straight sections containing insertions and 8 arcs. The Insertion Regions IR1, IR2, IR5, IR8 house the physics experiments. Then, for the other four IRs, we can find:

- on IR3, the momentum cleaning region with collimators and magnets to clean the protons with large momentum offset
- on IR4, the **R**adio – **F**requency (RF) system for the energy control
- on IR6, the dump system to be able to discard the beam properly
- on IR7, the betatron cleaning system to get read of protons with too high amplitude oscillations

The LHC ring, as already mentionned, had to be integrated in the tunnel of the former LEP accelerator. This brings some difficulties concerning the magnets, the space containing the ring being too small to contain two different magnets, the LHC requires a single magnet for both beams.

These magnets are superconducting magnets since it is the only technology allowing to reach the magnetic field required for 7 TeV nominal energy per beam. The LHC contains 1232 main superconducting dipoles which were designed to provide a field of 8 Teslas each. The dipole definition will be given in § 2.2.1. Anyway, the proton beams are circulating in two separated vacuum chambers inside the same magnet. Each magnet houses both beam pipes as can be seen in Fig. 1.3. The LHC has been designed to have instantaneous peak luminosity at IP1 and IP5 of 10^{34} cm^{-2} s^{-1}. The parameters which fulfil the requirements are listed in table 1.1. However, all these parameters have been optimized to maximize the integrated luminosity.

The optics design is based on FODO cells (described in § 2.5) where the insertions are included. Having a closer look on Fig. 1.2, we can see that one insertion region contains a Long Straight Section (LSS) and a Dispersion Suppressor respectively Right and Left (DSR and DSL). The right side of LSS1 for example is then the side going from IP1 to IP2. It can be confusing as in Fig. 1.2, the right side we talk about is located on the left.

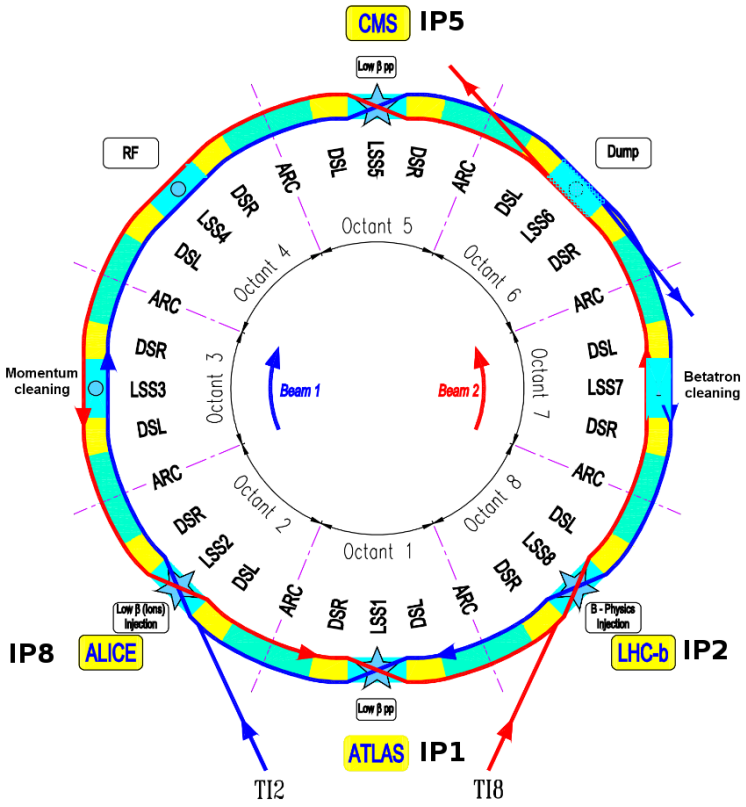

Figure 1.2: LHC layout divided in 8 sections with the four experiments, the eight Interaction Region IRs and the eight arcs. Following usual convention, beam 1 circulates clockwise and beam 2 counter – clockwise.

But right and left for IP1 are defined such as we look from inside the ring and not from above as in the figure.

This labelling concerning right and left side will be used to identify the magnets. As an exemple, starting from IP1, beam 1 will first meet magnets on the right side. Then, quadrupole (defined in § 2.2.2) Q4 will be named "MQY.4R1.B1". MQY is the magnet type, in this case it says that it's an insertion region wide aperture quadrupole with 3.4 m length. 4R1 means that it's quadrupole 4 on the right side of IP1 and B1 is beam 1. The same can be applied for the left side of IP1, Q4 will then be called "MQY.4L1.B1". IR1 and IR5 insertions have been made anti – symmetric.

1.2 The LHC operation

Bringing the protons to high energy requires several steps. The beam is injected in IP2 and IP8 in LHC from SPS by two transfer lines TI2 and TI8 as seen on Fig. 1.2. Then, the beam is ramped to high energy (from 450 GeV to 7 TeV) and squeezed[1] (from β^*=

[1] $*$ means the observable is evaluated at the Interaction Point.

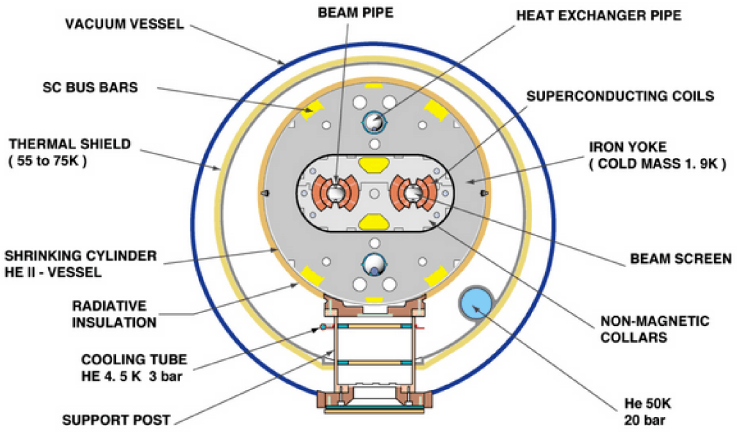

Figure 1.3: Sketch for the main LHC superconducting magnet dipoles located in the arcs, containing two separate chambers in the horizontal plane for both proton beams.

18 m to $\beta^* = 0.55$ m) at the Interaction Points IP1 and IP5 to reach higher luminosity. The β – function is also called the betatron function. It's the envelope around all the trajectories of the particles circulating in the accelerator. More details on the β – function will be given in chapter 2. LHC has started in 2011 with 3.5 TeV per beam and a β^* equals to 2 m. Decreasing β^* and increasing energy will also increase the peak luminosity as defined in chapter 3. During 2012, at 4 TeV, the beam was injected at a $\beta^* = 11$ m for IP1 and IP5 and was squeezed down to 0.6 m.

The nominal scheme in the LHC TDR is 2808 bunches injected in trains. Nominally, each train will have 72 bunches with 25 ns spacing between bunches as illustrated in Fig. 1.4. The 25 ns spacing is small, which means that to avoid collisions away from the Interaction Point, two bunches have to collide at a small angle (quasi head-on) at the center which keep the other bunches separated elsewhere. The number of parasitic collisions that can appear on each side of the IP were estimated at 15 extra more collisions for one collision point. The crossing angle value for the nominal collision scheme at 7 TeV at IP1 and IP5 is equal to 285 μrad as shown on Fig. 1.5. For special optics like the high β^* optics described in this PhD, no crossing angle will be required.

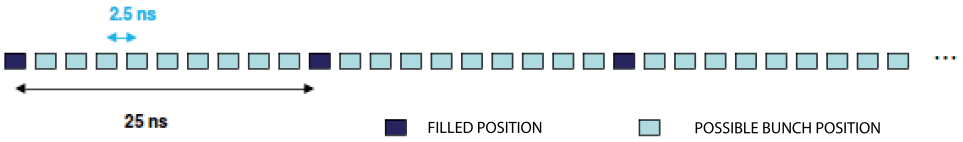

Figure 1.4: LHC bunch filling scheme [11].

During the squeeze phase where the beam size σ is reduced from the injection to its nominal value and during when no collisions occur, the two beams are kept separated

Table 1.1: Nominal LHC parameters [1].

		Injection	**Collision**
Beam Data			
Proton energy	[GeV]	450	7000
Relativistic gamma		479.6	7461
Number of particles per bunch		1.15×10^{11}	
Number of bunches		2808	
Longitudinal emittance ($4\,\sigma$)	[eVs]	1.0	2.5
Transverse normalized emittance	[μm.rad]	3.5	3.75
Circulating beam current	[A]	0.582	
Stored energy per beam	[MJ]	23.3	362
Peak Luminosity Related Data			
RMS bunch length	cm	11.24	7.55
RMS beam size at the IP1 and IP5	μm	375.2	16.7
RMS beam size at the IP2 and IP8	μm	279.6	70.9
Geometric luminosity reduction factor F		–	0.836
Peak luminosity in IP1 and IP5	[$\mathrm{cm^{-2}s^{-1}}$]	–	1.0×10^{34}
Peak luminosity per bunch crossing in IP1 and IP5	[$\mathrm{cm^{-2}s^{-1}}$]	–	3.56×10^{30}

to avoid the parasitic collisions. Only after the beams are put into collision. The separation should not be smaller than $7\,\sigma$ which is the minimum tolerable value for LHC aperture. The LHC standard injection and ramp use a separation which is horizontal in IP1 and a vertical crossing angle whereas at IP5 the separation is vertical with a horizontal crossing angle. The parallel separation is always orthogonal to the crossing angle. The separation scheme and collision scheme at 7 TeV for IP1 are shown on Fig. 1.6 and Fig. 1.7. The parallel separation bumps use three types of corrector magnets: MCBC, MCBY and MCBX, MCBX being common for the two beams and able to control horizontal and vertical planes. The same correctors will be used to put the beam into collision.

During 2012, LHC was mainly dedicated to high luminosity proton physics runs. After optimization, each time beams are put into collision and everything goes well, they are declared as stable beams.

1.3 LHC Instrumentation

Every accelerator complex needs to know the beam characteristics as precise as possible. With appropriate diagnostics it is possible to monitor and measure the position and the beam properties. Different devices have been developed at LHC to measure all these parameters such as BPMs (**B**eam **P**osition **M**onitors), BLMs (**B**eam **L**osses **M**onitors,

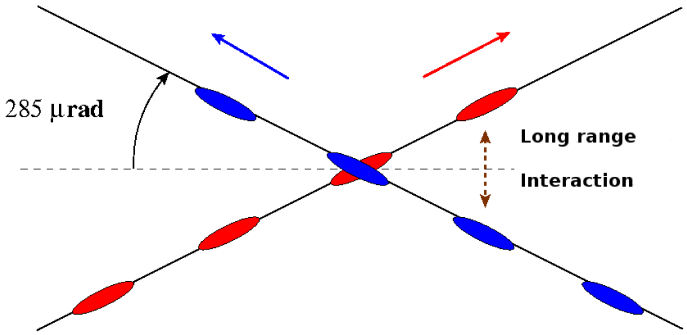

Figure 1.5: Nominal beam crossing scheme at the ATLAS interaction point in the vertical plane.

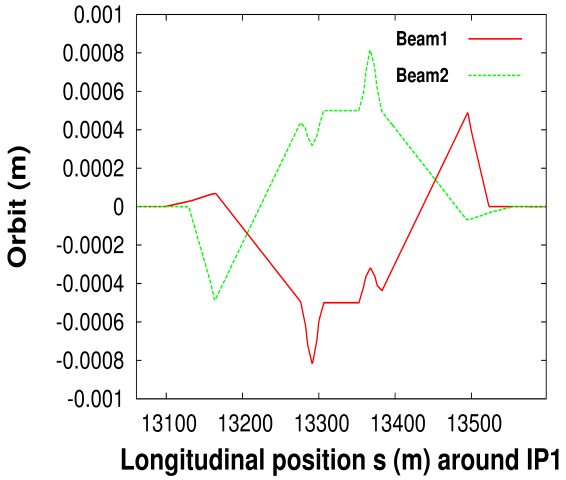

Figure 1.6: Horizontal parallel separation bump for IP1 located at s = 13329.594 in the figure for 7 TeV beam energy.

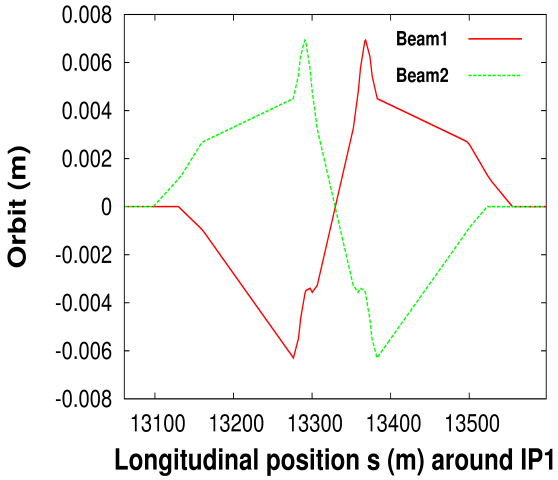

Figure 1.7: Vertical collision scheme for IP1 located at s = 13329.594 in the figure for 7 TeV beam energy.

WSs (**W**ire **S**canners) and BSRTs (**B**eam **S**ynchrotron **R**adiation **T**elescopes). These equipements are described in some more details in the following.

1.3.1 BPMs and orbit correction

The orbit represents the trajectories described by the particles going through the magnetic elements. The LHC orbit system has been studied in order to fulfil its specifications [12]. An example of the orbit measurement in stable beam condition used for high luminosity physics run is given on Fig. 1.8.

The BPMs are used to measure the beam position (horizontal and vertical) from which the orbit is deduced. They are non destructive devices. On the LHC ring, most of the BPMs are button electrode monitors measuring bunched beam position by detecting the induced current in the button. A total of over 1000 BPMs have been installed. Knowing the transverse position of the beam per turn, the correctors magnets, usually dipoles,

can be used to provide a better closed orbit. The closed orbit is defined by a particle trajectory followed by an ideal particle which closes on itself after one revolution in the case of circular accelerator.

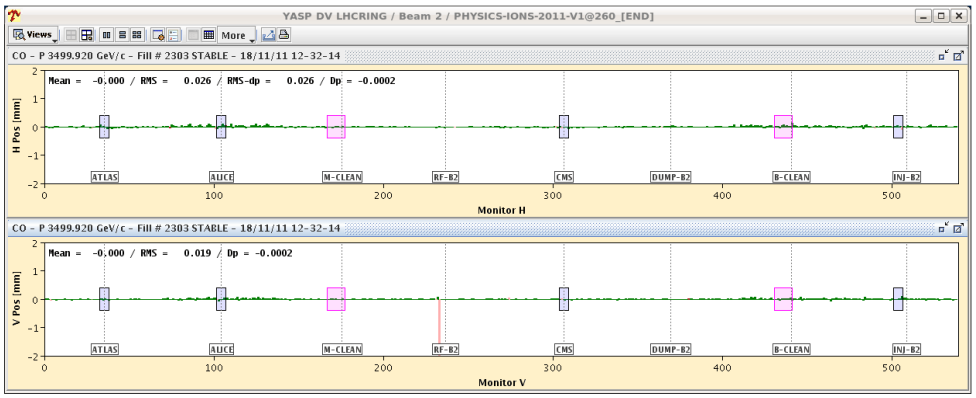

Figure 1.8: Screenshot from the Control Room of the orbit measurement with the BPMs during stable beams period meaning with high luminosity at 3.5 TeV performed in 2011. The position being close to zero means the beams are centered in the magnetic elements.

Most of the BPMs are located in the arcs, but some BPMs stripline monitors are used in the insertion regions like in IR1 where the closest BPMs around IP1 are located in front of the first quadrupole from the inner triplets Q1. They are named BPMWS and are equipped with warm directional stripline couplers. Using the left and right position of these BPMs, one can know the position and also the angle at the IP.

Four button pick – up BPMs have been added close to IP1 and IP5 to ensure no crossing angle at IP1 and IP5 specially for the high – β^* optics that are the subject of this PhD. These BPMs cannot distinguish between beam 1 and beam 2 and are called BPMWF.

1.3.2 Emittance measurements

Emittance measurements are briefly detailed here. More informations can be found in [13]. The emittance can be defined as the area occupied by the beam in phase space (position vs. phase). More details are given in chapter 2. On LHC, two principles leading to two different monitors are used: WSs and BSRTs.

- The **W**ire **S**canner (WS) principle consists of a thin carbon wire passing through the beam and producing secondary particles. These secondary particles are measured giving a signal proportionnal to the beam intensity crossing through the wire and provide a reliable result. Two WSs for both horizontal and vertical planes are installed on each beam at IR4. This gives a total number of eight WSs on LHC. WSs provide absolute measurements of the beam dimension but can be used up to a maximum intensity depending on the energy. The intensity limit at 4 TeV is 3.6×10^{12} protons per beam.

- The **B**eam **S**ynchrotron **R**adiation **Telescope** (BSRT) uses the synchrotron light as mentionned in the name. A devoted optics line is used to send the radiation on a photon detector. There are two monitors per beam in IR4.

Wire Scanners are controlled from the control room and give an instantaneous measurement when they're applied whereas BSRTs give a continuous measurement. Following the TDR, the nominal transverse emittance at 7 TeV per beam was expected to reach 3.75 μm.rad at high intensity. With lower total beam intensity, LHC has reached an even lower value of about 2 μm.rad at 3.5 TeV per beam which is a good achievement as far as the high luminosity is concerned.

1.3.3 Optics measurements

The optics parameters have to be measured to check the accuracy of the optics and correct for it. The optics parameters measured will be described in more details in chapter 2. A complete description of the measurements and the way they are done can be found in [14], and more specifically for the LHC in [15]. Different techniques can be used for optics measurements, two of them are of particular interest because results will be used in this work:

- One consists in using an AC dipole [16].
- Another is to introduce on purpose a quadrupole error.

AC dipole technique

The AC dipole technique [15] can be used to measure β beating ($\Delta\beta_{x,y}/\beta_{x,y}$) and correct for it. The β beating is a perturbation of the betatron function which vary around the ring. The specification for LHC is that the peak β beating shall not exceed 20 %.

The AC dipole introduces transverse oscillations without emittance growth and turn by turn data are acquired about approximately 2000 turns. Amplitude and phase are calculated using an interpolated FFT and several algorithms are used to calculate linear and non – linear optics at the BPMs. From the phase advance calculated between three BPMs, β – functions can be measured. The technique used to calculate optics functions at elements is called the *segment – by – segment* technique. This technique is also used to calculate the dispersion function and the transverse coupling.

K – modulation technique

When introducing a quadrupole error Δk, it also introduces a tune shift ΔQ that can be measured (these notions will be detailed in chapter 2). Knowing both, the average β – function can be measured with:

$$\beta(s) \approx \frac{4\,\pi\,\Delta Q}{\Delta k(s)\,L} \tag{1.1}$$

L corresponding to the quadrupole length. This technique also called the K – *modulation* technique can be used to calculate β^* – functions at the IP's [17]. This is done by applying quadrupole errors Δk in the nearest quadrupoles to the IP ie the inner triplets. The β^* value is found by taking into account the measurement of the tune response from left and right. A polynomial function $\beta^* = f((\Delta k_l(s))(\Delta Q_l)(\Delta k_r(s))(\Delta Q_r))$ is calculated.

1.3.4 LHC Collimation

The LHC collimation system is designed to protect the accelerator and to avoid quenches of superconducting magnet due to amount of energy deposited in it. Collimators are made of jaws approaching the beam to intercept halo particles. The distance between two jaws defines the gap.

Three types of collimators are used in LHC: primary (TCP), secondary (TCSG) and tertiary collimators (TCTs). The primaries collimators must be the one closest to the beam, the secondaries intercept the halo from the primaries and then the tertiaries intercepts the halo from the secondaries. This is called a multi stage cleaning system and it's illustrated in Fig. 1.9.

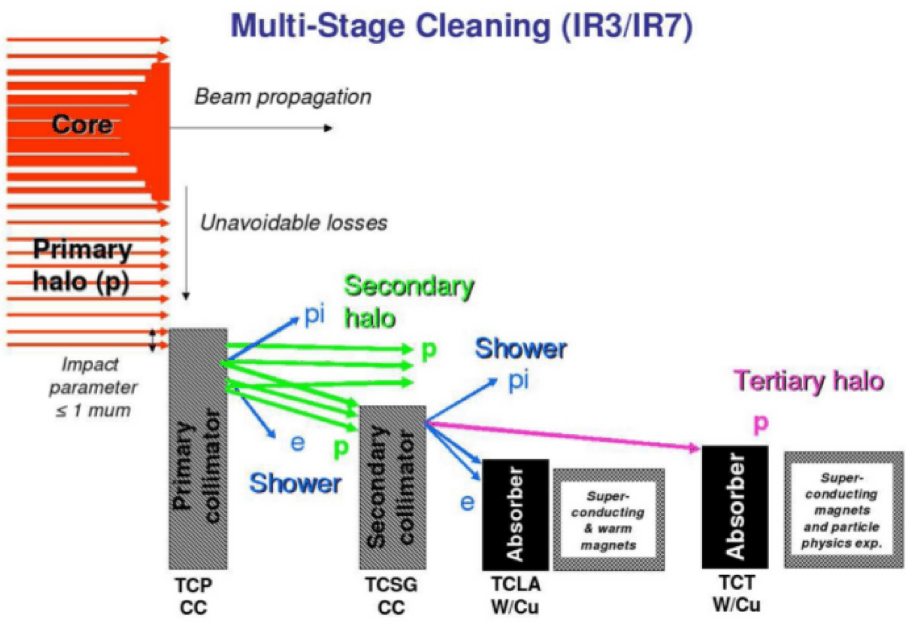

Figure 1.9: Multi stage cleaning scheme of the collimation system of the LHC from [18].

The collimation systems for LHC are located in IR3 and IR7. The location of the collimators on the LHC ring is shown in Fig. 1.10. The insertion regions used have two different purposes: one is dedicated to the momentum cleaning and the other one is dedicated to the betatron cleaning.

- The momentum cleaning insertion region intercepts off – momentum particles outside the allowed range ie more than $\pm 1 \times 10^{-3}$.

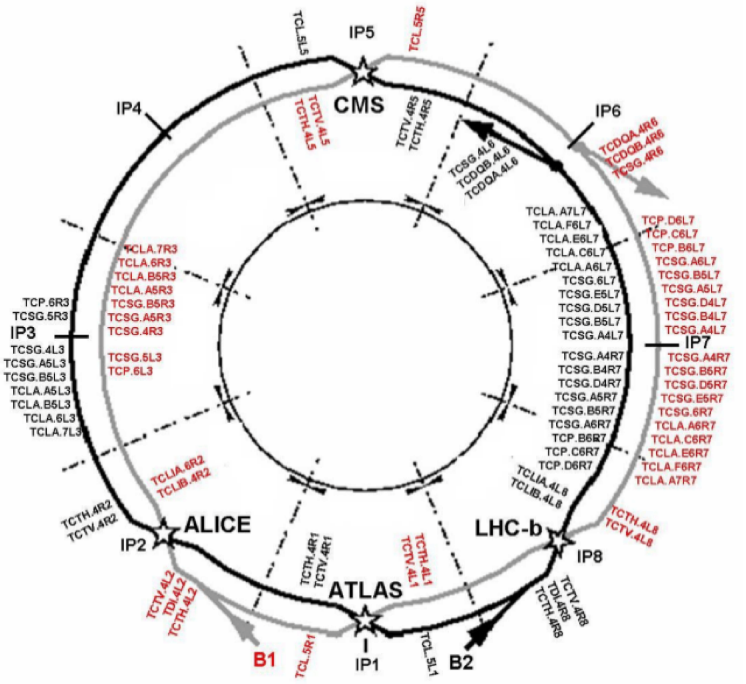

Figure 1.10: Schematic location of the collimators on the LHC ring [18]. They're many around IP3 and IP7.

- The betatron cleaning system removes large betatron oscillation amplitude protons.

For special optics dedicated to special ALFA run, the purpose is to approach the collimators as close as possible to the beam in order to reduce background in the dedicated detectors intercepting elastic protons from the IP.

1.4 The ATLAS experiment

1.4.1 ATLAS description

ATLAS is a multi purpose experiment. It allows to cover a wide range of physics studies and allows precision measurements. The ATLAS collaboration includes about three thousands people involved in the construction, analysis etc.... The ATLAS detector weights 7000 tons and it's the largest detector ever built (25 m height, 25 m large and 46 m long). The overall layout of ATLAS is shown in Fig 1.11. A complete description can be found in [19, 20]. ATLAS detector has been mainly built for the Higgs search and physics above standard model. It's made of different sub – detectors, each allowing to measure and identify various particles.

Starting from the collision point, a particle, as shown on Fig. 1.12, will go through:

- The Inner Detector and solenoid used to determine the charge tracks and to measure the momentum of charged particles.

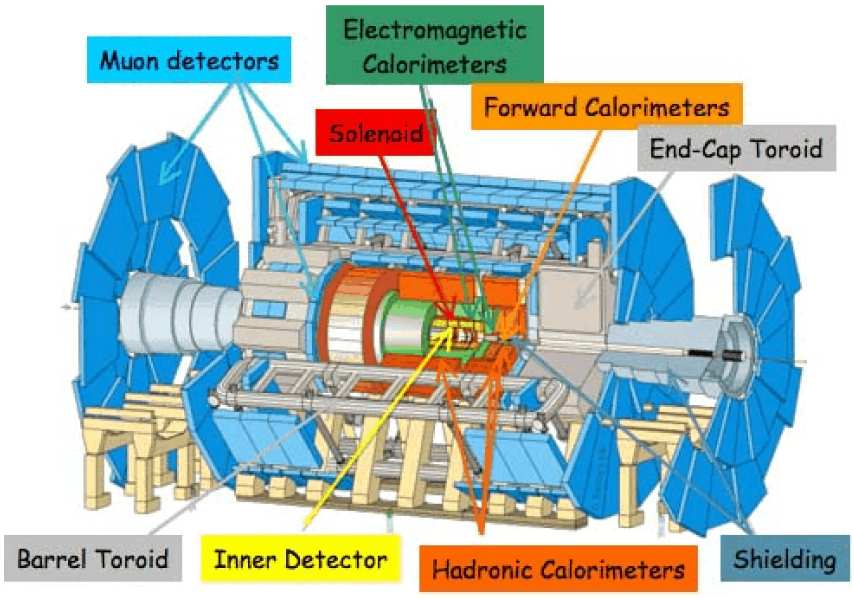

Figure 1.11: ATLAS detector with his sub-detectors.

- Electromagnetic and Hadronic calorimeters used for particle energy determination
- The Muon Spectrometer used to detect the muons.

All charged particles deposit some energy in the inner detector. Photons and electrons loose all their remaining energy in the electromagnetic calorimeter via electromagnetic showers. Protons and neutrons loose all their remaining energy in the hadronic calorimeter via hadronic showers. Muons go through all the sub – detectors leaving signals in all of them. Neutrinos go through the whole structure without any detection.

1.4.2 The Magnets system

The ATLAS magnetic system [21, 22] consists of four superconducting magnets: a solenoid, a barrel toroid and two end – cap toroids corresponding to a total stored energy of 1.6 GJ. A complete scheme of the magnet system is shown in Fig. 1.13.

The Solenoid

The solenoid produces a 2 T magnetic field parallel to the beam axis. It has a length of 5.3 m, an internal diameter of 2.44 m and an external diameter of 2.63 m. The inner detector is completely included inside the solenoid volume. The solenoid magnet shares the cryostat and vacuum vessel of the liquid argon calorimeter which also helps to minimize the amount of material upstream the electromagnetic calorimeter.

The Toroid

The toroid as seen on Fig. 1.14 allows to bend muons outside of the calorimeter ($9.4 < r < 20.1$ m) in addition to the solenoid effect. This solution allows to reduce the solenoid

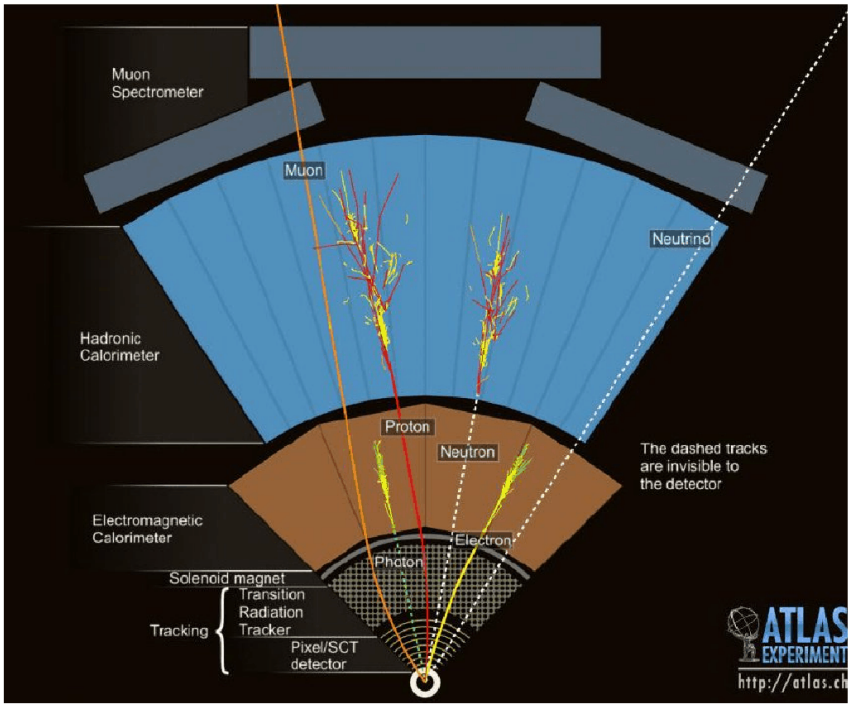

Figure 1.12: Particle identification. All charged particles give signals in the inner detector. Electrons and photons loose their remaining energy in the electromagnetic calorimeter. Protons and neutrons loose their remaining energy in the hadronic calorimeter.

field down to 2 T (instead of 4 T for CMS) but requires a huge detector volume specific for muons. Each toroid is made of eight coils installed symmetrically around the beam axis. Each ring segment nominally operates with a current of 20.5 kA. The maximum magnetic field achievable is 3.9 T for the barrel and 4.1 T for the endcap.

Conclusion

The LHC and his accelerator chain description made here gives us the informations on how the LHC has been divided and on all the labellings. Additionally, an overview of the experiments housed by the LHC was given. Then, the LHC operation description tells us how the accelerator works experimentally before the explanation on how optics parameters are measured which is directly linked on the accelerator performance. This method will be used during special optics measurements made for ALFA purpose. The LHC and the whole accelerator chain provide reliable beam conditions and collisions for the four experiments including ATLAS. The ATLAS description explains us the context as ATLAS has his own luminosity measurements program with different sub – detectors which will be described in chapter 3 including the sub detectors for this PhD.

The LHC higher performance in 2012 have allowed to reach a peak luminosity of 7.7×10^{33} cm^{-2} s^{-1}. This luminosity depends a lot from the optics parameters. Some of these parameters had much improved values than expected, leading to a higher luminosity at

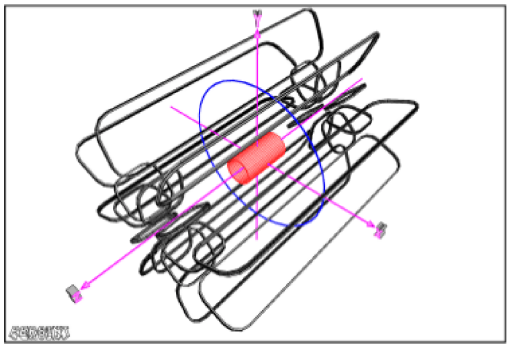

Figure 1.13: ATLAS magnetic system: the solenoid is located in the center. The toroid magnet is located in the outside.

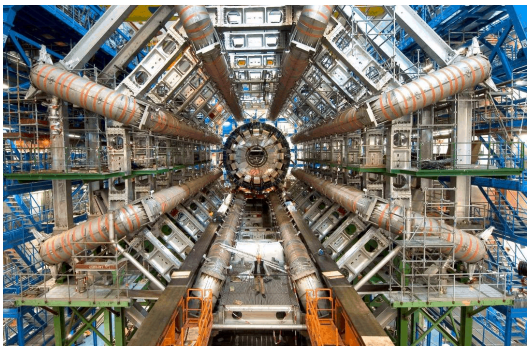

Figure 1.14: Toroid magnet before liquid argon cryostat insertion. The dimensions are given by the man located in between the two coils at the bottom.

3.5 TeV or 4 TeV. The description of these parameters will be given in chapter 2.

Chapter 2

Transverse Beam Dynamics

Contents

A small introduction to transverse dynamics in accelerators is given providing the main formulae that will be useful for the understanding of this report. More informations can be found in various references such as [23], [24] and [25].
To start, a small description with fundamentals is given before the definition of the magnetic field characteristics and the description of the reference particle with her associate reference system. Then the motion of particles inside the magnetic fields is defined to be able to introduce the transfer matrices. As for the ALFA project, the beam line used consists mainly on quadrupoles, the examples given will concern mostly the quadrupoles case. The particle motion brings to the definition of the twiss parameters leading directly to the transfer matrix with twiss parameters, an important tool for ALFA. A description of a FODO lattice is then given in order to introduce periodic structures like the LHC. Beam – beam effects is of importance in a collider like LHC, and a quick introduction will be given. Finally, the most important perturbations of the motion for our concerns will also be quickly introduced.

The motion of charged particles of velocity $\vec{v}$ in electromagnetic fields is governed by the Lorentz force:

$$\vec{F} = q\,(\vec{E} + \vec{v} \times \vec{B}) \tag{2.1}$$

q being the charge of the particles, $\vec{E}$ the electric field and $\vec{B}$ the magnetic field. The trajectory equation derived from this force is written as follows:

$$\frac{d\vec{p}}{dt} \;=\; \vec{F}_e + \vec{F}_m \text{ with } \vec{F}_e \;=\; q\,\vec{E} \text{ and } \vec{F}_m \;=\; q\,(\vec{v} \times \vec{B}) \tag{2.2}$$

where, in relativistic mechanics, the momentum is written:

$$\vec{p} \;=\; m_0\,\gamma_L\,\vec{\beta_L}\,c \tag{2.3}$$

In these equations, β_L is the relativistic factor equal to v/c, m_0 is the mass and γ_L is the relativistic lorentz factor equal to $\mathcal{E}/\mathcal{E}_0$ where $\mathcal{E}$ is the total energy and $\mathcal{E}_0$ the rest energy depending on the particle type. For 3.5 TeV or 4 TeV total energy, protons ($\mathcal{E}_0 = 938.272$ MeV/c^{-2}) have γ_L equal to 3730 or 4260 respectively.

If we compare magnetic and electric field strengths we obtain:

$$\frac{\vec{F_e}}{\vec{F_m}} = \frac{\left|q\,\vec{E}\right|}{\left|q\,(\vec{v} \times \vec{B})\right|} \leqslant \frac{\left|\vec{E}\right|_{V/m}}{\beta\,c_{m/s}\,\left|\vec{B}\right|_T} \tag{2.4}$$

For instance, for a relativistic particle with $v \approx c$, a magnetic field $B = 1$ T gives the same bending forces as an electric field of 300 MV/m which is far beyond technical limits. So for high energy beams whenever particles are needed to be guided (focused or bended), magnetic fields are preferably used. The electric field is used to accelerate the beam using for instance radio frequency (RF) superconducting cavities as for LHC.

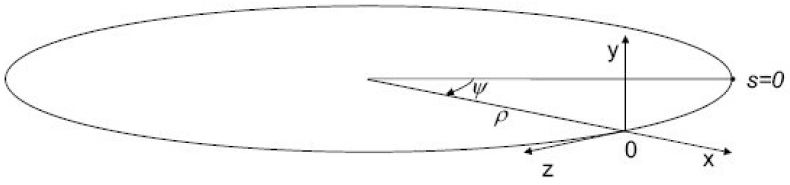

Figure 2.1: Cartesian coordinate system used to describe the particle motion in the LHC ring.

The magnetic part of the Lorentz force can be written:

$$\frac{d\vec{p}}{dt} = q\,(\vec{v} \times \vec{B}) \tag{2.5}$$

Integrating (2.5), with $\vec{B} \perp \vec{v}$ one can show that in 2D case, the particles travel on a circle with a radius ρ in the presence of a uniform magnetic field B, given by:

$$B\rho = \frac{p}{q} \tag{2.6}$$

where $B\rho$ is the beam rigidity. It links the curvature radius in the magnetic field and the energy of the particle.

An accelerator is a sequence of magnets which will guide the beam by bending and focusing depending on the magnet type. The magnetic configurations is described more precisely in § 2.2 after the definition of the coordinate system used for accelerators.

2.1 Coordinate system

A reference particle with a given momentum p_0 is chosen around which the motion is described. The trajectory described by this reference particle is known as the reference orbit.

More generally, all the particles trajectories will be described around the reference orbit in the coordinate system illustrated in Fig. 2.1 and will be defined by:

$$\vec{r}(s) = \vec{r_0}(s) + x(s)\,\vec{x}(s) + y(s)\,\vec{y}(s) \tag{2.7}$$

where r_0 denotes the position of the reference particle at the longitudinal s location along the reference orbit. The transverse coordinates are defined by x for the horizontal plane and y for the vertical plane. Any particle is described versus the reference particle and performs small oscillations around the reference orbit. We'll use the following notation to simplify the equations: $\dot{x} = \dfrac{dx}{dt}$, $x' = \dfrac{dx}{ds}$.

2.2 Magnetic elements

2.2.1 General case

Neglecting the fringe field, the magnetic field produced by a magnet can be described in polar coordinates as the sum of multipolar fields straight and skewed [23]:

$$\begin{cases} B_r(r,\theta) &= \sum_{n=1}^{\infty} r^{n-1} \left(b_n \sin(n\,\theta) + a_n \cos(n\,\theta)\right) \\ B_\theta(r,\theta) &= \sum_{n=1}^{\infty} r^{n-1} \left(b_n \cos(n\,\theta) - a_n \sin(n\,\theta)\right) \end{cases} \tag{2.8}$$

where b_n defines the multipolar straight coefficients and a_n the multipolar skewed coefficients.

For a straight perfect multipole with $2 \times n$ poles, the formulae can be written:

$$\begin{cases} B_r(r,\theta) &= b_n\, r^{n-1} \sin(n\,\theta) \\ B_\theta(r,\theta) &= b_n\, r^{n-1} \cos(n\,\theta) \end{cases} \tag{2.9}$$

$K_n = b_n / B\rho$ defines the normalized strength of the multipoles given by:

$$K_n = \frac{1}{B\,\rho}\,\frac{1}{(n-1)!}\,\left.\frac{\partial^{n-1} B_y}{\partial x^{n-1}}\right|_{\vec{r}=0} \tag{2.10}$$

Taking different values of n, we can find back each type of magnets: $n = 1$ corresponding to dipoles, $n = 2$ for quadrupoles, $n = 3$ to sextupoles and so on. A more complete description with other examples, like dipoles and sextupoles can be found in [23].

2.2.2 Example: Quadrupoles

The main quadrupole parameter linked to the current and the beam rigidity is called the normalized strength. Considering (x, y) as the transverse plane, the normalized strength for the quadrupole will be equal to:

$$K_2 = \frac{1}{B\rho}\frac{\partial B_y}{\partial x} \tag{2.11}$$

Due to the field pattern, a quadrupole is always focusing in one transverse plane and defocusing in the other (see Fig. 2.2). Furthermore, for a straigth perfect quadrupole, the gradient G is expressed as:

$$G = \frac{\partial B_x}{\partial y} = \frac{\partial B_y}{\partial x} \quad \text{and} \quad G = K_2\, B\, \rho = \frac{2\,\mu_0\, N\, I}{R^2} \tag{2.12}$$

where R is the quadrupole radius in meter, I the intensity of the coil in Ampere and N the number of turns. The quadrupole strength can then also be written as:

$$K_2 = \frac{1}{B\rho}\, G \tag{2.13}$$

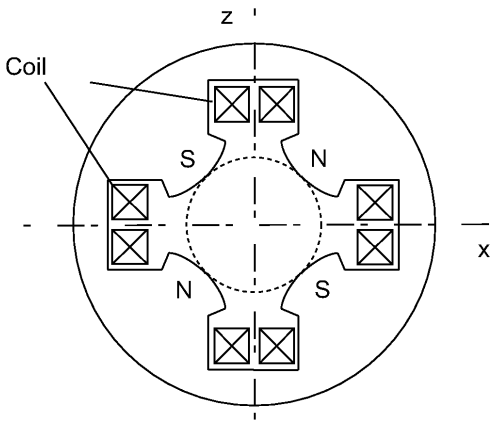

Figure 2.2: Scheme of a quadrupole in the transverse plane.

2.3 Transverse motion and Hill's equations

The particle motion inside the magnetic fields in the reference system is described here. The equation of motion is also called the Hill's equation for periodic systems as demonstrated in the following.

2.3.1 General case

We apply in the curved coordinate system defined in § 2.1, only in the (x, y) plane, the equation of motion of a charged particle into a pure magnetic field defined by (2.5). The particle velocity vector is $\vec{v} = d\vec{r}/dt$.

The amplitude of particle motion around the closed orbit is small and momentum deviations are also small and approximated by:

$$p = p_0 \, (1 + \delta) \tag{2.14}$$

where δ is the relative momentum deviation. We consider only the linear part of motion equations and after a complete demonstration detailed in [23], this gives the linear trajectory equations in the same system and describes the particles movements for the transverse plane:

$$\begin{cases} x'' + K_x(s)\, x &= f(s) \\ \\ y'' + K_y(s)\, y &= 0 \end{cases} \tag{2.15}$$

where $f(s) = \delta/\rho$ and $K_{x,y}(s)$ represents the focusing functions depending on the different magnet structure types. At first order, the vertical and horizontal motions are decoupled.

The different $K_{x,y}(s)$ values for different situation are listed below:

$$K_x(s) = \begin{cases} 0 \\ \dfrac{1}{\rho^2} \\ K_2 \end{cases} \quad \text{and} \quad K_y(s) = \begin{cases} 0 & \text{for a drift section} \\ 0 & \text{for a dipole} \\ -K_2 & \text{for a quadrupole} \end{cases} \tag{2.16}$$

Taking u to represent independantly the transverse dimension x or y, these equations are of the type:

$$u'' + K_u(s)\, u \;=\; f(s) \tag{2.17}$$

which are defined as the Hill′s equations where $K_u(s)$ is a periodic function which period is at most equal to the ring circumference.

2.3.2 Homogeneous equation

The second order differential linear trajectory homogeneous equation (2.15) has the following general solutions:

$$\begin{cases} u(s) &= C_u(s)\, u_0 + S_u(s)\, u'_0 \\ u'(s) &= C'_u(s)\, u_0 + S'_u(s)\, u'_0 \end{cases} \tag{2.18}$$

where $C_u(s)$ and $S_u(s)$ are the cosine and sine like independent solutions with the conditions $C_u(0) = 1$ and $C'_u(0) = 0$, $S_u(0) = 0$ and $S'_u(0) = 1$. This can be written with the matrix formalism:

$$\begin{pmatrix} u(s) \\ u'(s) \end{pmatrix} = T_{u=x,y} \begin{pmatrix} u(s_0) \\ u'(s_0) \end{pmatrix} \quad \text{with} \quad T_{u=x,y} = \begin{pmatrix} C_u(s) & S_u(s) \\ C'_u(s) & S'_u(s) \end{pmatrix} \tag{2.19}$$

All the elements seen by the beam can be described as a transfer matrix. The expressions of these transfer matrices can be found for instance in [24].

2.3.3 Inhomogeneous equation

The general solution from the inhomogeneous equation can be written as:

$$u(s) \;=\; C_u(s)\, u_0 + S_u(s)\, u'_0 + u_p(s) \tag{2.20}$$

where $u_p(s) = D_u(s)\, \delta$ is the particular solution of the homogeneous equation. As demonstrated in [26], the dispersion function $D_u(s)$ can be expressed in terms of $C_u(s)$ and $S_u(s)$:

$$D_u(s) \;=\; S_u(s) \int_0^s \frac{1}{\rho}\, C_u(s)\, ds - C_u(s) \int_0^s \frac{1}{\rho}\, S_u(s)\, ds \tag{2.21}$$

2.3.4 Example: Quadrupole transfer matrix

$T_{u=x,y}$ (2.19) is called the transfer matrix between s and s_0. This transfer matrix is calculated for each type of magnetic elements (dipoles, quadrupoles...) or drifts located along the ring. The overall matrix M for the whole structure is determined by the product of each transfer matrix.

The transfer matrices for a quadrupole in the (x, y) transverse plane in the curved coordinate system defined in 2.1 can be written as:

$$T_x = \begin{pmatrix} \cos\phi & \frac{1}{\sqrt{K}}\sin\phi \\ -\sqrt{K}\sin\phi & \cos\phi \end{pmatrix} \quad \text{and} \quad T_y = \begin{pmatrix} \mathrm{ch}\,\phi & \frac{1}{\sqrt{K}}\,\mathrm{sh}\,\phi \\ \sqrt{K}\,\mathrm{sh}\,\phi & \mathrm{ch}\,\phi \end{pmatrix} \tag{2.22}$$

where $\phi = \sqrt{K}\,L$ and L is the length of the quadrupole. This matrix is used for focusing quadrupole. By convention, the focusing is in the horizontal plane. We would have the opposite for a defocusing quadrupole in the horizontal plane (but focusing in the vertical plane).

The quadrupole transfer matrix can also be calculated in thin lens approximation in order to simplify the calculation. In that case, quadrupoles are replaced by thin lenses with the focal length $f = 1/K\,L$. Furthermore the focal length is much larger than the quadrupole length. The quadrupole is focusing or defocusing depending the sign of f : if $f > 0$, the quadrupole is focusing and if $f < 0$, the quadrupole is defocusing. Then the new quadrupole matrices are written as:

$$R_Q = \begin{pmatrix} 1 & 0 \\ -1/f & 1 \end{pmatrix} \tag{2.23}$$

2.4 Twiss parameters

2.4.1 Courant Snyder Invariant

We take u_1 and u_2 as the general solutions of (2.15) in the form $u(s) = a_0\,u_1(s) + b_0\,u_2(s)$ where a_0 and b_0 are constants and $u_1(s)$ and $u_2(s)$ are two independant solutions. Then we take the function W called the Wronskian:

$$W \;=\; u_1\,u_2' - u_1'\,u_2 \tag{2.24}$$

We have $dW/ds = u_1\,u_2'' - u_1''\,u_2 \;=\; 0$ which gives that W is constant. We can write the solutions as [23]:

$$\begin{cases} u_1(s) \;=\; C(s) + i\,S(s) \\ u_1^*(s) \;=\; C(s) - i\,S(s) \end{cases} \tag{2.25}$$

Inserting (2.25) in the general solution $u(s) \;=\; a_0\,C(s) + b_0\,S(s) + u_p(s)$, we find:

$$\begin{cases} u(s) \;=\; a_0\,\dfrac{u_1(s) + u_1^*(s)}{2} + b_0\,\dfrac{u_1(s) - u_1^*(s)}{2i} + u_p(s) \\ \qquad\;\; = A\,u_1(s) + A^*\,u_1^*(s) + u_p(s) \end{cases} \tag{2.26}$$

We take $z(s) = u(s) - u_p(s)$. The solution can be written on a matrix form:

$$\begin{pmatrix} z(s) \\ z'(s) \end{pmatrix} = \begin{pmatrix} u_1(s) & u_1^*(s) \\ u_1'(s) & u_1'^*(s) \end{pmatrix} \begin{pmatrix} A \\ A^* \end{pmatrix} \tag{2.27}$$

If we invert this matrix, it gives:

$$\begin{pmatrix} A \\ A^* \end{pmatrix} = \frac{1}{W^*} \begin{pmatrix} u_1'^*(s) & -u_1^*(s) \\ -u_1'(s) & u_1(s) \end{pmatrix} \begin{pmatrix} z(s) \\ z'(s) \end{pmatrix} \tag{2.28}$$

This gives the formulae:

$$|A^*|^2 \;=\; \text{constant} \;=\; A\,A^* \;=\; \frac{1}{W^2}\,(u_1^{*\prime}\,z - u_1^*\,z')(-u_1'\,z + u_1\,z') \tag{2.29}$$

And calculating the Wronskian expression:

$$\begin{cases} W \;=\; u_1\,u_1'^* - u_1^* u_1' \;=\; (C + i\,S)\,(C' - i\,S') - (C - i\,S)\,(C' + i\,S') \\ W \;=\; 2\,i\,(SC' - CS') \\ \text{with} \\ W(0) \;=\; 2\,i\,(S(0)\,C'(0) - C(0)\,S'(0)) = -2\,i \;\;\Rightarrow\;\; W^2 \;=\; -4 \end{cases} \tag{2.30}$$

This gives finally:

$$|A|^2 \;=\; \frac{u_1'\,u_1^{*\prime}}{4}\,z^2 - \frac{u_1^*\,u_1' + u_1'^*\,u_1}{4}\,z\,z' + \frac{u_1\,u_1^*}{4}\,z'^2 \tag{2.31}$$

We choose: $\beta(s) = u_1\,u_1^*$, $\gamma(s) = u_1'\,u_1'^*$ and $-2\alpha(s) = u_1^*\,u_1' + u_1'^*\,u_1$. This gives the final equation:

$$\gamma(s)\,z^2 + 2\;\alpha(s)\,z\,z' + \beta(s)\,z'^2 \;=\; 4\,|A|^2 \;= U \tag{2.32}$$

where U is defined as the Courant Snyder invariant and is a constant of the motion. The equation is an ellipse corresponding to the area in the phase space coordinate system (u, u'). The phase space ellipse described by the particle motion is shown on Fig. 2.3. The ellipse has a different orientation depending on the location in the ring. But the area $\mathcal{A}$ enclosed by the ellipse remains constant and is defined by $\mathcal{A} = U\,\pi$.

$\alpha(s),\ \beta(s)$ and γ(s) are defined as the twiss parameters. The twiss parameters are linked to each other by the relation $\beta(s)\,\gamma(s) = 1 + \alpha^2(s)$. This can be demonstrated as in the following:

$$\begin{cases} \beta \;=\; |u_1|^2 \;=\; C^2 + S^2 \\ \gamma \;=\; |u_1'|^2 \;=\; C'^2 + S'^2 \\ -2\,\alpha \;=\; 2\,(C\,C' + S\,S') \;\;\Rightarrow\;\; \alpha^2 \;=\; (C\,C' + S\,S')^2 \end{cases} \tag{2.33}$$

This gives the final relation:

$$\beta\,\gamma - \alpha^2 \;=\; (C\,S' - S\,C')^2 = \frac{W^2}{-4} \;=\; 1 \tag{2.34}$$

$\beta(s),\ \alpha(s)$ and $\gamma(s)$ are independant of $z(s)$.

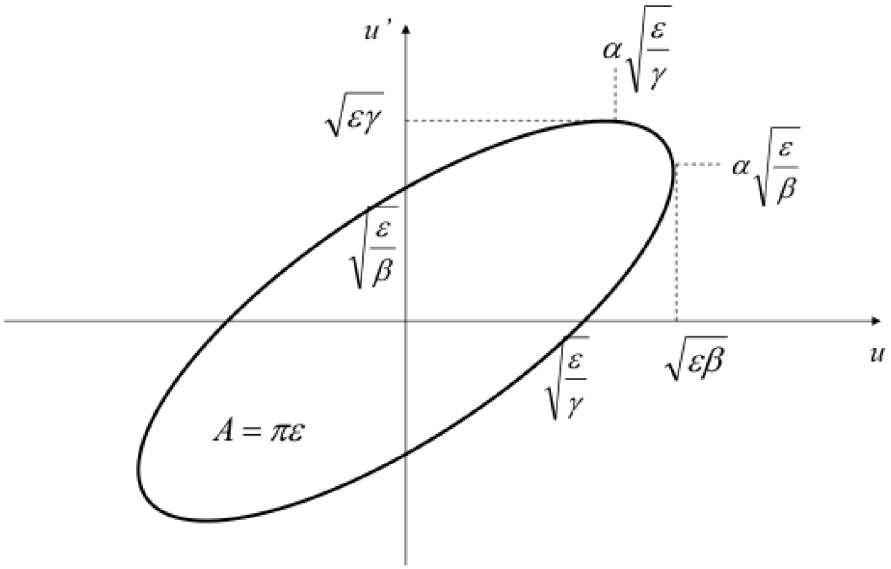

Figure 2.3: Phase space ellipse.

The solution z of the ellipse as in (2.32) can be written in a parametric form, with $\phi(s)$ a function increasing with s:

$$\begin{array}{rcl} z(\phi(s)) & = & a_1\,\cos(\phi(s)-\phi_0) \\ z'(\phi(s)) & = & b_1\,\cos(\phi(s)-\phi_0)+c_1\,\sin(\phi(s)-\phi_0) \end{array} \tag{2.35}$$

where a_1, b_1 and c_1 are constants. These parametric solutions are inserted into (2.32) and by identification, we find:

$$\left\{\begin{array}{rcl} \beta\,b^2+\beta\,c^2+\gamma\,a^2+2\alpha\,a\,b & = & 2\,U \\ \beta\,b^2-\beta\,c^2+\gamma\,a^2+2\alpha\,a\,b & = & 0 \\ 4\beta\,b\,c+4\alpha\,a\,c & = & 0 \end{array}\right. \tag{2.36}$$

Combining these three equations, we find the a_1,b_1 and c_1 parameters such as:

$$\left\{\begin{array}{rcl} a_1 & = & \sqrt{U}\sqrt{\beta} \\ b_1 & = & -\alpha\dfrac{\sqrt{U}}{\sqrt{\beta}} \\ c_1 & = & -\dfrac{\sqrt{U}}{\sqrt{\beta}} \end{array}\right. \tag{2.37}$$

This gives finaly, the quasi-harmonic solution form of (2.15).

$$z(s) \;=\; \sqrt{U}\,\sqrt{\beta(s)}\,cos(\phi(s)-\phi_0) \tag{2.38}$$

$$z'(s) = -\frac{\sqrt{U}}{\sqrt{\beta(s)}}\left(\sin\left(\phi(s)-\phi_0\right)+\alpha\,\cos\left(\phi(s)-\phi_0\right)\right) \tag{2.39}$$

where U and ϕ_0 are constants depending on initial conditions. $\beta(s)$ is called the betatron function given by the focusing properties of the lattice. If now we calculate the derivative of (2.38), it gives:

$$z'(s) \;=\; \sqrt{U}\left[\frac{1}{2}\frac{\beta'}{\sqrt{\beta}}\cos(\phi(s)-\phi_0) - \phi'(s)\sqrt{\beta}\sin(\phi(s)-\phi_0)\right] \tag{2.40}$$

And if we identify (2.39) and (2.40):

$$\begin{cases} \dfrac{1}{2}\dfrac{\beta'}{\sqrt{\beta}} \;=\; -\dfrac{\alpha}{\sqrt{\beta}} \;\Rightarrow\; \alpha \;=\; -\dfrac{1}{2}\beta' \\ \dfrac{1}{\sqrt{\beta}} \;=\; \phi'\sqrt{\beta} \;\Rightarrow\; \phi' \;=\; \dfrac{1}{\beta} \end{cases} \tag{2.41}$$

where we define the link between α and β and the other parameter called the betatron phase or phase advance which is related to the β – function and defined by:

$$\phi(s) \;=\; \int_0^s \frac{1}{\beta(s)}\,ds \tag{2.42}$$

The phase advance gives the number of oscillations between $z = 0$ and $z = s$ in the lattice.

2.4.2 Beam matrix

The covariant matrix also called the Σ matrix is:

$$\Sigma \;=\; \begin{pmatrix} \langle u^2\rangle & \langle uu'\rangle \\ \langle uu'\rangle & \langle u'^2\rangle \end{pmatrix} \tag{2.43}$$

The emittance is defined as in (2.44):

$$\epsilon \;=\; \sqrt{\det\,\Sigma} \;=\; \sqrt{\langle u^2\rangle\langle u'^2\rangle - \langle uu'\rangle^2} \tag{2.44}$$

The Σ matrix can also be written as $\Sigma = \langle X\,.\,X^T\rangle$ with X representing the trajectory vector. At $s = 0$, $X = X_0$. Knowing $X = T\,.\,X_0$, the transport of the Σ matrix between s and s_0 is made as:

$$\begin{cases} \Sigma &= \langle T\,.\,X_0\,.\,X_0^T\,.\,T^T\rangle \\ &= T\,.\,\langle X_0\,.\,X_0^T\rangle\,.\,T^T \\ &= T\,.\,\Sigma_0\,.\,T^T \end{cases} \tag{2.45}$$

Finally, we find:

$$\det\,\Sigma \;=\; \det\,T\,.\,\det\,\Sigma_0\,.\,\det\,T^T \;=\; \det\,\Sigma_0 \tag{2.46}$$

with $\det\,T \;=\; 1$ as for the transfer matrices $\det\,M = CS' - SC' = 1$ as shown in (2.30). This gives that ϵ is a constant. The emittance is the area of the phase space ellipse which

has the same value at every point in a beam transport system. To determine the Σ matrix value, starting from (2.43), it follows:

$$\begin{cases} \langle u^2 \rangle &= \beta(s)\langle U_u \rangle \langle \cos^2(\phi_u - \phi_0) \rangle &= \dfrac{\beta(s)\langle U_u \rangle}{2} \\ \\ \langle u\, u' \rangle &= -\alpha(s)\langle U_u \rangle \dfrac{1}{2} \\ \\ \langle u'^2 \rangle &= \dfrac{\langle U_u \rangle}{2}\,\gamma(s) \end{cases} \tag{2.47}$$

Which gives at the end:

$$\Sigma \;=\; \frac{\langle U_u \rangle}{2} \begin{pmatrix} \beta(s) & -\alpha(s) \\ -\alpha(s) & \gamma(s) \end{pmatrix} \tag{2.48}$$

And $\det \Sigma \;=\; \epsilon^2 \;=\; \dfrac{\langle U_u \rangle^2}{4}$

Also if we consider beam particle trajectory with ϵ as the beam emittance, we can also define the rms beam enveloppe and rms beam divergence as in (2.49).

$$\begin{cases} \sigma_u(s) &= \sqrt{\beta_u(s)\,\epsilon_u} \\ \sigma'_u(s) &= \sqrt{\gamma_u(s)\,\epsilon_u} \end{cases} \tag{2.49}$$

The adiabatic damping phenomenon described in [13] implies that the emittance of the beam shrinks as $1 \,/\, \beta_L\,\gamma_L$. Here $\beta_L\,\gamma_L$ are the relativistic factors already defined in the introduction. The emittance which is then conserved is the normalized emittance defined by (2.50).

$$\epsilon_N \;=\; \beta_L\,\gamma_L\,\epsilon_u \tag{2.50}$$

The emittance values given will be the one of the normalized emittance in most cases.

2.4.3 Twiss parameters transport

Considering two positions in the ring and the fact that the emittance is a constant value and inserting the inverse trajectory transformation.

$$\begin{pmatrix} u_0 \\ u'_0 \end{pmatrix} = T^{-1} \begin{pmatrix} u \\ u' \end{pmatrix} = \begin{pmatrix} S'_u & -S_u \\ -C'_u & C_u \end{pmatrix} \begin{pmatrix} u \\ u' \end{pmatrix} \tag{2.51}$$

we can state that:

$$\gamma\, y_0^2 + 2\,\alpha\, y_0\, y'_0 + \beta\, y'^2_0 \;=\; \gamma_0\,(S'y - Sy'^2) + 2\,\alpha_0\,(S'y - Sy')(-C'y + Cy') + \beta_0\,(-C'y + Cy')^2$$

giving the following twiss values:

$$\begin{cases} \beta(s) &= C^2\,\beta_0 - 2\,S\,C\,\alpha_0 + S^2\,\gamma_0 \\ \alpha(s) &= -C\,C'\,\beta_0 + (SC' + S'C)\,\alpha_0 - S\,S'\,\gamma_0 \\ \gamma(s) &= C'^2\,\beta_0 - 2\,S'\,C'\,\alpha_0 + S'^2\,\gamma_0 \end{cases} \tag{2.52}$$

which can be written in matrix notation

$$\begin{pmatrix}\beta\\ \alpha\\ \gamma\end{pmatrix}_s = \begin{pmatrix} C^2 & -2SC & S^2 \\ -CC' & CS'+SC' & -SS' \\ C'^2 & -2C'S' & S'^2 \end{pmatrix} . \begin{pmatrix}\beta\\ \alpha\\ \gamma\end{pmatrix}_0 \tag{2.53}$$

This expression gives the possibility to calculate the twiss parameters in the ring knowing them at any point. This matrix is based on the focusing properties elements of the lattice.

2.4.4 Transfer matrix with twiss parameters

The C_u, S_u, C'_u, S'_u coefficients are based on the transfer matrix M which gives the knowledge of the coordinates at location s knowing the coordinates at an initial location s_0. They follow:

$$\begin{pmatrix} u(s) \\ u'(s) \end{pmatrix} = M \begin{pmatrix} u(s_0) \\ u'(s_0) \end{pmatrix} = \begin{pmatrix} C_u(s) & S_u(s) \\ C'_u(s) & S'_u(s) \end{pmatrix} \begin{pmatrix} u(s_0) \\ u'(s_0) \end{pmatrix} \tag{2.54}$$

Taking into account the expression (2.38) and (2.39), we get:

$$u(s) = \sqrt{U}\,\sqrt{\beta_u}\,(\cos\phi_s\,\cos\phi_0 + \sin\phi_s\,\sin\phi_0) \tag{2.55}$$

$$u'(s) = -\frac{\sqrt{U}}{\sqrt{\beta_u}}(\alpha_u\cos\phi_s\cos\phi_0 + \alpha_u\sin\phi_s\sin\phi_0 + \sin\phi_s\cos\phi_0 - \cos\phi_s\sin\phi_0) \tag{2.56}$$

And knowing that $u_0 = u(0)$ is the starting point and that $\phi(0) = 0$ by definition, we get:

$$\begin{cases} \cos(\phi_0) &= \dfrac{u_0}{\sqrt{\beta_0\,U}} \\ \sin(\phi_0) &= \dfrac{\alpha_0\,u_0 + \beta_0\,u'_0}{\sqrt{\beta_0\,U}} \end{cases} \tag{2.57}$$

Inserting into the solution $u(s)$ and $u'(s)$:

$$\begin{cases} u(s) = & \sqrt{\dfrac{\beta_u}{\beta_0}}(\cos\phi_s + \alpha_0\sin\phi_s)\,u_0 + (\sqrt{\beta_0\beta_u}\sin\phi_s)\,u'_0 \\ u'(s) = & -\dfrac{1}{\sqrt{\beta_0\beta_u}}\,((\alpha_u-\alpha_0)\cos\phi_s) + (1+\alpha_u\alpha_0)\sin\phi_s)\,u_0 + \sqrt{\dfrac{\beta_0}{\beta_u}}\,(\cos\phi_s - \alpha_u\sin\phi_s)\,u'_0 \end{cases} \tag{2.58}$$

We finally find the transfer matrix M by comparison with (2.54).

$$M = \begin{pmatrix} \sqrt{\dfrac{\beta_u}{\beta_0}}(\cos\phi_s + \alpha_0\sin\phi_s) & \sqrt{\beta_0\beta_u}\sin\phi_s \\ -\dfrac{1}{\sqrt{\beta_0\beta_u}}\,[(\alpha_u-\alpha_0)\cos\phi_s + (1+\alpha_u\alpha_0)\sin\phi_s] & \sqrt{\dfrac{\beta_0}{\beta_u}}(\cos\phi_s - \alpha_u\sin\phi_s) \end{pmatrix} \tag{2.59}$$

Any single particle trajectory between two positions can be calculated knowing only the twiss parameters α_u, β_u and γ_u at the entrance and exit.

If now we consider periodic solutions with the twiss parameters, α_u, β_u and γ_u are defined as periodic functions over one turn with length L as in (2.60).

$$\alpha_u(s+L) = \alpha_u(s),\ \beta_u(s+L) = \beta_u(s) \text{ and } \gamma_u(s+L) = \gamma_u(s) \tag{2.60}$$

the matrix M becomes when the beam is matched:

$$M = \begin{pmatrix} (\cos\phi_u + \alpha \sin\phi_u) & \beta \sin\phi_u \\ -\gamma \sin\phi_u & (\cos\phi_u - \alpha \sin\phi_u) \end{pmatrix} \tag{2.61}$$

where ϕ_u represents the phase advance over one turn as defined in (2.42).

The tune $Q_u = \dfrac{\phi_u}{2\pi}$ corresponds to the number of betatron oscillations per turn and has the following value:

$$Q_u = \frac{1}{2\pi} \int_0^L \frac{ds}{\beta_u} \tag{2.62}$$

In the periodic solution case, if instead of applying one turn, we perform many turns, it can be demonstrated that for a periodic structure, the stability condition on matrix (2.61) is $|Tr\,(M)| \leq 2$ [23].

2.5 FODO Lattice

There are different ways to build circular colliders, more precisely different kind of lattices. All type of lattices won't be described but we'll focus on the one used for LHC: the FODO lattice (Fig. 2.4). A basic FODO lattice is based on an alternance on quadrupoles gradient: one focusing quadrupole, and one defocusing. Dipoles can be inserted in between two quadrupoles. This forms the cell of the lattice.

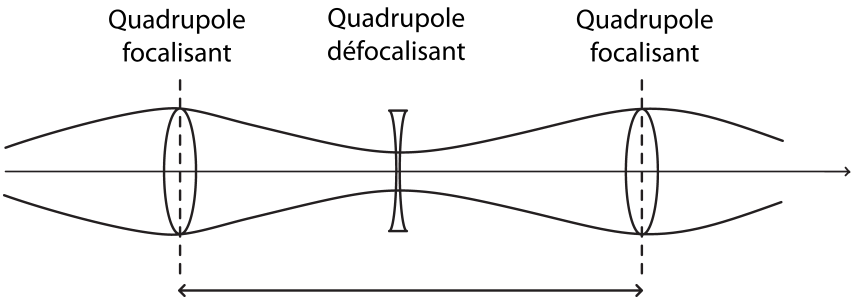

Figure 2.4: Symmetric FODO cell with a focusing quadrupole QF in the horizontal plane and a defocusing quadrupole QD in the horizontal plane.

Colliders are made of straight and arc sections. Straight sections are used to house, for instance, experiments at collision points or RF devices and arc sections are used to bend the beams. They can still be made as a FODO lattice. Parameters of FODO cells are

calculated with beam optics programs like MAD–X [27].

A FODO matrix is written as the matrix product of quadrupoles and dipoles. From this we can check the stability criteria of the periodic lattice already shown i.e. $|Tr(M)| \leq 2$. And we can check the optics parameters α_u, β_u and ϕ_u. FODO cells are easier to calculate in thin-lens approximation. An example of the FODO cells used in LHC arcs is given in Fig. 2.5 illustrating the betatron motion.

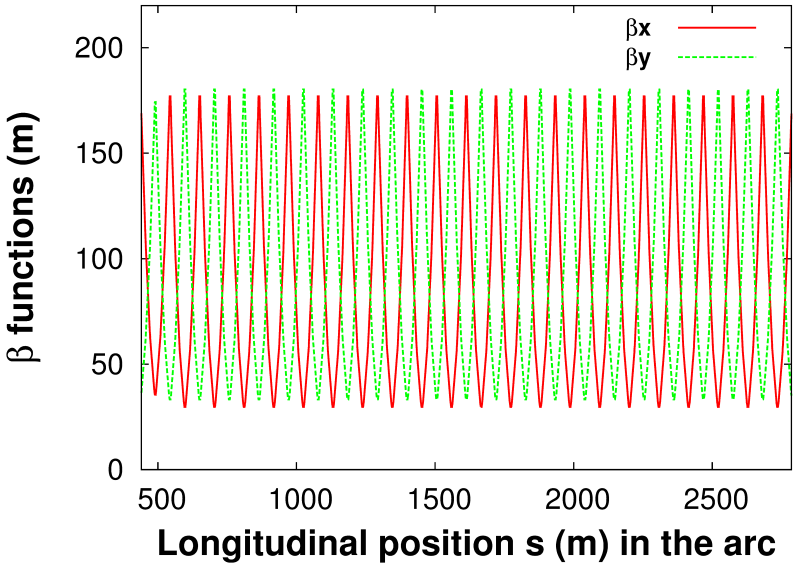

Figure 2.5: β – functions corresponding to the FODO cell in the LHC arcs. IP1 is at s = 0.0 m and the approximate length on the plot is 2345 m.

2.6 Beam – beam effect

A brief introduction of beam – beam effect is given in this section as it's often a limiting factor for the collider's luminosity.

2.6.1 Beam – beam force

A beam is a distribution of charges. It represents an electromagnetic potential for other charges. Therefore it induces a force on himself (space charge) and on opposing beam (beam – beam effect). On particle colliders, the force will act only when two beams cross each other. The effect is important for high density beams. The beam – beam interactions are then a limiting effect for high luminosity. More details on beam – beam effect can be found on [28].

In a Gaussian two dimensional beam with density distributions $\rho(x, y) = \rho(x)\rho(y)$ in the

transverse plane, the distribution of particles has the analytical expression:

$$\rho_u(u) = \frac{1}{\sigma_u\sqrt{2\pi}} \exp(-\frac{u^2}{2\sigma_u^2}) \quad \text{where} \quad u = x, y \tag{2.63}$$

where σ_x and σ_y are the beam sizes. It gives the two dimensional potential:

$$U(x, y, \sigma_x, \sigma_y) = \frac{n\,e}{4\,\pi\,\epsilon_0} \int_0^\infty \frac{\exp(-\frac{x^2}{2\,\sigma_x^2+q} - \frac{y^2}{2\,\sigma_y^2+q})}{\sqrt{(2\sigma_x^2+q)(2\sigma_y^2+q)}}\,dq \tag{2.64}$$

where n is the line density of particles in the beam, e is the elementary charge and ϵ_0 the permittivity of free space. We calculate then $\vec{E} = -\vec{\nabla}(U)$ If we concentrate only on round beams ($\sigma_x = \sigma_y = \sigma$), we can express the radial force:

$$F_r(r) = -\frac{ne^2(1+\beta_L^2)}{2\pi\epsilon_0}\,\frac{1}{r}\,\left[1 - \exp\left(\frac{r^2}{2\sigma^2}\right)\right] \tag{2.65}$$

2.6.2 Beam – beam parameter

The beam is receiving a kick from the opposite beam that can be calculated. From the expression of the two dimensional force for gaussian beams multiplied by its longitudinal distribution, assuming r constant, and neglecting the location of the kick, the radial kick $\Delta r'$ coming from the integration of this force is expressed by:

$$\Delta r' = -\frac{2Nr_0}{\gamma}\,\frac{1}{r}\,\left[1 - \exp\left(-\frac{r^2}{2\sigma^2}\right)\right] \tag{2.66}$$

where N is now the total number of particles and considering r_0 as the classical proton radius defined by:

$$r_0 \;=\; \frac{e^2}{4\,\pi\,\epsilon_0\,m\,c^2}$$

At small amplitudes $r << \sigma$, the radial kick can be expressed as:

$$\Delta r'|_{r\to 0} = -\frac{Nr_0 r}{\gamma\sigma^2} \tag{2.67}$$

From this we can express the linear beam – beam parameter:

$$\xi = \frac{N\,r_0\,\beta^*}{4\,\pi\,\gamma\,\sigma^2} \tag{2.68}$$

The linear beam – beam parameter represents the tune shift due to the beam – beam force at small amplitudes. This parameter is equal to the linear tune shift ΔQ for small values.

2.7 Perturbations of the motion

In a real accelerator, imperfections appear like magnetic field errors or misalignments. For the accuracy of the beam behaviour, these errors have to be taken into account.

2.7.1 Chromaticity

Focusing errors provided by a particle reaching a quadrupole with a momentum offset is called chromatic aberration. This leads to a tune shift with energy. The chromaticity is defined as:

$$\xi \;=\; \frac{\Delta Q_u}{\Delta p/p} \tag{2.69}$$

ξ is always created if the beam focussed, it's determined by the focusing strengths $K(s)$ of all quadrupoles. The general formulae for the chromaticity is:

$$\xi \;=\; -\frac{1}{4\,\pi}\oint K(s)\beta(s)ds \tag{2.70}$$

The chromaticity can be corrected with sextupoles magnets. A better description can be found in [25].

2.7.2 Coupling

Coupling in transverse plane between x and y is often induced by errors on the rotation of quadrupoles or by solenoids. The new quadrupole matrix after rotation can be find with:

$$R_{final} \;=\; S_\theta \,.\, R_{element} \,.\, S_\theta^{-1} \tag{2.71}$$

Using the rotation matrix S given by:

$$S_\theta \;=\; \begin{pmatrix} \cos\theta & -\sin\theta \\ \sin\theta & \cos\theta \end{pmatrix} \tag{2.72}$$

For instance, a skew quadrupole (a quadrupole rotated by 45°) induces a coupling between the two planes. The transfer matrix R_{SQ} of a skew quadrupole with thin lens approximation can be found with the rotation matrix for 45° angle:

$$M_{\pi/4} = \begin{pmatrix} \cos(\pi/4).I_2 & \sin(\pi/4).I_2 \\ -\sin(\pi/4).I_2 & \cos(\pi/4).I_2 \end{pmatrix} \tag{2.73}$$

And the well known quadrupole transfer matrix called here R_Q in thin lens approximation. With both matrix, we can write:

$$R_{SQ} = M_{\pi/4} \,.\, R_Q \,.\, M_{-\pi/4}. \tag{2.74}$$

This gives:

$$R_{SQ} = \begin{pmatrix} I_2 & K_2/f \\ K_2/f & I_2 \end{pmatrix} \tag{2.75}$$

with $K_2 = \begin{pmatrix} 0 & 0 \\ 1 & 0 \end{pmatrix}$ and I_2 is the identity matrix. More details and a complete demonstration concerning coupling can be found in [29]. To summarize the results, we can say that inserting the skew quadrupole matrix R_{SQ} in a beam line and after the calculation

of the σ matrix, the geometrical emittances values with coupling in the transverse plane can be found using:

$$\begin{cases} \epsilon_x^2 = \det(\sigma_{xx}) = \epsilon_1 \left(\epsilon_1 + \dfrac{\beta_x \beta_y}{f^2}\,\epsilon_2\right) \\ \epsilon_y^2 = \det(\sigma_{yy}) = \epsilon_2 \left(\epsilon_2 + \dfrac{\beta_x \beta_y}{f^2}\,\epsilon_1\right) \end{cases} \tag{2.76}$$

$\epsilon_{1,2}$ being intrinsic emittances and constants coming from the diagonalisation of the σ matrix. Correction of coupling can then be done using skew quadrupole corrector magnets. The LHC will have several skew quadrupoles around the ring for this purpose.

Conclusion

An overview of the main optics parameters concerning transverse beam dynamics have been given here. The most important and critical parameter for ALFA, as it will be seen in the following, will be the transfer matrix with twiss parameters. But before going into the detailed ALFA optics design, we need to describe the ALFA context and the way the luminosity and total elastic cross section can be measured.

Chapter 3

Luminosity measurement in ATLAS

Contents

The luminosity is one of the most important parameter of a collider. Indeed, the luminosity is linked to the cross section by:

$$\dot{N} = \mathcal{L}\,\sigma \tag{3.1}$$

where σ is the cross section, $\mathcal{L}$ the luminosity and $\dot{N}$ the event rate. $\mathcal{L}$ is expressed in unit of $\mathrm{cm}^{-2}\,\mathrm{s}^{-1}$ or $\mathrm{barn}^{-1}\,\mathrm{s}^{-1}$. From (3.1), measuring and calibrating the luminosity is directly related to the cross section determination. An absolute luminosity measurement is then necessary if we want to measure absolute cross section. The precision on these parameters is of importance to explore physics above the standard model. The errors on the luminosity will propagate to the cross section error.

Measurement of the absolute luminosity in collider experiments is not easy. The relative luminosity is often enough, for instance to control the luminosity evolution with time and correct for the pile – up.
This chapter is dedicated to luminosity and total cross section measurement for ATLAS. Firstly, the detectors used for relative luminosity measurements are described and then the method for an absolute luminosity measurement is detailed leading to the measurement method that is used for ALFA (**A**bsolute **L**uminosity **F**or **A**TLAS) with the need for a new optics for LHC. We will see that the total cross section comes from the same measurement.

3.1 Relative luminosity in ATLAS

Different devices in the forward region are used to measure relative luminosity in ATLAS: The BCMs, the MBTS, the ZDC and the LUCID (the dedicated one).

3.1.1 Beam Condition Monitors

The **B**eam **C**ondition **M**onitor (BCM) [30] includes four stations on both sides of the pixel detector around the beam pipe at the longitudinal position of $z = \pm 184$ cm from the Interaction Point and at a radius $r = 5.5$ cm. It has been built to monitor beam losses and provide fast signals that will abort the beam safely if the loss rates become too high for ATLAS safety. Each station has four diamond sensors like the one shown on Fig. 3.1.

3.1.2 MBTS

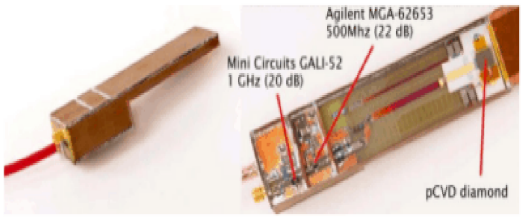

Figure 3.1: Diamond sensor for BCM [31].

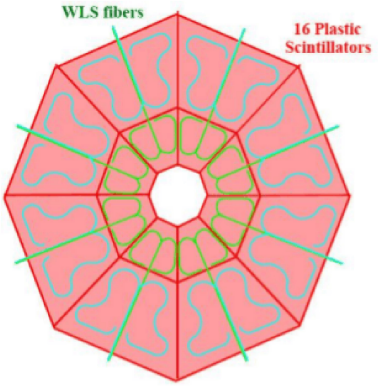

Figure 3.2: Disk of the MBTS with 16 scintillator tiles. Figure from [32].

The relative luminosity with the MBTS (**M**inimum **B**ias **T**rigger **S**cintillator) is measured by counting the number of minimum bias events. The two detectors of the MBTS are installed on the inner face of the end-cap calorimeter cryostat. They are located at ± 3.6 m

from the ATLAS Interaction Point. MBTS is not expected to run at a luminosity higher than 10^{33} $cm^{-2}\,s^{-1}$ as scintillators are sensitive to radiations. So it will be effective only for the first running period and shall not be used when the LHC restarts in 2015. The disk of the MBTS are shown on Fig. 3.2.

3.1.3 ZDC

The primary purpose of the ATLAS **Z**ero **D**egree **C**alorimeter (ZDC) [33] is to detect forward neutrons and photons in both proton – proton and heavy – ion collisions. Recent studies have shown that the relative luminosity achievable on ZDC is close to $10^{33}cm^{-2}\,s^{-1}$ [34].

The ZDC is located at 140 m from the Interaction Point. ZDC modules are included in the **T**arget **A**bsorbers for **N**eutrals (TAN) as shown on Fig. 3.3. Each ZDC detector has one electromagnetic module and 3 hadronic modules. It is a sampling calorimeter using tungsten as absorber.

3.1.4 LUCID

The method used by LUCID (**L**uminosity monitor **U**sing **C**erenkov **I**ntegrating **D**etectors) [35] to determine the luminosity is to use inelastic events on a bunch – to – bunch basis. The number of charged particles is proportional to the number of inelastic events and though to the luminosity. In case it's capable of counting all the particles, the measurement is linear. To be used as an absolute luminometer, LUCID has to be calibrated.

LUCID shown on Fig. 3.4 is dedicated for relative luminosity measurement. It consists on 200 Aluminum tubes filled with C_4F_{10} gas at 17 m from the Interaction Point and surrounds the beam pipe. The tubes are pointing to the proton – proton interaction region. This system allows Cerenkov light emission when a charged high energy particle crosses the gas. The light is reflected in the tube. The Cerenkov angle is about 3° with an average of 3 reflections inside the tube. The light is collected at the end of the tubes to reach the PhotoMultipliers (PMTs).

LUCID has a limited background due to the high Cerenkov threshold of 10 MeV for electrons and 2.8 GeV for pions. Furthermore, the fast response (few ns) allows for single bunch crossing detection.

3.2 Absolute luminosity measurement and total cross section introduction

An non exhaustive list of methods to measure absolute luminosity is given, summarizing the ones used by ATLAS.

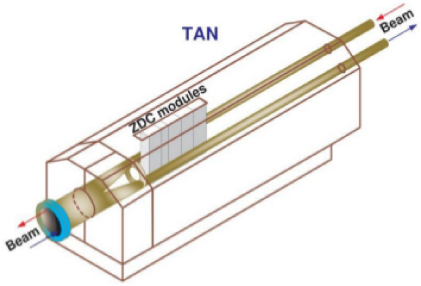

Figure 3.3: View of the TAN showing the Zero Degree Calorimeter ZDC. The interaction point is located on the left.

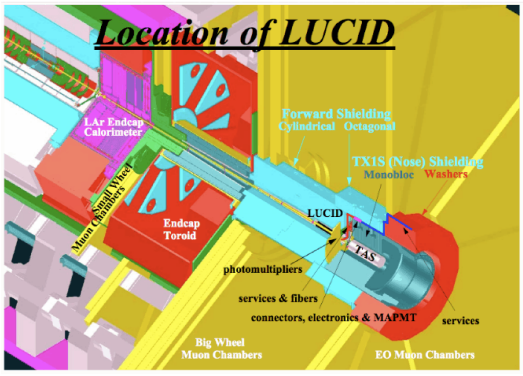

Figure 3.4: LUCID location in ATLAS forward region.

3.2.1 Luminosity from accelerator parameters

Description

The absolute luminosity can be measured directly from beam parameters [36]. Two gaussian beams which collide without offset, without crossing angle and without hourglass effect has a luminosity given by (3.2).

$$\mathcal{L} = \frac{N_b\, f\, N_1\, N_2}{4\,\pi\,\sigma_x^*\,\sigma_y^*} \tag{3.2}$$

where N_1 and N_2 are the number of particles that collide for each beam, N_b is the number of bunches, f the revolution frequency and $\sigma_{x,y}$ the transverse RMS beam size. Here, N_1, N_2, σ_x^* and σ_y^* are assumed to be the same for all bunches.

The simplest luminosity formulae assuming gaussian beams with different sizes and no other effects is:

$$\mathcal{L} = \frac{N_b\, f\, N_1\, N_2}{2\,\pi\,\sqrt{(\sigma_{1x}^*)^2+(\sigma_{2x}^*)^2}\,\sqrt{(\sigma_{1y}^*)^2+(\sigma_{2y}^*)^2}} \tag{3.3}$$

If now we add an horizontal crossing angle, it becomes:

$$\mathcal{L} = \frac{N_b\, f\, N_1\, N_2}{4\,\pi\,\sigma_x^*\,\sigma_y^*}\,F \qquad \text{where} \qquad F \approx \frac{1}{\sqrt{1+(\frac{\sigma_s}{\sigma_x^*}\frac{\phi}{2})^2}} \tag{3.4}$$

F being the reduction factor coming from the fact that the beams collide with an angle ϕ, assuming that σ_x and σ_y are much smaller than the bunch length σ_s. Other effects can also affect the luminosity like presence of an offset, linear coupling and hour glass effect. Also the formulae is modified assuming the beams are not gaussian. The beam sizes σ_x and σ_y at the Interaction Point are estimated via the Van der Meer scans.

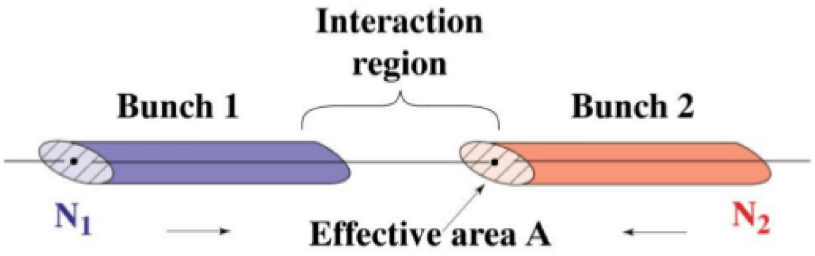

Figure 3.5: Luminosity for two colliding beams with the effective area represented.

Van der Meer scan

This method was first introduced by S. Van der Meer at CERN Intersection Storage Ring ISR [37]. This topic is well explained and developped in more details for LHC in [38]. A Van der Meer scan provides, by moving one beam through the other, the measured counting rates versus transverse displacements and gives the effective beam sizes in the two transverse planes.

The effective transverse area A_{eff}, in which the collisions take place, can be expressed as in (3.5) and is illustrated in Fig. 3.5 with N_1 and N_2 the number of particles per bunch measured continously with beam current transformer and f the revolution frequency well estimated in a collider.

$$\mathcal{L} = \frac{N_1 N_2 f}{A_{eff}} \tag{3.5}$$

The effective beam size σ_{ueff} is defined by:

$$\sigma^*_{ueff} = \sqrt{(\sigma^*_{1,u})^2 + (\sigma^*_{2,u})^2} \tag{3.6}$$

Taking into account the luminosity formulae for gaussian beams (3.3), it can be reformulated as:

$$\mathcal{L} = \frac{N_1 N_2 f N_b}{2\pi \sigma^*_{xeff} \sigma^*_{yeff}} \text{ and } A_{eff} = 2\pi \sigma^*_{xeff} \sigma^*_{yeff} \tag{3.7}$$

In LHC, due to machine protection, the scan is performed step by step within a range of $\pm 2\sigma_u$ by moving the two beams at the same time in opposite directions [39]. Indeed, the displacement is generated by a bump in the closed orbit which also generates a change of orbit at the tertiary collimators located in the triplets. This displacement has to stay in a limited range due to the collimators apertures.

All this leads to the fact that from accelerator parameters, the luminosity would have an accuracy estimated not better than 5 – 10 % [38]. To reach lower values, another method is required. ATLAS decided to use elastic scattering at very small angle [5].

Figure 3.6: Elastic scattering principle characterized by the angle θ.

3.2.2 Elastic scattering at very small angles

Elastic scattering

As illustrated in Fig. 3.6, for elastic scattering, two incoming protons with initial momentum p ($p1 = p2 = p$) exchange a momentum t that can be written, for very small scattering angles:

$$t = (p1 - p3)^2 = (p2 - p4)^2 = -2\,p^2(1 - \cos(\theta)) \approx -p^2\,\theta^2 \tag{3.8}$$

Optical theorem

The principle of this method is the use of the optical theorem [40]. The elastic and inelastic scattering rates $\dot{N}_{el}$ and $\dot{N}_{inel}$ are related to the luminosity $\mathcal{L}$ and total cross section σ_{tot} by:

$$\sigma_{tot}\,\mathcal{L} = \dot{N}_{el} + \dot{N}_{inel} \tag{3.9}$$

The optical theorem states that the total cross section is related to the elastic cross section for small values of momentum transfer t. Following [5], the luminosity can be calculated from experimental rates with:

$$\mathcal{L} = \frac{1+\rho^2}{16\,\pi}\,\frac{(\dot{N}_{inel} + \dot{N}_{el})^2}{(d\dot{N}_{el}/dt)_{t=0}} \tag{3.10}$$

where ρ is the ratio of the real to the imaginary part of the elastic scattering amplitude [5]. Its value is of interest to distinguish between forward physics models.

This method requires a good detector coverage to get a precise measurement on the inelastic rate for $t \approx 0$ or $\theta \to 0$. This is also the method used by TOTEM [41]. However, this method can not be used for ATLAS due to the lack of precise forward coverage. Instead, the measurement will be done using Roman Pots detectors described in § 3.3.2. This method is not easy to implement as it needs special runs with dedicated optics, the subject of this PhD.

Coulombian diffusion

At very small diffusion angle θ, the cross section becomes sensitive to the Coulomb interaction, which can be exactly calculated. The final expression for the differential elastic

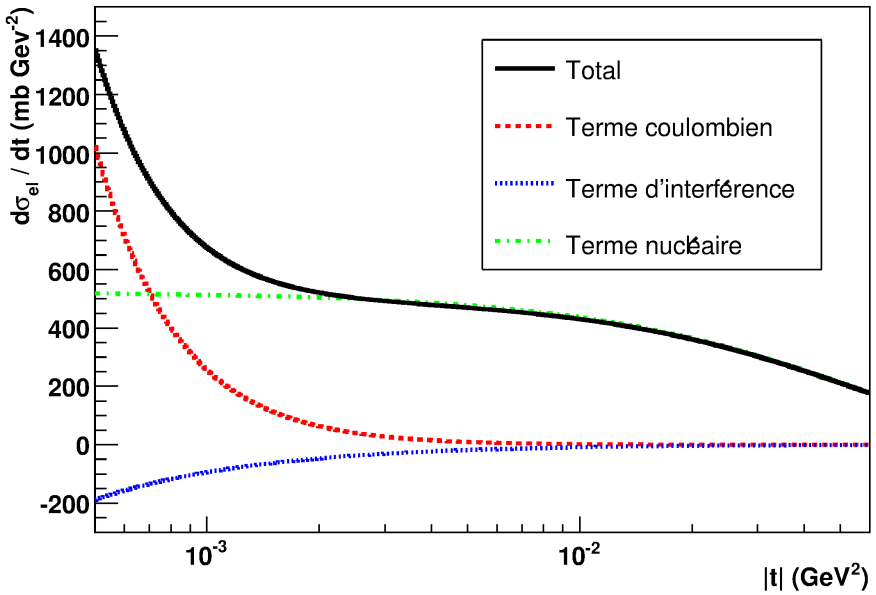

Figure 3.7: Differential elastic cross section at 7 TeV with $\sigma_{tot} = 100\,\text{mb}$, $\rho = 0.13$ and $b = 18\ \text{GeV}^2$.

cross section may be expressed following [42]:

$$\frac{d\sigma_{el}}{dt}(t) = \frac{4\,\pi\,\alpha^2\,G^4(t)}{|t|^2} - \frac{\sigma_{tot}\,\alpha\,(\rho - \alpha\,\phi)\,G^2(t)\,\exp(-b\,|t|/2)}{|t|} + \frac{(1+\rho^2)\,\sigma_{tot}^2\,\exp(-b|t|)}{16\,\pi} \tag{3.11}$$

where α, G, ϕ and b are forward physics parameters. This expression has three terms that lead to three different regions that can be seen on Fig. 3.7:

- A pure electromagnetic term dominant for $|t| < 10^{-3}\ \text{GeV}^2$ ("Coulomb regime").
- A pure nuclear term dominated for $|t| > 10^{-2}\ \text{GeV}^2$.
- An interference term sensitive to both coulomb and nuclear term for $10^{-3} < |t| < 10^{-2}\ \text{GeV}^2$.

The differential elastic cross section is linked to the luminosity by:

$$\frac{d\dot{N}_{el}}{dt}(t) = \mathcal{L}\,\frac{d\sigma_{el}}{dt}(t) \tag{3.12}$$

where $d\dot{N}_{el}/dt$ is the elastic scattering rate. The whole idea is to be as much as possible in the Coulomb regime ($t \to 0$) to be able to measure $\mathcal{L}$ with the highest precision by measuring $\dot{N}_{el}$. However, a measurement in the interference region will allow to access at the same time $\mathcal{L}$ and σ_{tot}, with lower precision.

The measurement and detection of the elastic scattered protons will allow to reconstruct the differential elastic cross section spectrum as a function of the scattering angle θ. By

fitting the reconstructed spectrum as a function of t, we determine the absolute luminosity, the total cross section and the other forward physics parameters [5].

Quantitatively, this means being sensitive enough to reach the Coulomb interference region where $|t| < 10^{-3}$ GeV^2. The typical diffusion angle for LHC at 7 TeV is 3.5 μrad which comes from a t – value of 6.5 $\times$ 10^{-4} GeV^2. It can be noted that this type of measurement was performed in 1984 [6] at $Sp\bar{p}S$, but with a typical diffusion angle of 120 μrad.

As shown in [42], we cannot intercept elastic scattered protons with such small angles before the inner focusing triplet located at 23 m from the IP. To solve this problem, the leading idea is to intercept the elastic scattered protons further than the inner triplets by modifying the optics and use appropriate detectors.

3.3 ALFA description for absolute luminosity and total elastic cross section measurement

3.3.1 Modified optics

A complete description of the nominal optics is given in chapter 4, but we introduce here the main parameters taken into account to build this nominal optics. The optics choice for ALFA is a parallel to point focusing optics set in the vertical plane providing a 90° phase advance between the Interaction Point and the detectors with $\alpha^* = 0$ at the Interaction Point. If now we take the transfer matrix (2.59) with twiss parameters as described in chapter 2, the particle position u_{det} at the detector in the LHC beam line is linked to the position at IP1 by:

$$\begin{aligned} u_{det} &= \sqrt{\frac{\beta_{det}}{\beta^*}}(\cos(\Delta(\mu)) + \alpha^* \sin(\Delta\mu))\, u^* + \sqrt{\beta_{det}\,\beta^*} sin(\Delta\mu)\, u'^* \\ &= \sqrt{\beta_{det}\,\beta^*}\, u'^* \end{aligned} \tag{3.13}$$

u corresponding to the transverse coordinates x or y. Taking into account the vertical transverse coordinates and using (3.13), we easily find the link between the vertical position at the detector and the vertical angle at the IP:

$$y_{det} = \sqrt{\beta_{det}\,\beta^*}\,\theta_y^* \tag{3.14}$$

The t – value can be re – calculated as:

$$-t_{min} = (p\,\theta_y^*)^2 = \frac{p^2\, y_{det}^2}{\beta_{det}\,\beta^*} \tag{3.15}$$

Using the beam size σ, the position at the detector can also be written as:

$$y_{det} = n\,\sigma_{det} = n\sqrt{\epsilon\,\beta_{det}} \tag{3.16}$$

where n represents the smallest possible distance to the beam center. In the following, the distance of approach will always be given by n ie in number of beam size σ. The resulting t – value is:

$$-t_{min} \;=\; p^2\, n^2 \frac{\epsilon}{\beta^*} \tag{3.17}$$

β^* can then be determined. With a normalized emittance of 1 μm.rad and $n = 15$, one obtains:

$$\beta^* \;=\; p^2\, n^2 \frac{\epsilon}{-t_{min}} \;=\; 2273 \text{ m} \tag{3.18}$$

This very high value has to be compared with the one used routinely in LHC ($\beta^* < 11$ m). The lower n is, the lower is β^*. Following (3.15), t_{min} is proportional to $1/\beta_{det}\,\beta^*$ and β_{det} should not be too low. The minimum n is fixed at about 1.5 mm due to the detectors possible approach. With $\beta^* = 2300$ m, β_{det} must be larger than 70 m to reach $-t_{min} = 6.5 \times 10^{-4}$ GeV^2.

Another requirement to reach such small angles is to minimize the angular divergence $\sigma^{*\prime}$ at the IP. The angular divergence has to be much smaller than the minimum scattering angle we want to measure. Looking at (2.49), we understand that this is also why a small emittance is needed. The initial requirements for the optics required by ALFA can be summarized by:

- A vertical phase advance at the Roman Pots equals to 90°.
- $\beta^* \geq 2300$ m.
- $\alpha^* = 0.0$.
- $\epsilon_N \leq 1$ μm.rad.
- $\beta_{RP} \geq 70$ m.

First high β^* optics for the LHC have been studied in [43] to [47]. The optics has been modified by then with a $\beta^* = 2625$ m in [48].

One crucial input to achieve the measurement is the overall experimental acceptance, i.e. the proportion of particles entering the active area of the detector compared to the generated ones. This experimental acceptance is computed as a function of t. It cannot be known or deduced from the experiment, it has to be done using the tracking of the protons from the IP to the detectors. The ultimate goal of the ALFA experiment was to reach 2 – 3 % accuracy on the absolute luminosity but also mainly to perform the measurement of the total cross section from proton – proton scattering.

3.3.2 ALFA detectors

For the purpose of measuring the trajectories of elastic scattered protons using the previous method, **R**oman **P**ots (RPs) have been installed on each side around IP1 at 240 m in between the DQR (Dump Resistor Boxes). A more detailed description of the beam line will be given in chapter 4. Concerning the Roman Pots, a description of their position on

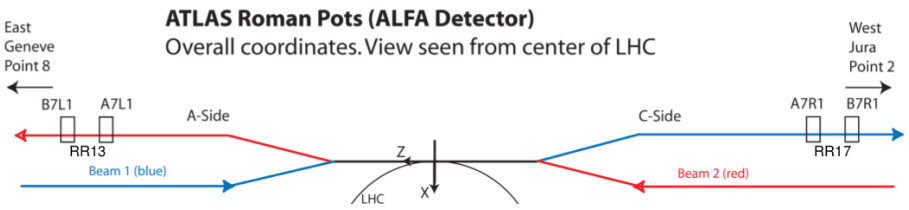

Figure 3.8: Roman Pots position and labelling on the LHC [49].

the LHC is given in Fig. 3.8.

The labelling for the ALFA Roman Pots are XRPV.A7R1.B1 and XRPV.B7R1.B1 on beam 1 in LHC sequence notation and on beam 2, XRPV.A7L1.B2 and XRPV.B7L1.B2. In the following, to simplify the notation for Roman Pots, we'll used, as shown on Fig. 3.8, the shortest notation A7R1, B7R1 for RPs on beam 1 and A7L1, B7L1 for RPs on beam 2.

The RPs are the technology chosen and used because they allow to approach the detectors as close as possible to the beam as shown on Fig. 3.9 and catch the elastic scattered protons with small angles. The name "roman" comes from the fact that the first group using these pots was the CERN Rome group in the 70s to study physics at CERN Intersection Storage Ring (ISR).

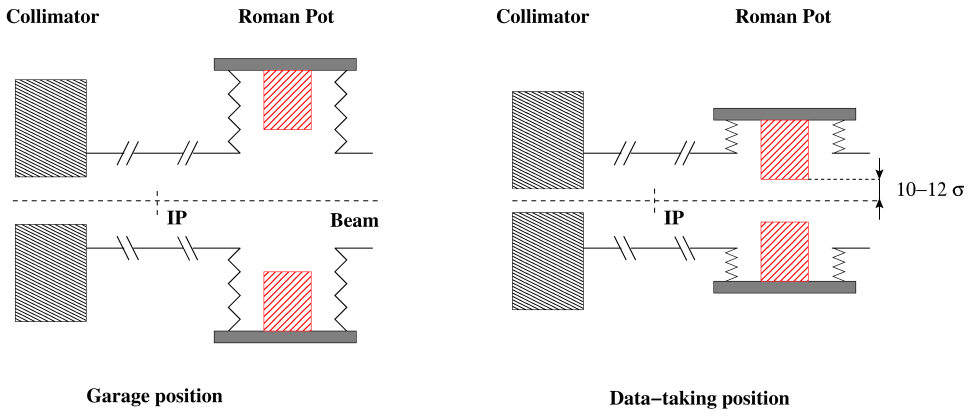

Figure 3.9: Mechanical Roman Pots technique within a gap of the order of 2 – 3 mm.

Two RPs stations are installed on beam 1 and two others on beam 2. They have 4 m distance between them on each side. In total, ALFA has eight Roman Pots.

Roman Pot Mechanics

The RPs technique has been used for other previous experiment like UA4/2 at CERN [50, 51] to measure the real elastic scattering amplitude for proton – antiproton. This is also the one used by the TOTEM experiment.

With the mechanical system of the ALFA Roman Pots, the detectors can be approached vertically to the beam, from below and above, within a millimetre range to intercept the scattered protons. Small gaps of the order of 3 mm can be reached. They can be approached close to the beam axis during a run and retracted when they're not used. Furthermore, the mechanical system has been made to allow the RPs to retract in case of the power cut for instance. To maximize the maximum available distance n, the bottom window is specially thin. The thickness value is about 200 – 250 μm. The mechanical system consists on bellows where the RPs are installed to allow them to move. The upper and lower RPs can be adjusted independently when approaching the beam due to high precision roller screw linked to a step by step motor. Then, to compensate the force coming from the LHC beam pipe primary vacuum of about 2.7 kN, compensation bellows are added directly connected to the vacuum, a little larger than the bellows around the RPs.

Electronics and Detectors

Each station house an upper and a lower detector build up with scintillating fibers representing the active part of the detector also called the **M**ain **D**etectors (MDs) used for tracking particles. This active part located inside the Roman Pots is in the vacuum. For alignment, **O**verlap **D**etectors (ODs) have been added.

The scintillating fibers have been chosen to answer to the different requirements of importance in ALFA. These requirements are:

- the possibility to approach the detectors close to the beam.
- negligible inactive edge zone.
- be radiative resistant.
- reach a spatial resolution of 30 μm.
- be as insensitive as possible to the electromagnetic background.

Main Detectors

Each Main Detector is made with a 20×64 scintillating fibers tracker. Each plane has two perpendicular layers. Most fibers have a 45° cut at the end whereas the others have a 90°. The fibers end cut at 90° are coated with an Al film in order to make a mirror which improves the light yield.

Then the scintillating fibers are readout by a 64 channels **M**ulti **A**node **P**hoto **M**ultiplier **T**ube (MAPMT) outside the Roman Pots which convert the light from the fibers into an electrical signal. The compact front end electronics **P**hoto**M**ultiplier **F**ront–end electronics (PMFs) is mounted on top of the MAPMT as seen on Fig. 3.10 for the charge readout. Each station has one fan to cool the PMFs. Nevertheless, during 90 m β^* optics LHC runs, the temperature has increased due to RF losses. It has increased enough to study it for higher β^* optics and future runs. Decision has been taken to add a cooling system on the RPs for future runs during the LHC Long Shutdown (LS1) in 2013.

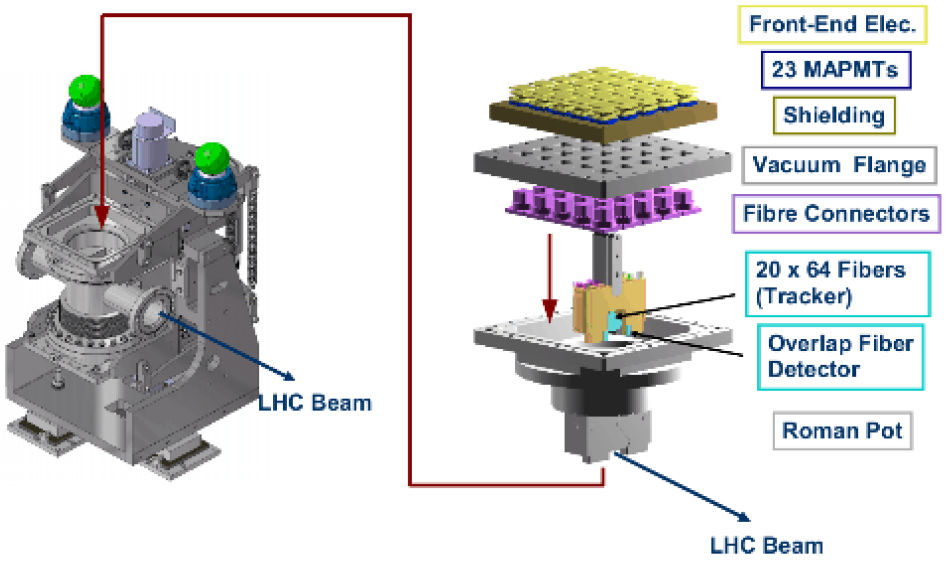

Figure 3.10: Roman pots layout showing the electronic scheme and how it's inserted in the Roman Pot.

Overlap Detectors (ODs)

The ODs give the relative position of the detectors. The layout is shown on Fig 3.11. This detectors measure only the vertical position of particles halo. They're made of 3×30 fibers similar to the Main Detectors fibers. Added to the ODs, BPMs are installed in between two stations, called BPMSA, to help for the positioning reading. A fine positionnement is then made by couting the rates in upper and lower pot and equalizing them. The estimated relative precision positioning on the vertical distance between two detectors in one station must be about 10 μm.

Conclusion

As it has been shown in this chapter, the absolute luminosity can be determined by different methods. The one chosen for ALFA to measure the absolute luminosity and the total cross section uses proton – proton scattering at very small angles. This method implies a new optics described as the high β^* optics. After the description of the main optics specifications and the RPs detectors necessary for the measurement, the nominal ALFA configuration needs now to be described in more details, more precisely the complete ALFA simulation and the nominal optics taken into account in the simulation at the beginning. This will be done in Chapter 4.

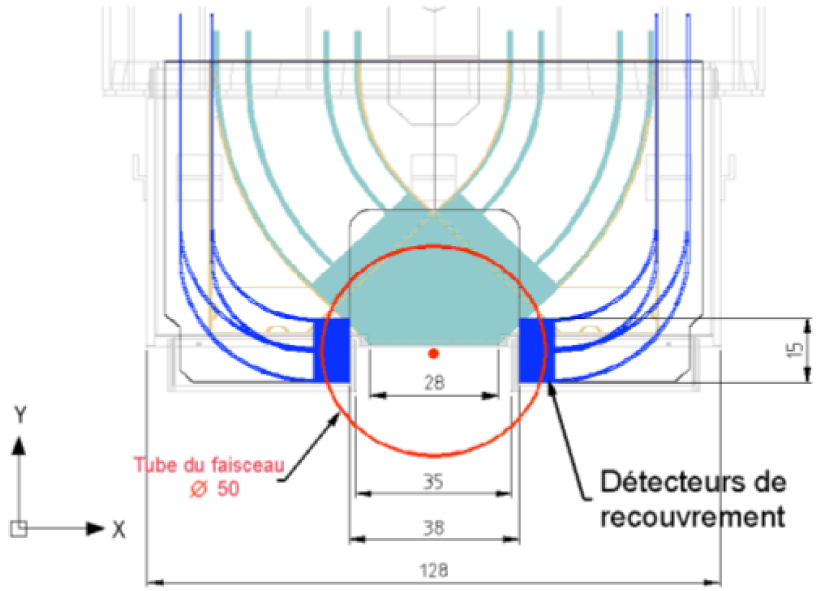

Figure 3.11: Overlap detectors integrated with the rest of the detector.

Chapter 4

Nominal ALFA configuration

Contents

This chapter is a description of the $\beta^* = 2625$ m optics that I used for both the elastic proton generation and the tracking of particles up to the detectors.

The method used for ALFA in order to compute the t – spectrum consists of a complete simulation divided in three main steps:

- Firstly, the Monte – Carlo generator Pythia [52] is used to generate elastic scattering protons including energy dispersion, vertex smearing and angular divergence.
- Once all events have been generated by the Monte – Carlo, we keep the momentum, the position and the angle of the protons after the interaction to reach the second steps of the particle tracking with MAD–X [53] from IP1 to the RPs.
- Then, the knowledge of the position with respect to the beam center together with the geometry of the detectors allow to tag the relevant protons that would be used for the determination of the luminosity and the total cross section. This last step is also used to calculate the experimental acceptance.

We'll now go through a more detailed description of the three different steps.

4.1 Elastic protons generation

As detailed in [42], elastic protons are generated randomly with Pythia 8.1. The simulation takes into account elastic parameters coming from (3.11) namely ρ, σ_{tot} and the nuclear slope b. The size, divergence of the beam, vertex smearing and energy dispersion are also specified and taken into account in the generation. The parameters values used for generation at 7 TeV energy are listed in table 4.1.

Table 4.1: Elastic parameters values used in elastic protons generation for ALFA [5].

Parameters	7 TeV
σ_{tot} (mb)	100
b (GeV^{-2})	18
ρ	0.12
$\frac{\Delta E}{E}$	1.0×10^{-4}
σ_x^*, σ_y^* (μm)	593
$\sigma^{*'}$ (μrad)	0.226

σ_{tot} and ρ values come from the COMPETE collaboration [54]. Fig. 4.1 shows an example of elastic generated protons defined by the previous parameters at 7 TeV in a logarithmic scale. A t lower limit needs to be fixed to cover the entire spectrum. This lower limit has been chosen at $-t_{min} = 4 \times 10^{-5}$ GeV^2.

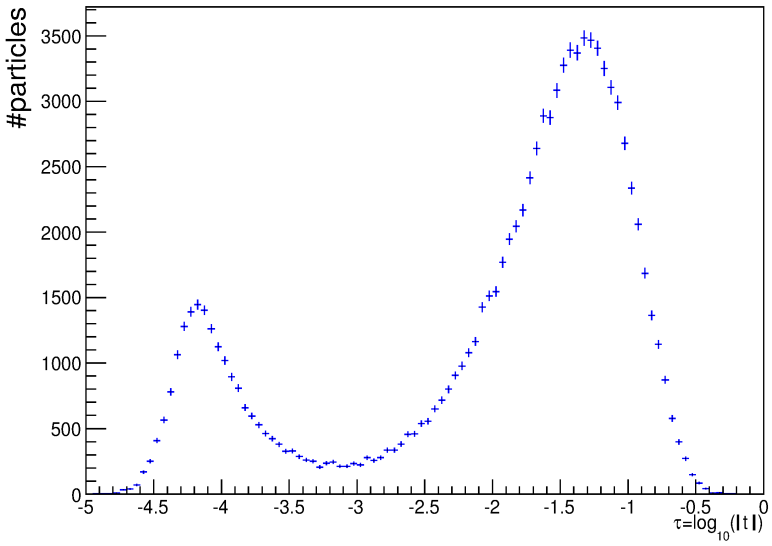

Figure 4.1: Elastic protons generation as a function of t in a logarithmic scale with $\sigma_{tot} = 100$ mb, $b = 18$ GeV^{-2} and $\rho = 0.12$.

This generated spectrum will be kept in order to be used in the t – reconstruction after the complete simulation ie after tracking has been performed. The results of the generation

takes the form of several files containing the useful informations for the tracking coming next, such as the cartesian coordinates of each particle (x, y), their transverse momentums (p_x, p_y) which can give angular informations and the energy error divided by the reference momentum times the velocity of light $\Delta E/(p_0\, c)$.

All output from generation files are compatible with MAD – X coordinates used for the tracking. Before describing the MAD – X tracking used in the complete ALFA simulation, one need to detail the way the optics called the high β^* optics has been established and the complete optics definition.

4.2 High β^* optics

4.2.1 Matching

ALFA won't be able to use the nominal LHC optics at 7 TeV with a β^* of 0.55 m. As described in Chapter 3, special high β^* optics have to be introduced to fulfil the ALFA requirements. Different optics have been studied and the ones that have already been tested will be introduced in the next chapters.

To obtain these new optics, what is called matching needs to be performed. This is implemented by the function *match* in MAD – X. Matching means finding adapted quadrupoles strengths k to respect the constraints imposed by ALFA and all constraints of the LHC as currently installed in oder to build the ALFA modified optics.

LHC constraints

Looking more closely at the LHC constraints, limit constraints in Insertion Region 1 (IR1) have to be respected in order to try to avoid the modification of the rest of the ring. IR1 consists in 13 quadrupoles. Accelerator sequence and elements (longitudinal position and magnetic field of the magnets along the ring) was fixed before ALFA has started to put in place the absolute luminosity and total cross section measurement. This removes a lot of flexibility concerning the magnetic elements located in IR1. Thus, matching becomes more complicated. An example of the ALFA beam line is shown on Fig. 4.2. A list of the

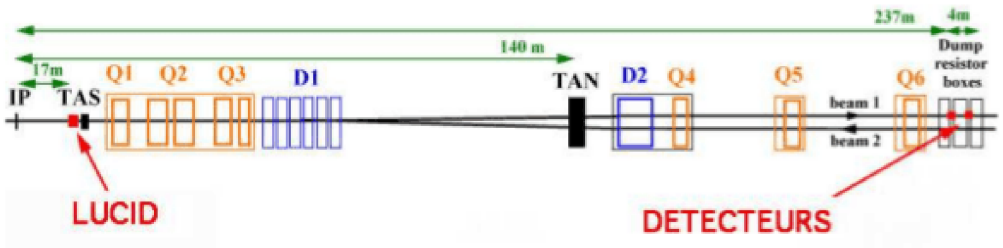

Figure 4.2: Schematic layout of one side of IR1 [1] indicating also LUCID location and the place of the detectors at 240 m.

corresponding quadrupoles MAD – X names and their strengths for beam 1, that have

been used for matching is shown in table 4.2. One can see that the triplets are described by an addition of two strengths instead of only one as for Q4.

Table 4.2: Quadrupoles and gradients using MAD – X names labelled as defined in § 1.1.2.

Quadrupoles	Quadrupoles MAD–X names	k gradient MAD–X names
Q1	MQXA.1R1	kqx.r1 + ktqx1.r1
Q2a	MXQB.A2R1	-kqx.r1 - ktqx2.r1
Q2b	MXQB.A2R1	-kqx.r1 - ktqx2.r1
Q3	MQXA.3R1	kqx.r1
Q4	MQY.4R1.B1	kq4.r1b1
Q5	MQML.5R1.B1	kq5.r1b1
Q6	MQML.6R1.B1	kq6.r1b1
Q7	MQML.7R1.B1	kq7.r1b1
Q8	MQML.8R1.B1	kq8.r1b1
Q9	MQM.9R1.B1	kq9.r1b1
Q10	MQML.10R1.B1	kq10.r1b1
Q11	MQTLI.11R1.B1	kqtl11.r1b1
Q12	MQT.12R1.B1	kqt12.r1b1
Q13	MQT.13R1.B1	kqt13.r1b1

The most useful quadrupoles for ALFA are located between IP1 and RPs. They are the ones from Q1 to Q6. Q1, Q3 (MQXA type) and Q2 (MQXB) are the single aperture triplets quadrupoles used to focus the beam at IP1 and the same strengths are applied for both beams. These triplets are superconducting quadrupoles, 6.6 m long for Q1 and Q3 and 5.7 m long for Q2. The layout is shown on Fig. 4.3. These magnets are completed

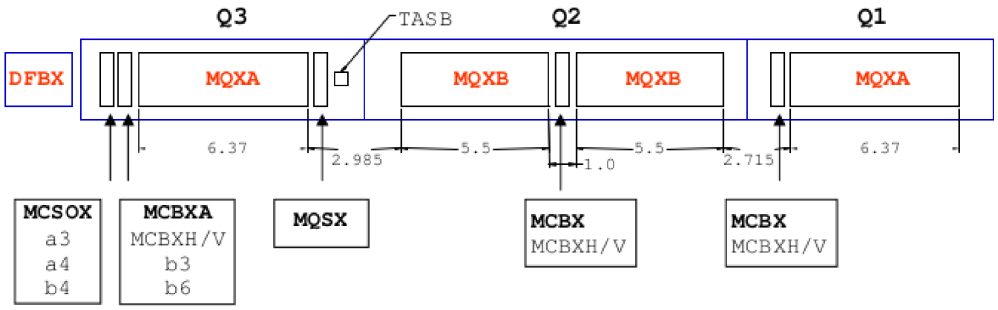

Figure 4.3: Schematic layout of Q1, Q2 and Q3 quadrupoles in the ATLAS triplet [1].

with correctors in between them. Furthermore a skew quadrupole has been added which will allow to correct coupling as it will be seen later.

Q4 to Q6 are common quadrupoles for beam 1 and beam 2 with different strengths for each beam. They provide two different beam pipes where each beam can circulate. They are superconducting quadrupoles. Q4 (MQY) has a 3.4 m length and an enlarged 70 mm

aperture whereas Q5 and Q6 (MQML) are 4.80 m length and 56 m aperture. For instance, Q4 quadrupole is shown on Fig. 4.4. On beam 1, Q4 is defocusing, Q5 focusing and Q6

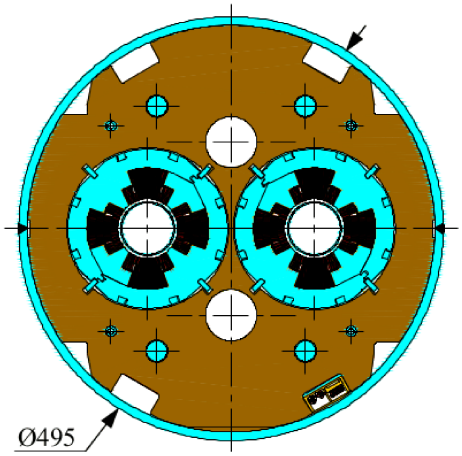

Figure 4.4: Schematic layout of Q4 quadrupole showing the two beam apertures.

again defocusing. Two dipoles, located between the triplets and the quadrupoles Q4, Q5 and Q6, are used for separation and bending.

Beam 1 and beam 2 are matched separately. They have some differences in the beam lines used for ALFA tracking more precisely on the longitudinal position of some correctors. The main quadrupoles from Q1 to Q7 have the same longitudinal positioning. Furthermore, for convenient reason, and also because of the anti – symmetry of the LHC, the matching is done on IP5 first with RPs located at 220 m as for TOTEM and translated only after for IP1 with the 240 m RPs position.

Another constraint to be taken into account in the matching and resulting also in a loss of flexibility, concerns the existence of a quadrupole gradient ratio r between beam 1 and beam 2 for quadrupoles Q4 to Q10. This ratio comes from the way cabling of magnets power supply has been done which gives an upper and a lower limit for r. The allowed range between both beams is $0.5 < r = b1/b2 < 2$. This ratio needs to be checked each time new strengths files are created.

ALFA constraints

The list of constraints coming from ALFA input described in chapter 3, are summarized in the following:

- A phase advance at the Roman Pots equals to 90°.
- Obviously, β^* equals to the needed value of 2625 m for the ultimate optics.
- $D^*_{x,y} = 0.0$.
- $\alpha^*_{x,y} = 0.0$.

Taking into account all these constraints, a solution for a new LHC optics for ALFA has been found and new quadrupoles gradient files specific for high β^* optics have been produced. It will be included in the MAD – X setup used for the ALFA tracking simulation part. A more detailed description of the MAD – X setup and the 2625 m β^* optics, the ultimate optics for ALFA, is given in § 4.2.2.

4.2.2 7 TeV high β^* ALFA optics

A solution for the ALFA ultimate optics with the required optics parameters ie a $\beta^* =$ 2625 m has been firstly designed by [46] and re – designed in [38] to respect the fact that, after LHC revisited its parameters, it occured that some quadrupoles strengths were above the tolerances.

The optics parameters are listed in table 4.3. As seen in Figs. 4.5 and 4.6, the ALFA requirements concerning the β^* – function equals to 2625 m and the phase advance equals to 90° are fulfiled for beam 1 as shown on Fig. 4.7. The phase advance for beam 2 is the same as for beam 1. The ratio of the β for beam 1 and beam 2 can be seen in Fig. 4.8.

Table 4.3: $\beta^* = 2625$ m optics parameters for beam 1, at 7 TeV beam energy and for an emittance of $\epsilon_N = 1\,\mu$m.rad. D is the dispersion and σ' the beam divergence with LHC version V6.503.

IP1		**RPs**	
ϵ_n (μm.rad)	1.0	β_x (m)	95.2 – 97.9
β_x^* (m)	2625	β_y (m)	123.9 – 117.1
β_y^* (m)	2625	σ_x (μm)	113 – 114
α_x^*	0.0	σ_y (μm)	129 – 125
D_y^* (m)	0.0	σ_x' (μrad)	1.19 – 1.17
$D_y^{*\prime}$	0.0	σ_y' (μrad)	1.04 – 1.07
σ^* (mm)	0.593	$\Delta\mu_x$ (2π)	0.534 – 0.541
$\sigma^{*'}$ (μrad)	0.226	$\Delta\mu_y$ (2π)	0.247 – 0.252

But due to the limited flexibility on the magnets, the 2625 m β^* optics found has the Q4 quadrupole polarity inverted. This means that a manual intervention of the power convertor is needed during an access ie with no beam. Then, it will be kept for a whole operation cycle. As a result, the injection scheme will need to be changed and this will also required special optics and runs which will mean more avalaible time for experiments like ALFA and TOTEM. Solutions for injection have also been studied [38].

Another requirement is to keep head – on collisions and avoid crossing angles. This is why bunches are limited to a maximum small number of 156 bunches per beam instead of the 2808 bunches planned for LHC at 7 TeV. Anyway low intensity bunches are enough for ALFA measurement as detailed in chapter 3.

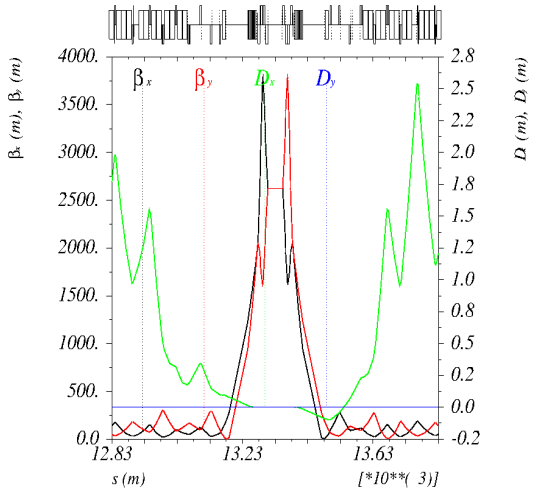

Figure 4.5: β – functions for beam 1 for the 2625 m high β^* optics with IP1 at the center of the figure.

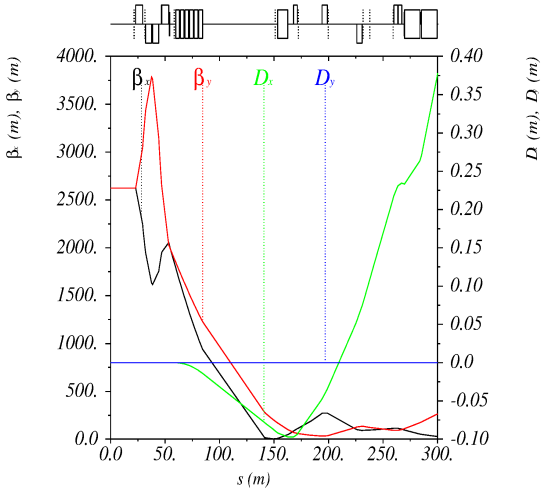

Figure 4.6: Zoom of β – functions for beam 1 for the 2625 m high β^* optics on the right side of IP1 where the RPs are located.

One of the critical point with high β^* optics is to check the apertures (specially at the triplets or the TAS) which also depend on the normalized emittance value that could be achieved. Some calculations were performed and it has been shown that the 2625 m β^* optics does not fulfil the apertures constraints if the nominal normalized emittance $\epsilon_N = 3.75$ μm.rad is used and even for $\epsilon_N = 2.0$ μm.rad, apertures in the triplets are too small as can be seen on Fig. 4.9. Both apertures with two different normalized emittances $\epsilon_N = 1$ μm.rad and $\epsilon_N = 2$ μm.rad, computed with MAD – X, are shown in Fig. 4.9.

Nevertheless, this fit with the fact that ALFA requires a much smaller normalized emittance ϵ_N ie close to 1 μm.rad. This value is not yet achievable but is planned be tested. $n1$ is the parameter for aperture check with MAD – X which with the geometrical aperture also takes into account the alignment tolerances of the magnets. The limit for LHC is fixed at $n1 = 7\,\sigma$. For 1 μm.rad normalized emittance, aperture values for ALFA are above the limitations.

It has already been demonstrated that tune decreases exponentially when β^* increases looking at the tune contribution around IP1 at $\pm\,26$ m [48]. Nominal overall tune values for LHC, that in a ideal situation we would like to keep for high β^* optics, are $Q_x = 64.31$ and $Q_y = 59.32$ during collisions for high luminosity physics runs. But, for the 2625 m β^*, these tune values differ. The new overall tune values are $Q_x = 64.12$ and $Q_y = 58.79$ if ALFA experiment is running alone (without TOTEM) which gives a difference $\Delta Q_x = 0.2$ and $\Delta Q_y = 0.5$. Furthermore, the loss in tune won't be the same by running both experiments TOTEM and ALFA together and in this case, the difference is $\Delta Q_x = 0.36$ and $\Delta Q_y = 0.98$. It will increase the gap.

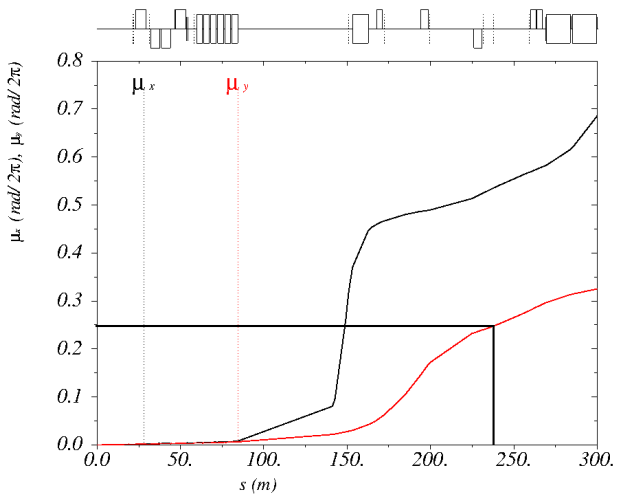

Figure 4.7: Phase advances for beam 1 for the 2625 m high β^* opticswith IP1 at $s = 0.0$ and the 0.25 phase advance at 240 m as indicated by the straight line.

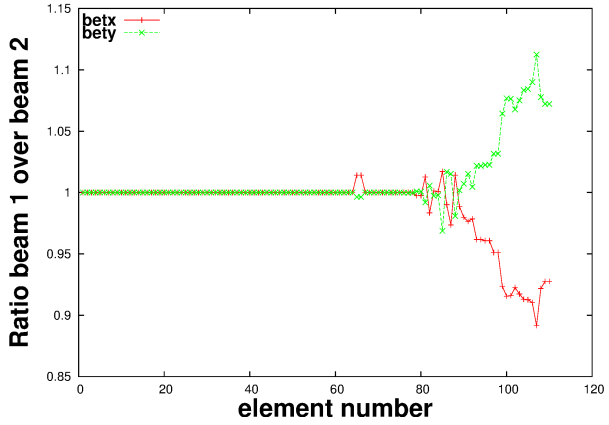

Figure 4.8: Ratio of β for beam 1 and beam 2 from each side of IP1.

This loss in tune will have to be compensated as it was not possible to compensate the tune values in the local matching. To compensate fully, it will be necessary either to use other insertions or to use the main quads in the ring. Optics measurements will be explained and detailed more for experimental 90 m high β^* optics in chapter 6.

The requirements of a 1 μm.rad normalized emittance is smaller than currently achieved at the LHC. Moreover, the inversion of the polarity of the Q4 magnet is not compatible with the present LHC operation. This makes $\beta^* = 2625$ m optics extremely challenging.

The optics parameters required to reach the 2 – 3 % precision with $\beta^* = 2625$ m are defined in the ALFA TDR [5] and are summarized in table 4.4. These values are rather demanding and need special studies.

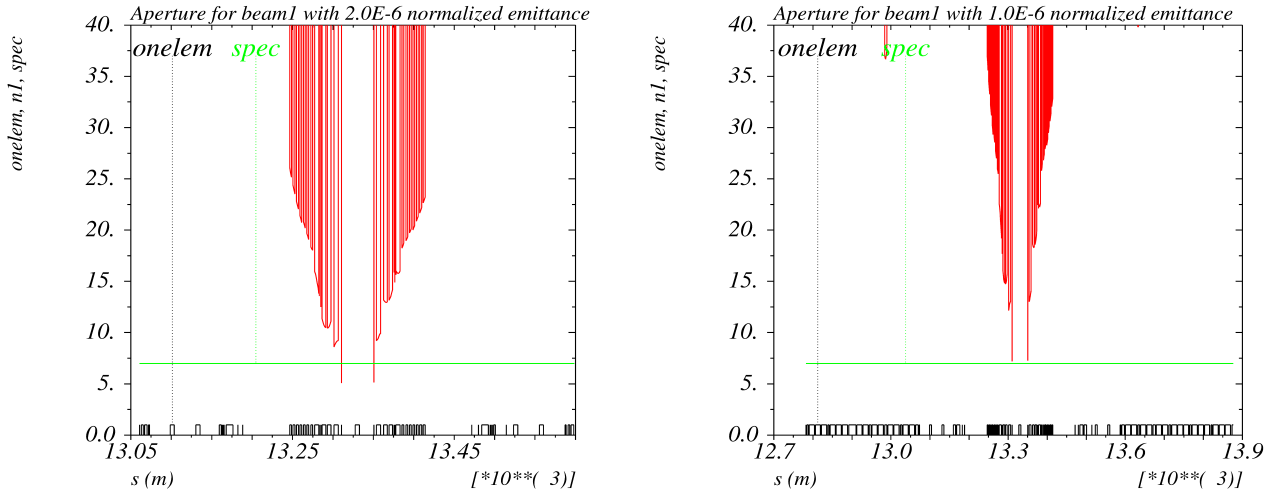

Figure 4.9: Apertures with 2 μm.rad (left) and 1 μm.rad (right) normalized emittance for beam 1 and for $\beta^* = 2625$ m.

Table 4.4: Initial requirements on optics parameters for 2625 m β^* optics [5].

Optics parameters	Precision
β^*	± 1 %
β_{RPs}	± 2 %
μ_{RPs}	$\pm 0.5°$
$\sigma^{*\prime}$	± 10 %
Crossing angle	$\pm 0.2\,\mu$rad

4.2.3 MAD – X tracking setup

The gradient files extracted from matching will then be used in the elastic protons tracking. The tracking will be performed with MAD – X as the software is already extensively used for LHC and contains all the elements sequence needed for ALFA but separatly from the matching.

The first studies I've done were including two different tracking methods integrated in MAD – X that we could call thin tracking and thick tracking. The thin tracking is based on thin lens approximation and the tracking computation is much more faster than with the **P**olymorphic **T**racking **C**ode (PTC) [55, 56] thick tracking module which is a symplectic integrator.

It has been demonstrated that there is a difference on the ALFA t – reconstruction results between both tools and that ptc – track looks more precise for ALFA. We then perform all the trackings with this tool. Tracking starts by using previous generated files. As seen in Fig. 4.2 the beam line around IP1 where the Roman Pots for ALFA are located is made of several magnetic elements. This beam line is part of the LHC ring sequence and

defined with MAD – X element names from table 4.2.

The MAD – X setup has two goals:

- producing twiss files that can be used by the ALFA community for different purposes like tracking with ATHENA [57], the ATLAS software, calculating the lever arm L_{eff}.
- tracking up to 1 million particles from IP1 to the Roman Pots taking into account the generation files.

For both issues, the setup contains LHC beam 1 or 2 sequences, an added file containing Roman Pots names to be added in the LHC sequence, collision strengths file and the file issued from matching solution containing the strength quadrupoles values for high β^* optics. Beam 1 and beam 2 are runned separately.

This MAD – X setup for both beams can be found on ALFA twiki pages to allow the community to perform the complete simulation or have access to the relevant twiss files.

Twiss files production has been done for different optics and takes into account every new parameters that could be added in the setup coming from experimental results for instance. These files are updated. A summary of the main optics parameters from the twiss files is also made with beam size calculations depending on the normalized emittances. This summary is also made for each optics and used for each data taking.

Once twiss files are produced, tracking starts with the coordinates of the particles compatible with MAD – X coordinates conventions coming from the generation. To speed up the tracking, the maximum number of particles is fixed to 20 000 particles by file and is run into a loop. Then to reach 100 000 elastic protons tracked one need 5 input generated files.

The PTC tracking used allows to observe, after tracking, the position of the elastic events at the Roman Pots location and takes into account the element apertures. The output of the tracking files is divided in four main parts, each containing the coordinates of each particle (position and momentum) who passed the tracking at the start, at the Roman Pots and at the end. The tracking results allows us to collect all the particles that have reached the detector, calculate the acceptance and the t – spectrum as it will be described in § 4.3.

4.3 Events collection and acceptance calculation

An important parameter for the measurement is the experimental acceptance which can only be estimated by simulation. Indeed, when elastic protons are collected at the RPs, the way to know the initial t – spectrum goes through the acceptance value.

To describe the acceptance more precisely, one need to look at Fig. 4.10 which shows that most of the protons are scattered with small angles thus passing between the upper

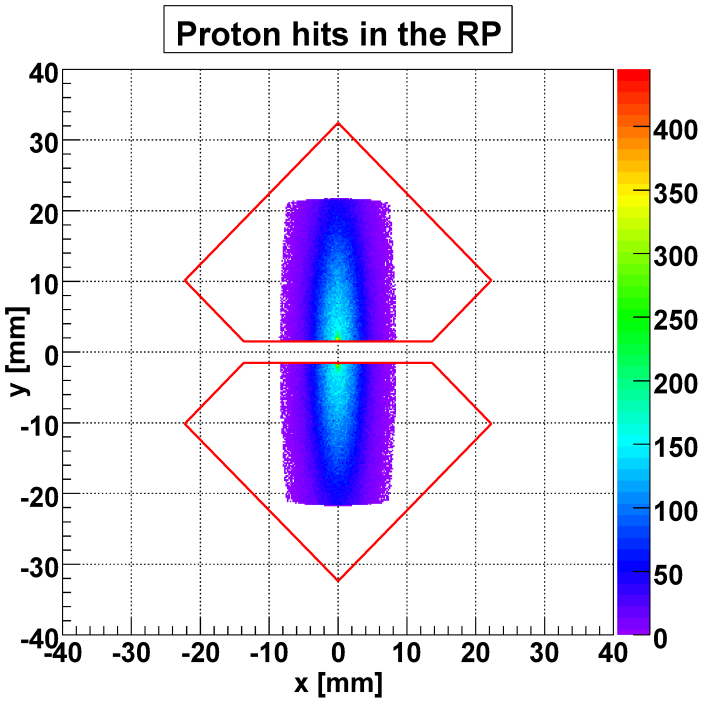

Figure 4.10: Intercepted elastic protons at the first RP on beam 1 with 2625 m β^* optics for 4 mm gap between upper and lower detectors. The diamond shape represents ALFA sensitive area [42].

and lower part of the detectors. One can see that the upper and lower extremities of the scattering pattern are cut. This is due to the physical aperture of the magnetic elements.

Once the reconstruction is done, we have two distinct information:

- The generated spectrum which contains all protons (real information).
- The reconstructed spectrum which contains only protons that have passed the tracking and hit the sensitive area of the detectors (detected information). This spectrum depends upon the distance d we can bring the detector to the beam center. We usually used 1.5 mm which is equivalent to $12\,\sigma$.

The ratio of these two distributions defines the acceptance which can be seen on Fig. 4.11. On this plot we can distinguish two parts: above $\log_{10}(|t|) = -1.2$ where the lowering is mainly due to the losses during the transport, whereas below this value, it can only be attributed to the detector geometry. Thus, to recover the generated spectrum from the reconstructed spectrum we have for each part of the spectrum to weight it using the inverse of the acceptance. An example of the t – reconstructed spectrum is shown in Fig. 4.12.

This illustrates the different steps for the t – spectrum.

- The red one is the $p - p$ elastic scattering generated t – spectrum at the IP.

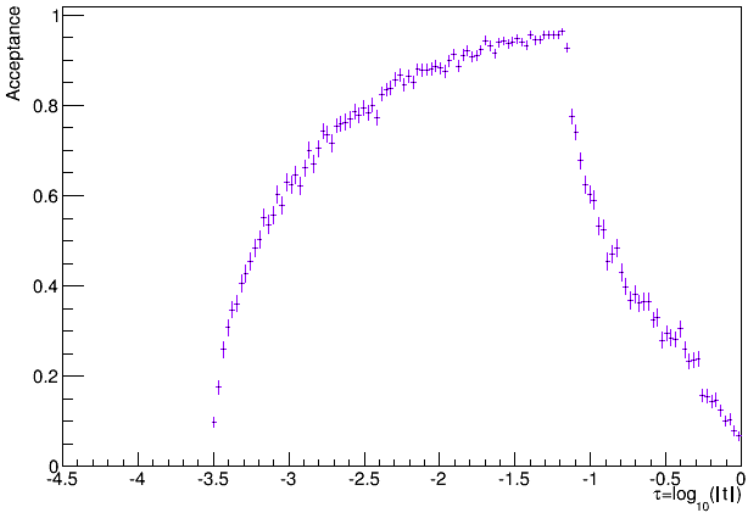

Figure 4.11: Acceptance for 100 000 events with $\beta^* = 2625$ m optics, $\epsilon_N = 1$ μm.rad and detector opening $n = 12$.

- the green reconstructed t – spectrum comes from what has been reconstructed using particle coordinates at the Roman Pots.
- The last one in blue is the corrected t – spectrum which comes from the reconstructed t – spectrum corrected by the acceptance.

Reconstruction method uses the position and the lever arm to determine the t – spectrum. The method can be briefly summarized looking at some equations. This is done for each collected particle at the Roman Pot and for both x and y planes taking opposite Roman Pots for both beams. (4.1) gives the scattering angle at the IP for each particle. The same can be done for $\theta_{x,2}$. (4.2) gives the overall scattering angle and (4.3) use both overall angles x and y in the t – reconstruction.

$$\theta_{x,1} = \frac{1}{2}\left(\frac{x_{a7r1}}{L_{eff,x,a7r1}} - \frac{x_{a7l1}}{L_{eff,x,a7l1}}\right) \text{ with } L_{eff,x} = \sqrt{\beta\,\beta^*}\,\sin\psi \tag{4.1}$$

$$\theta_x^* = \frac{1}{2}\left(\theta_{x,1} + \theta_{x,2}\right) \tag{4.2}$$

$$t = p^2\left(\theta_x^{*2} + \theta_y^{*2}\right) \tag{4.3}$$

Any parameter (magnet currents, beam properties...) that is not known perfectly and given as input for the simulation is a source of error on the acceptance determination thus on the luminosity and total cross section determination. The misalignment of the quadrupoles is one of these for instance.

Even, if all the methods cannot be explained in detail, some other reconstruction methods can also be used. For instance:

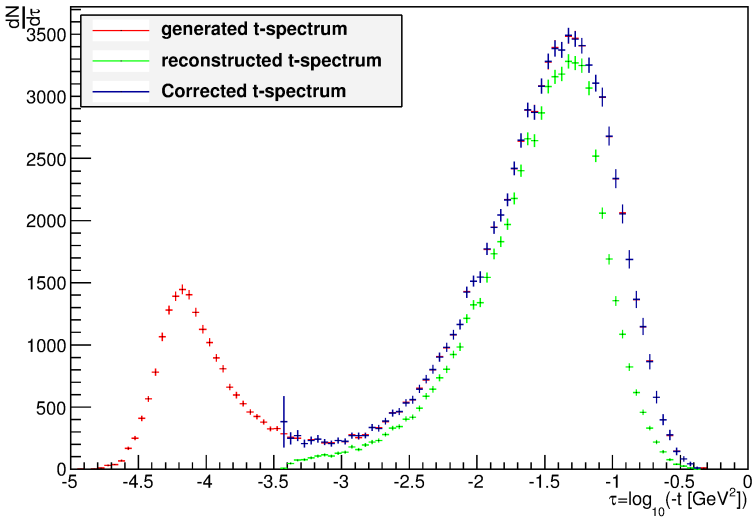

Figure 4.12: Comparison of the different t – spectrum with the one corrected with the calculated acceptance for $\beta^* = 2625$ m (Fig. 4.11).

- the substraction method (as already detailed in (4.2)).
- the local angle method using the measured angles from left and right and the M_{22} matrix term as in (4.4).

$$\theta_x^* = \frac{\theta_{x,left} - \theta_{x,right}}{M_{22,left} + M_{22,right}} \tag{4.4}$$

- the lattice method using the invert matrix to retrieve the angle position at the IP as in (4.5).

$$\theta_x^* = x\, M_{12}^{-1} + \theta_x\, M_{22}^{-1} \tag{4.5}$$

- the local substraction method using position from inner and outer detectors but including the M_{11} matrix term as in (4.6).

$$\theta_x^* = \frac{M_{11}^{outer}\, x_{inner} - M_{11}^{inner}\, x_{outer}}{M_{11}^{outer}\, M_{12}^{inner} - M_{11}^{inner}\, M_{12}^{outer}} \tag{4.6}$$

All these methods must converge in one single final total elastic cross section value. The method which is the most sensitive on the optics is the substraction method as it uses position in vertical and in horizontal plane which was less studied. But the other methods are based on the local angle which is poorly measured.

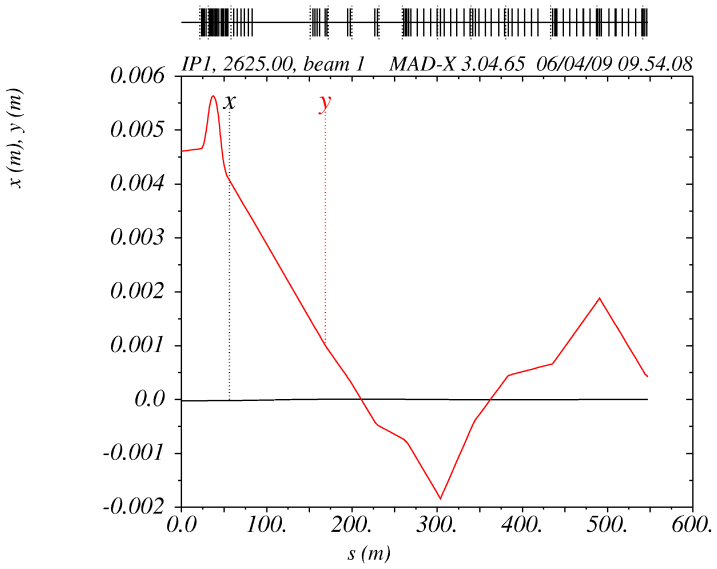

Figure 4.13: Displacement of the closed orbit for the +++ configuration meaning Q4, Q5 and Q6 displaced vertically by + 250 μm (see text for details).

4.4 Magnet misalignements for ATLAS high β^* optics

4.4.1 Impact of quadrupoles misalignement

In this study [58], the main magnetic elements are the inner triplets, the separation dipoles and three quadrupoles called Q4, Q5 and Q6 [1]. The complete simulation needs tracking on both beams. To evaluate the worst misalignment configuration, only one beam is modified for the tracking, the beam 1 which circulates clockwise in the LHC conventions. Only the quadrupoles misalignments will be studied. The accuracy on the quadrupole alignment is expected to be 250 microns [1]. To begin, we misalign Q4, Q5 and Q6 one after the other. Then all combination will be done following the schemes given in table 4.5.

Table 4.5: Different configurations with corresponding vertical displacements in micron.

	Q4	Q5	Q6	+ + +	+ + -	+ - +	+ - -
Q4	+250	0	0	+250	+250	+250	+250
Q5	0	+250	0	+250	+250	-250	-250
Q6	0	0	+250	+250	-250	+250	-250

We have done the three first cases for horizontal and vertical displacements. However due to the fact that the parallel to point focusing optics is set in the vertical plane, an horizontal displacement has no impact on the detector acceptance and a small one on the reconstruction. On Fig. 4.13, one can see the impact of the +++ configuration on the

closed orbit.

Fig. 4.14 displays the effect of different misalignment configurations on the acceptance. From this we can foreseen how such an effect could be damaging not only for the luminosity measurement but also for the accelerator settings. In the LHC sequence, such cases has

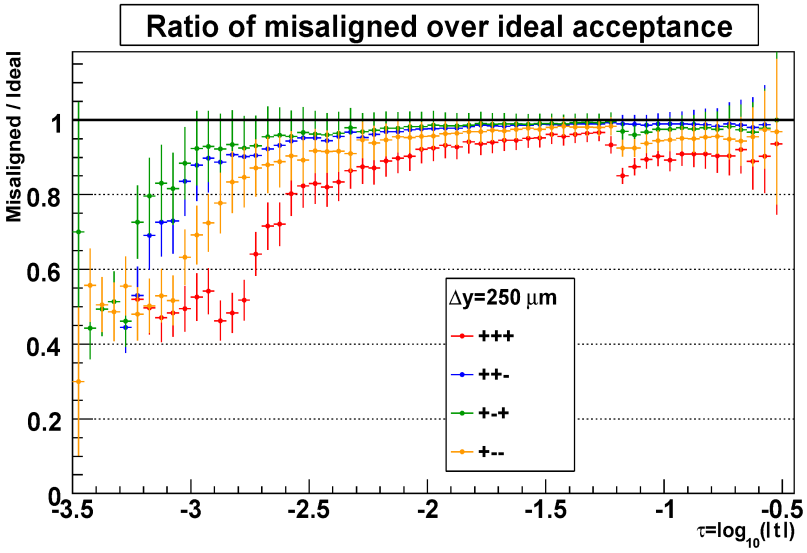

Figure 4.14: Ratio of the acceptance determined for different configurations of quadrupole misalignement over the ideal one.

been anticipated introducing a BPM and a corrector in front of all quadrupoles between the ATLAS IP and the RPs. The BPMs measure the displacement of the beam with respect to the magnetic axis. This information is used to determine the corrections to apply. This procedure is done using the MICADO correction algorithm within MAD–X. For the luminosity measurement it is very important that the correction converges before the protons reach the first RP in order that no effects are visible. The correction is done with all the different configurations of misalignments already mentioned. We assume that the BPM measurement error is negligible.

Due to the linear treatment of the optics, any misalignment has a linear impact on the position and the angle of the tracked protons. As a consequence, the impact can be measured in terms of position and angle offset at the RPs. These results have shown that we are able to correct up to a 2 mm vertical offset in the RPs. If for some configurations, the correction allows to retrieve the initial settings, some cases still show a little difference as we can see on Fig. 4.15 where the + + + configuration and the + - - could not be perfectly corrected before the RPs.

4.4.2 Acceptance and luminosity

A former study [59] has shown that considering errors on β and β^* measurements as well as on the phase advance, a total contribution on the systematic uncertainties for the beam

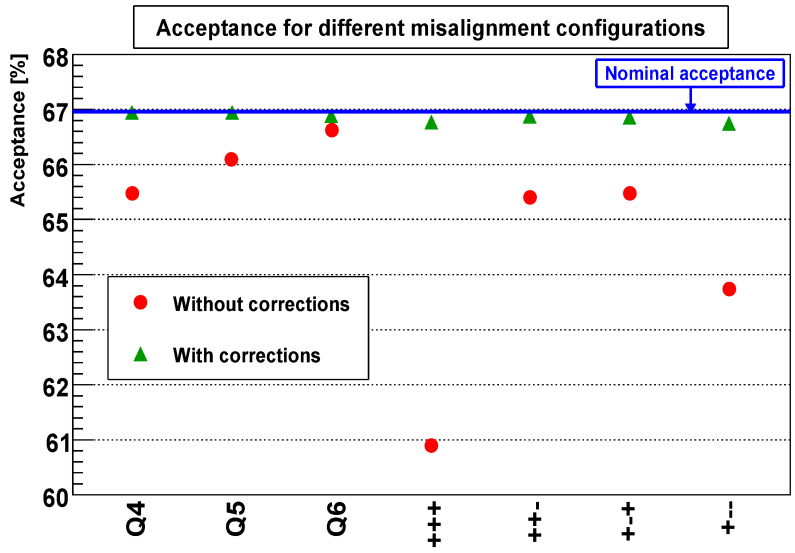

Figure 4.15: Acceptance variation as a function of the misalignment configurations, integrated over the full t – spectrum.

properties should be about 0.7 % on the luminosity. However this figure does not take into account the magnet misalignments. To minimize statistical effects, we have generated 10 million events. The luminosity and the total cross section are strongly correlated. Futhermore, the effect of the misalignment can only lower the acceptance as it introduces a skewness in the proton distribution which is not counter – balanced in the other arm of ALFA. The consequence is that the luminosity is underestimated whereas the total cross section is overestimated. In the worst case (+ + +), we obtain +1.9 % of uncertainty on the luminosity and -0.8 % on the cross section.

Considering the worst case of vertical misalignment for one beam, we have shown that assuming a perfect correction introduces a systematical uncertainty of 1.9 %. This large effect comes from the fact none of the alignement information is taken into account in the simulation. This will be needed for the final analysis. The key issue will be to achieve the corresponding correction in the short range going from IP to RP during the operation of the accelerator. A complete study including the inner triplets should be done. Furthermore all misalignment and rotations should be considered and one should allow to set boundary conditions.

Conclusion

The 2625 m high β^* optics has been described and studied including the possible errors due to transverse quadrupoles misalignements. An overview of the complete simulation scheme and a description of the t – reconstruction method has been given. This optics is challenging and needs first special run tests. Therefore, an intermediate optics to integrate in the complete ALFA simulation has then been implemeted and is shown in chapter 5.

Chapter 5

Intermediate High β^* 90 m optics

Contents

LHC has provided collisions at 4 TeV beam energy from 2012 till february 2013. It has been followed by the first LHC Long Shutdown (LS1) to prepare LHC for operation at higher energy. The 2625 m high β^* optics could not be achieved before LS1 because of two different reasons. Firstly because of the quadrupole Q4 inversion leading to new injection scheme dedicated for this optics. Secondly because of the aperture critical limit imposing to reduce the emittance to 1 μm.rad which is an important item for ALFA to reach the Coulomb nuclear interference region. Both items, new injection and emittance, need first to be tested. But other accelerator issues need also to be tested and time becomes then a critical issue. The main goal for ALFA is ultimately to reach a very high β^* optics of 2625 m. But before, intermediate optics need to be approved and tested on the LHC.

The idea was then to start with optics as close as possible to the nominal optics but with higher β^*. The 90 m intermediate optics [60] has then been chosen as a first intermediate optics study. In this chapter, my work on the 90 m β^* optics will be described as it has been more precisely studied to fulfil the requirements for the LHC and ALFA.

5.1 90 m β^* optics

5.1.1 Matching and de – squeeze

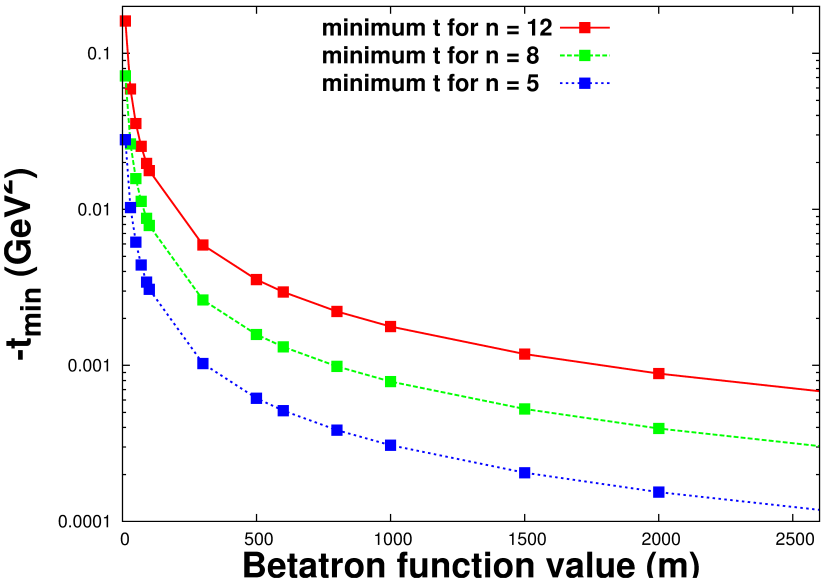

Figure 5.1: t value evolution as function of β^* for three different openings of RPs n = 5, 8 and 12 σ, with 3.5 TeV energy and with a normalized emittance equals to 3.75 μm.rad.

Fig. 5.1 summarizes the minimum t – value coming from (3.15) that can be achieved for a normalized emittance of 3.75 μm.rad and 3.5 TeV energy per beam. With $\beta^* = 90$ m, the minimum $|t|$ – value reacheable is 3.42×10^{-3} GeV^2 for a distance to the beam at 5 σ. This illustrates and confirms that the 90 m high β^* optics is not sufficient to reach the Coulomb nuclear interference region and that to reach it, higher β^* optics will be needed and will have to be studied. Nevertheless, it has some advantages which are that the optics can be tested on the LHC quite soon so as to check the feasibility of high β^* optics and check the important parameters for future developments. And still, it allows first results on total cross section measurements from data taking with the Roman Pots.

As explained in chapter 4, optics matching needs to be done in order to create new optics corresponding as close as possible to ALFA requests. The injection scheme for LHC starts at $\beta^* = 11$ m. A de – squeeze is then needed to be able to go smoothly from $\beta^* = 11$ m to $\beta^* = 90$ m at IP1. This de – squeeze is a rather demanding part as, at each time, the ratio of quadrupole strengths between both beam lines ($0.5 < r < 2$) needs to be checked.

The limitations must be respected as relevant for the first year of operation for the first 90 m high β^* optics runs and identically to the 2625 m high β^* optics matching, beam 1, beam 2 have to be treated separatly.

A study has been made in order to evaluate the impact on the tune when increasing the β^*. The curve as seen on Fig. 5.2 [48] has been made for this purpose. The larger tune reduction appears between 11 and 90 m during the de – squeeze. This is the reason of the choice of $\beta^* = 90$ m for the first optics above $\beta^* = 11$ m on LHC.

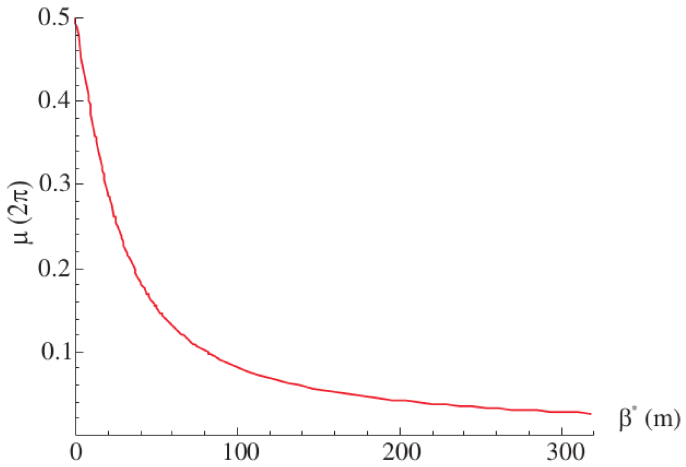

Figure 5.2: Tune contribution in terms of β^* at $\pm$ 26 m from IP1 for the LHC [48].

Further iterations are needed, everything being done on IP5 first, to simplify the calculation. Several reasons lead to that choice: the first one is that the LHC sequence used in MAD – X starts at IP1. Secondly, ALFA and TOTEM will work with quasi – similar optics during the same beam time and as TOTEM was more advanced, optics matching were first calculated for IP5. To match the entire insertion IR1, the sequence needs to be started elsewhere. This is possible and has been checked after experimental studies, but not taken into account for the matching.

Furthermore, as LHC is quasi – symmetric, to simplify at first, only the last step could be calculated for IP1 with Roman Pots located at 240 m instead of 220 m for TOTEM. An example of the de – squeeze showing the evolution of the normalized strengths at each β^* step is shown on Fig. 5.3. This has been done for each quadrupole located in IR1 (from Q1 to Q13 listed in table 4.2).

This shows that nineteen steps have been needed to go from the $\beta^* = 11$ m at injection to desqueeze smoothly to $\beta^* = 90$ m after ramp and keep the spacing between the steps adequate. The same layout of IR1 and IR5 have made, in principle, possible to operate the LHC with identical optics in IR1 and IR5. The size of the beam evolution during the de – squeeze for both σ_x and σ_y is shown on Fig. 5.4.

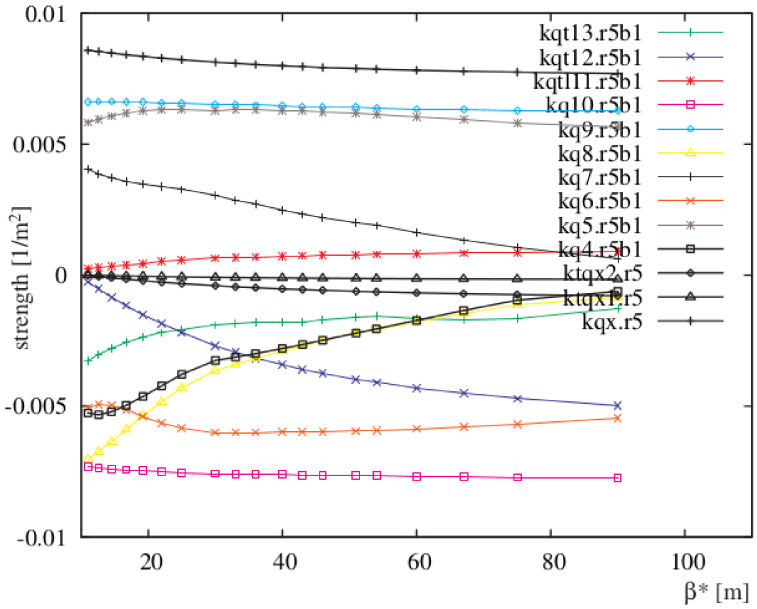

Figure 5.3: Quadrupole strengths evolution in IR1 for each β^* step during the de – squeeze. 19 steps are enough to go smoothly from 11 m to 90 m.

As expected, the beam size described in (2.49) in the horizontal and vertical direction at IP1 is always growing from $\sigma = 112$ μm at the first step of about $\beta = 12$ m to reach it's maximum size of 300 μm at 90 m. At the Roman Pots, vertical and horizontal beam sizes are also growing with the β^* value. For the first RP, (A7R1), the vertical beam size goes up to 928 μm and for the horizontal beam size up to 374 μm.

On the opposite, the divergence (see (2.49)) decreases as β^* increases. But the dominant term for the divergence is the emittance. The evolution of the horizontal and vertical divergences are shown on Fig. 5.5. The smaller the divergence, the better for the elastic total cross section measurement with ALFA. Hence, this is another reason why increasing β^* up to higher than 90 m will be necessary. Very high β^* optics, rematched starting from 90 m β^* optics including the same limit conditions, will be described in chapter 7.

5.1.2 Main parameters

The parameters of the 90 m β^* optics are listed in table 5.1 for a normalized emittance equals to 3.75 μm.rad which was the emittance expected for LHC as indicated in [1]. The main parameters used in the 2625 m β^* optics have been kept in the 90 m β^* optics. In particular, the vertical phase advance between the IP and the RPs is equal to 90°, dispersion and α at IP1 are equal to zero. With these values, the vertical and horizontal beam sizes at IP1 reach 300 μm. The internal tune compensation cannot be done internally. This optics is fully compatible with beam at 3.5 TeV beam energy with a normalized emittance of 3.75 μm.rad but also it has been checked that it's compatible with 7 TeV beam energy.

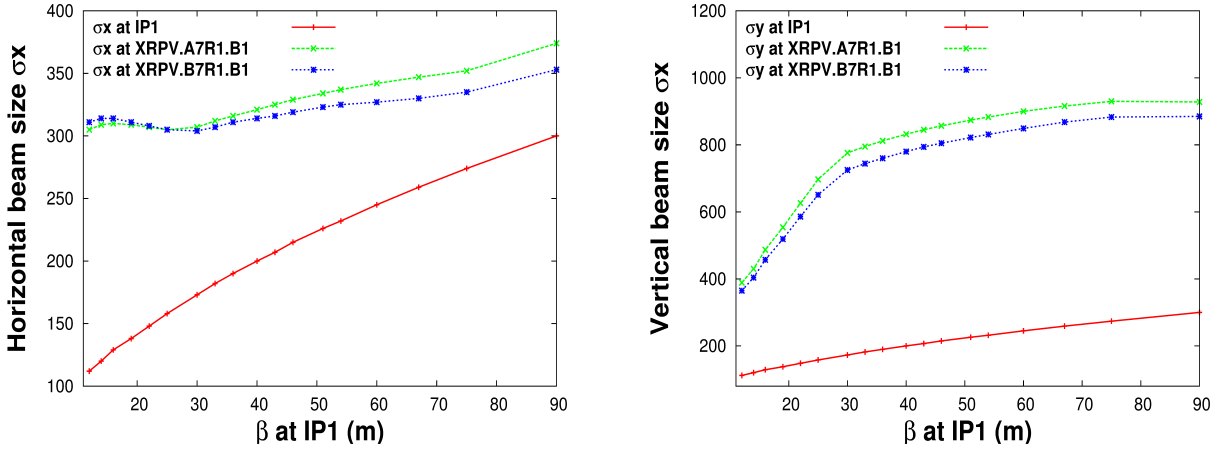

Figure 5.4: Horizontal (left) and vertical (right) beam size evolution during the de – squeeze from $\beta^* = 11$ m up to $\beta^* = 90$ m with $\epsilon_N = 3.75$ μm.rad and 3.5 TeV energy.

Table 5.1: 90 m β^* optics parameters for beam 1 (LHC version V6.503).

IP1		**RPs**	
ϵ_n (μm.rad)	3.75	β_x (m)	193.5 – 124.2
β_x^* (m)	90	β_y (m)	857.5 – 780.4
β_y^* (m)	90	σ_x (μm)	374 – 353
α_x^*	0.0	σ_y (μm)	926 – 883
D_y^* (m)	0.0	σ_x' (μrad)	2.67 – 2.83
$D_y^{*'}$	0.0	σ_y' (μrad)	1.08 – 1.13
σ^* (mm)	0.3	$\Delta\mu_x$ (2π)	0.515 – 0.519
$\sigma^{*'}$ (μrad)	3.33	$\Delta\mu_y$ (2π)	0.249 – 0.250

The final rematched optics for IP1 is shown on Fig. 5.6. The 90 m optics can also be found on the LHC optics database under the name `IP1_beta90.str` and also all the steps for the de – squeeze. Fig. 5.7 shows that the calculated aperture at 90 m is not critical and well above the specification. The calculation was done for the standard normalized emittance of 3.75 μm.rad at 3.5 TeV. The specification is that the aperture, shown in terms of a figure of merit value "$n1$"[2], remains well above the specified value of 7 including separation over the full interaction region.

As for the squeeze in standard operation, it is planned to keep the beams separated during the de – squeeze to 90 m using parallel separation at the IPs. Standard injection and ramp uses horizontal parallel separation and a vertical crossing angle in IP1 and vertical parallel separation and crossing angle in IP5. The crossing angle will be turned off before

[2]The notation $n1$ is the one traditionnaly used at CERN.

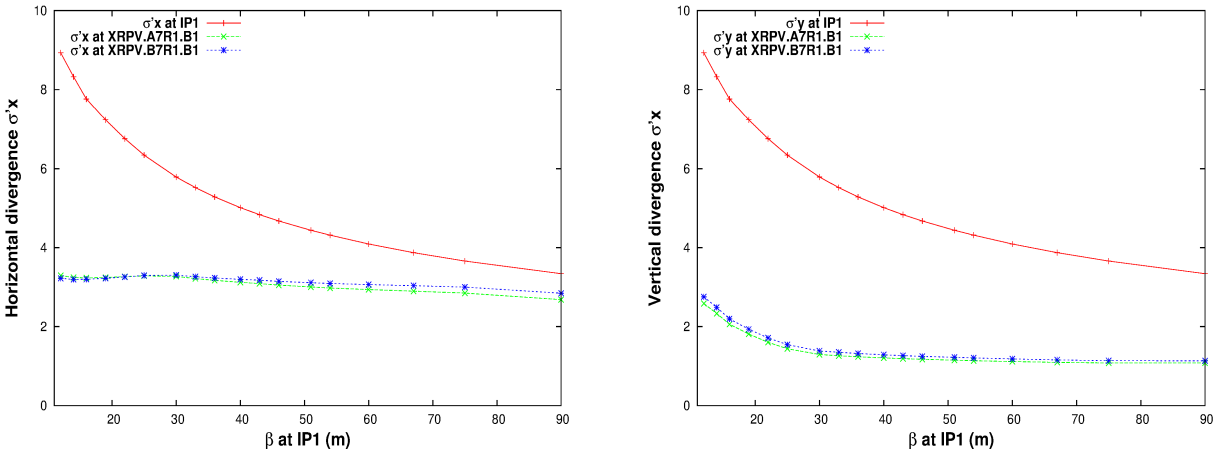

Figure 5.5: Horizontal (left) and vertical (right) beam divergence evolution during the de – squeeze from $\beta^* = 11$ m up to $\beta^* = 90$ m with $\epsilon_N = 3.75$ μm.rad and 3.5 TeV energy.

the de – squeeze to 90 m. The separation bump shape is shown in Fig. 5.8. The parallel separation is kept constant at IP1 and IP5 during the de – squeeze. For the 90 m β^* optics for ALFA and for all intermediate de – squeeze optics, the separation bumps had to be recalculated since opposite planes are used for IP1 and IP5. The same scaling is used in IR1 and IR5 for the MCBX1 corrector starting with a kick of 10 μrad at 11 m which scales during the de – squeeze as $\frac{\sqrt{11\text{ m}}}{\sqrt{\beta^*}}$.

The de – squeeze from $\beta^* = 11$ m to 90 m results in a significant loss in phase advance which has to be compensated in the rest of the LHC to keep the overall tunes constant. This change will result in some β beating. The numerical values are given in Table 5.2. They are very similar for IP1 and IP5. Commissioning of both optics together implies a doubling of the external tune compensation and an increased β beating.

For tune compensation, alternatives have been found in [48]:

- To use IR4, where is located the RF system. But this has some consequences on the instrumentations and damper as to be able to change the tune to a maximum value of 0.2. This has to take into account the damping and the synchrotron light monitor.

- To use the trim quadrupoles instead of the main quadrupoles. This will introduce β beating of 2.2 % rms in x and 0.4 % rms in y.

- To use the main quadrupoles in the arcs.

In these three cases, the most attractive alternative is to use the main quadrupoles in the arcs and ramp them up during the de – squeeze.

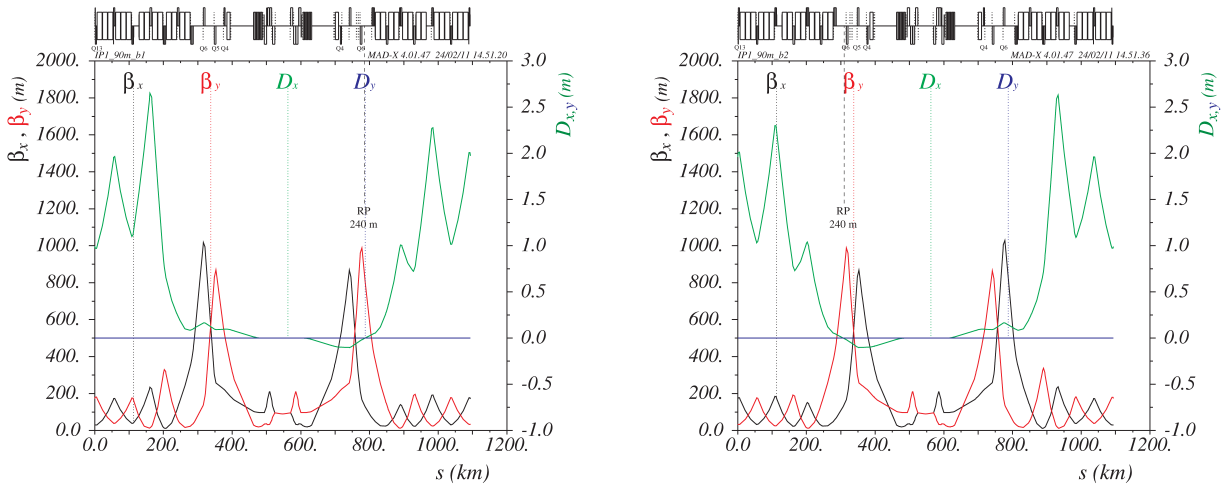

Figure 5.6: 90 m ALFA optics parameters $\beta_{x,y}$ and dispersion $D_{x,y}$ for beam 1 (left) and beam 2 (right).

5.1.3 90 m β^* optics commissioning strategy

A commissioning strategy for the 90 m β^* optics has been established [61]. To summarize, the first step for machine commissionning was to use standard injection and ramp. Then the de – squeeze was done with no crossing angle using the matched files which will allow ± 2 mm separation constant during the de – squeeze. In parallel, the feasibility for external tune compensation using the main quadrupoles in the arcs was checked. Both IP1 and IP5 were commissionned simultaneously.

A machine study performed earlier 2011 in the LHC has demonstrated, that it is possible to provide the external tune compensation by ramping up all main LHC arc quadrupoles (QF, QD) during the de – squeeze, such that the tunes are kept constant and the beam lifetime is not reduced [62]. The experimental study will be explained in more details in chapter 6.

Table 5.2: External tune compensation required for the 90 m optics in IP1 and IP5.

	beam 1		beam 2	
	ΔQ_x	ΔQ_y	ΔQ_x	ΔQ_y
IP1, 90 m	0.225	0.057	0.224	0.055
IP5, 90 m	0.222	0.055	0.220	0.053
Total	0.447	0.112	0.444	0.108

Strategy for 90 m β^* optics has a lot been discussed. During 2011 and 2012, the strategy has evolved due to the experience acquired in the runs dedicated to the high β^* optics. In

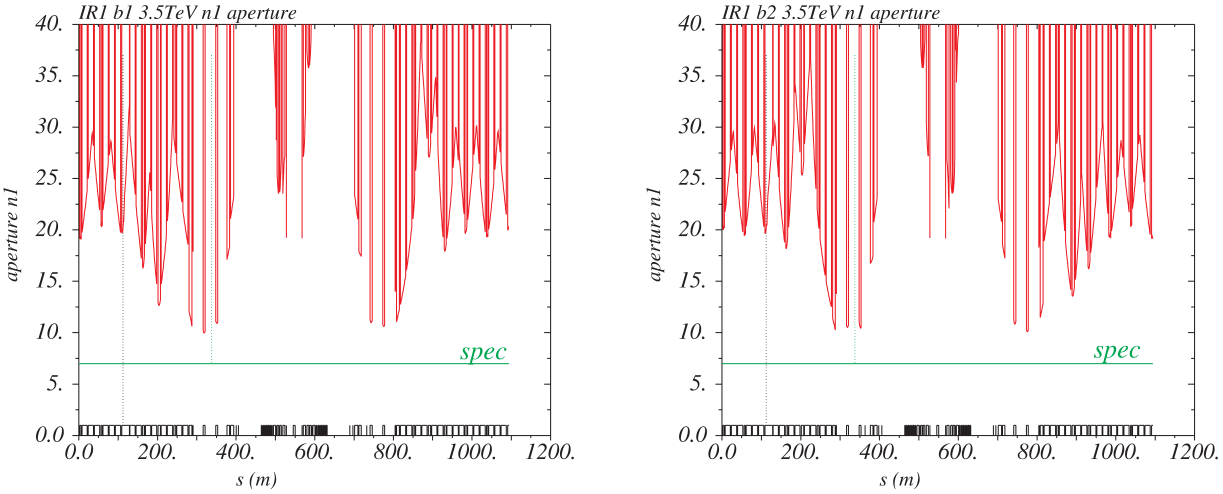

Figure 5.7: 90 m ALFA optics apertures with 3.75 μm.rad normalized emittance at 3.5 TeV in IR1, for beam 1 (left) and beam 2 (right). The green line figures the limit $n1$ for the aperture ($n1 = 7$ in LHC specifications).

2011, it was planned to commission in one run both high β^* optics for IP1 and IP5. The first step was to study the feasibility of the de – squeeze with external tune compensation with main quads using standard injection and ramp optics and crossing angle in IP1 and IP5 off during the whole run.

5.2 ALFA Acceptance simulation with the 90 m β^* optics

For the transfer momentum t – reconstruction, which is needed to give the total elastic cross section, the two main parameters are the experimental acceptance and the lever arm L_{eff}. First, we'll look at the acceptance as defined in chapter 4 with a complete simulation including tracking and reconstruction. Then, the lever arm will be defined and its importance highlighted.

5.2.1 Generation and tracking

All the simulations in this study have been made for 3.75 μm.rad but as it will be seen in chapter 6, during the commissioning of the optics, the emittance value is close to 2.0 μm.rad. This smaller emittance will be very useful as it was highlighted in chapter 4.

PYTHIA generation has been adapted to the 90 m β^* optics parameters and nominal LHC for 2011. The new set of parameters used are the following:

- Emittance value is 2 μm.rad.
- Beam energy 3.5 TeV.

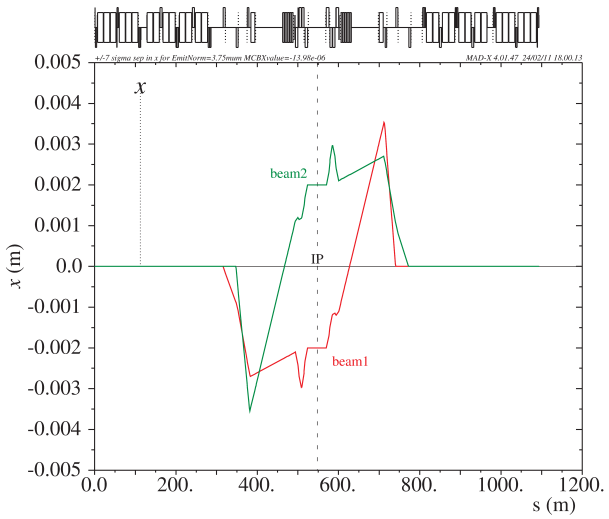

Figure 5.8: Horizontal separation bump scheme at IP1 for $\beta^* = 90$ m.

- Beam divergence $\sigma^{*\prime}_{x,y} = 2.44$ μrad.
- Beam size $\sigma^{*}_{x,y} = 220$ μm.

A minimum limit has been set for t which is $-t_{min} = 4 \times 10^{-5}$ GeV^2. But, for acceptance calculation only, corresponding to the ratio of intercepted protons on generated protons, the generation can be simplified. Instead of generating elastic scattering events, one can generate a pulse in the same t – values range as in the PYTHIA generation. This was done with ROOT using the uniform distribution provided by the random number generator. The generated protons spectrum represented in a flat uniform density distribution is shown on Fig. 5.9.

The file computed here is in fact divided into 5 files for beam 1 and beam 2 containing positions and angles which are opposite between both beams. Each file contains 20 000 particles to gain in computering calculation time for the tracking. Putting all files in one is too time consuming. Furthermore, the generated spectrum has to be kept because it will be used after tracking to calculate the acceptance. For this, a special text file containing only the t – values is produced at the same time during the generation. The tracking has been performed for 100 000 elastic protons using the 90 m β^* optics at IP1 for 3.5 TeV energy per beam.

After tracking, all the elastic particles are collected and all the files are put again together in order to be able to calculate the acceptance with a MAD – X setup like it was described in chapter 4 for the 2625 m β^* optics. The MAD – X setup has two purposes: one is to track all the elastic generated protons from IP1 to the RPs to collect the events at the RPs and determine the acceptance. The other one is to calculate the beam matrix elements using the corresponding optics. Both purposes can be done separatly and are defined in § 5.2.2 and § 5.2.3.

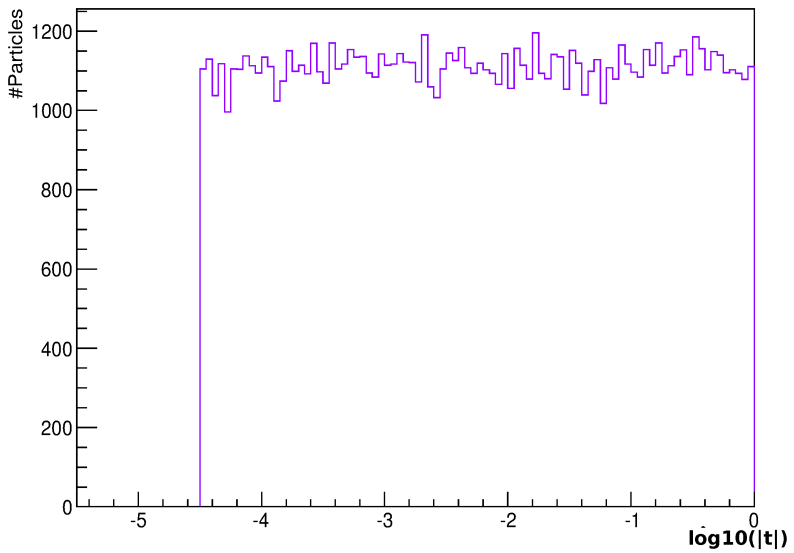

Figure 5.9: Random generated spectrum for the 90 m β^* optics for ALFA for 100 000 entries.

5.2.2 Acceptance

The energy is 3.5 TeV per beam as relevant for LHC first year of operation. The acceptance has been calculated for different $y = n\,\sigma$ distances. The normalized emittance used in the calculation has been set to 2 μm.rad which leads to a geometrical emittance of $\epsilon_{x,y}$ = 5.36×10^{-10}m.rad. Table 5.3 lists the minimum t – value achievable using (3.15) when approaching the beam at a vertical distance y which depends on the number n of σ. This confirms that the closer we approach vertically, the minimum t – value is reached.

Table 5.3: Minimum t values for different values of n.

n	y (mm) at A7R1	t_{min}(GeV^2)
6	4.1	0.0026
8	5.4	0.0047
10	6.8	0.0073
12	8.1	0.0105

The acceptance corresponding to these different distances n have been calculated and are shown on Fig. 5.10. The plot shows two different parts: one above $\log_{10}(|t|) = -1.2$ linked to the losses due to the transport and the other one below the same value, linked to the detector geometry. What is relevant, looking at the acceptance plot, is the values above 50 %. We can see that the acceptance is much bigger with a peak of 0.84 for 6 σ when the distance of the pots is closer to the beam.

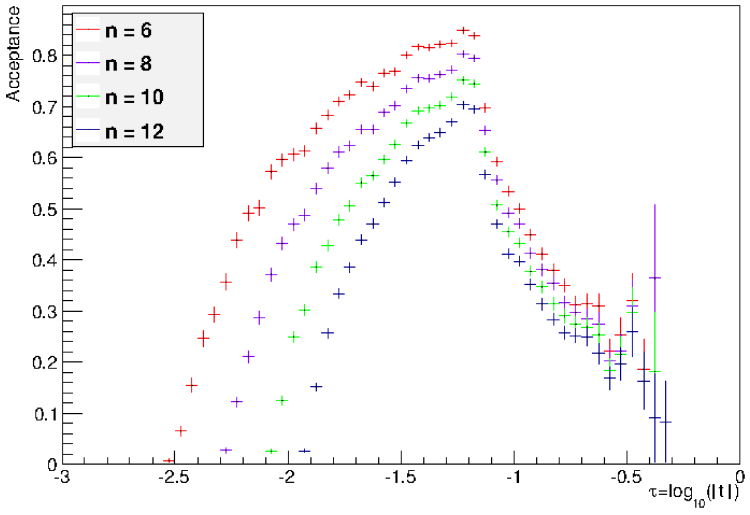

Figure 5.10: Acceptance as a function of $\log_{10}(|t|)$ for different σ values with $n = 6$, 8, 10 and 12.

This illustrates the great interest to put ATLAS/ALFA detectors close to the beam. Going down to $6\,\sigma$ able to reach an acceptance of 50.1 % which is closer to the value that we can achieve with the nominal 2625 m β^* optics of the order of 67 %.

But the acceptance is not the only important parameter concerning optics. The lever arm defined as a matrix term in optics convention needs to be defined and studied as it has a lot of impact on the t – reconstruction.

5.2.3 Lever arm (M_{12} or M_{34})

The lever arm as called for ALFA is in fact the M_{12} term in the matrix beam formalism (2.59). This is an important term as the lever arm is used in the t – reconstruction methods and is part of the systematics errors for the total elastic cross section. Despite the more important role of M_{12}, the other matrix terms have also to be calculated. A reminder of all the matrix elements considered without coupling that can be applied for both horizontal x and vertical y are listed in (5.1).

$$\begin{pmatrix} x(s) \\ x'(s) \\ y(s) \\ y'(s) \end{pmatrix} = \begin{pmatrix} M_{11} & M_{12} & 0 & 0 \\ M_{21} & M_{22} & 0 & 0 \\ 0 & 0 & M_{33} & M_{34} \\ 0 & 0 & M_{43} & M_{44} \end{pmatrix} \begin{pmatrix} x_0 \\ x'_0 \\ y_0 \\ y'_0 \end{pmatrix} \tag{5.1}$$

with:

$$\begin{cases} M_{11} = M_{33} = \sqrt{\frac{\beta_{u(s)}}{\beta_{u_0}}}\left(\cos\phi(s) + \alpha_{u_0}\sin\phi(s)\right) \\ M_{12} = M_{34} = \sqrt{\beta_{u_0}\beta_{u(s)}}\sin\phi(s) \\ M_{21} = M_{43} = -\frac{1}{\sqrt{\beta_{u_0}\beta_{u(s)}}}\left[(\alpha_{u(s)} - \alpha_{u_0})\cos\phi(s) + (1 + \alpha_{u(s)}\alpha_{u_0})\sin\phi(s)\right. \\ M_{22} = M_{44} = \sqrt{\frac{\beta_{u_0}}{\beta_{u(s)}}}\left(\cos\phi(s) - \alpha_{u(s)}\sin\phi(s)\right) \end{cases}$$

With $u = x$ or y depending on the matrix term. The matrix formalism allows to retrieve the position at the Roman Pots from the position and slope at IP1 taking into account all the matrix terms depending on the method used.

A set of lever arm values, with 3.5 TeV energy and no crossing angles found with the 90 m β^* design optics for each Roman Pots at their initial position are listed in table 5.4.

Table 5.4: Lever arm L_{eff} for each ALFA Roman Pots for beam 1 and beam 2.

	s (m)	$L_{eff,x}$ (m)	$L_{eff,y}$ (m)
A7R1	237.398	-10.294	277.804
B7R1	241.538	-13.017	265.022
A7L1	-237.398	-10.292	277.836
B7L1	-241.538	-13.016	265.073

As the lever arm are different for each beam, each of them for each pot has to be taken into account in the t – reconstruction with the substraction method (4.1).
To obtain the beam matrix terms, twiss files are produced from the MAD – X setup giving the different optics values and therefore the matrix elements. The lever arm is not exactly identical for both beams because both sides on LHC around IP1 are not exactly identical. This leads to small differences on the optics parameters and then on the lever arm. All the simulation and twiss files are given and produced for the ALFA community in order to give different setup for different needs.

5.3 Parametric study

5.3.1 Study with and without tune compensation

The 90 m β^* optics setup is very close from the 2625 m β^* optics. The quadrupoles strengths files providing the 90 m β^* optics are used with all the LHC sequences needed. The files have been updated and were put in a common location in order to able all ALFA community to use them. The collision points IP1 and IP5 have head on collisions.

It has been demonstrated in [48] that there was different solutions for tune compensation during the run. The solution chosen for 90 m β^* optics and included in the commissionning strategy is to compensate the global tune by using the quadrupoles in the arcs. That's why initially for the whole simulation the setup includes a global matching for tune compensation. Table 5.5 shows a comparison of the twiss parameters with and without tune compensation around IP1.

Table 5.5: Comparison of MAD – X setup with and without tune compensation for beam 1 on the first three columns and beam 2 on the last three columns. IP1.B1 indicates the Interaction Point for beam 1 and IP1.B2 indicates the Interaction Point for beam 2.

	IP1.B1 (%)	A7R1 (%)	B7R1 (%)	IP1.B2 (%)	A7L1 (%)	B7L1 (%)
$\Delta\beta x/\beta x$	3.9	4.0	3.97	3.3	3.8	3.4
$\Delta\beta y/\beta y$	0.19	0.16	0.15	0.4	0.4	0.4
$\Delta\mu/\mu$	0.0	0.12	0.16	0.0	0.09	0.13
$\Delta\mu/\mu$	0.0	1.2	1.2	0.0	0.04	0.04
$\Delta L_{effx}/L_{effx}$	0.0	0.0	0.0	0.0	0.0	0.0
$\Delta L_{effy}/L_{effy}$	0.0	0.0	0.0	0.0	0.0	0.0

As we can see, tune compensation doesn't act at all on the lever arm L_{eff}. Even if the optics parameters are different, the lever arm remains the same. This was predictible as for tune compensation, only quadrupoles strengths in the arcs are modified. Then, there will be no need to add the tune compensation in the tracking for ALFA. ALFA MAD – X setup and tracking can be treated as a beam line. Only what happens in between IP1 and the RPs has some influence.

5.3.2 Beam line vs ring – Betatron function

Due to the fact that the lever arm has the largest importance and that crossing angles, tune compensation etc... does not act on it between IP1 and the RPs, further studies to search for the elastic total cross section including systematics are done using a beam line MAD – X setup. The fact that the lever arm won't change even if the rest of the ring is modified can be well understood looking at the fact that it's a matrix term which depends only on the quadrupoles located in between IP1 and RPs.

The β^* – function is one of the important parameter for the lever arm calculation. MAD – X allows to change the β^* – function in the twiss file by imposing initial conditions to see if the impact on the lever arm is large or not. To evaluate this impact on the lever arm, one need to go back to the definition as stated in (5.1).

M_{12} called lever arm L_{eff} is a constant term in the matrix unless the optics line is changed. To change the value in the matrix, one need to change the optics ie modification of the

line. To understand better what happens to the optics functions, we use the following formalim:

$$\begin{pmatrix}\beta\\ \alpha\\ \gamma\end{pmatrix}_s = \begin{pmatrix} C^2 & -2SC & S^2 \\ -CC' & CS'+SC' & -SS' \\ C'^2 & -2C'S' & S'^2 \end{pmatrix} . \begin{pmatrix}\beta\\ \alpha\\ \gamma\end{pmatrix}_0 \tag{5.2}$$

The β – functions have been modified by ± 5 m. The study has been done for beam 1 but the result is similar for beam 2. Two different methods have been used: an analytical one using matrix formalism in mathematica and the twiss MAD – X module with specified initial parameters in order to calculate the lever arm. The same results have been obtained such as $\Delta L_{effx}/L_{effx}$ and $\Delta L_{effy}/L_{effy}$ are both equals to 0.0.

Regardless the β – functions given in input, the lever arm keeps the same value and is not changed which was predictible regardless the matrix formalism. Indeed, as can be seen on table 5.6 for $\sqrt{\beta\beta^*}$ on beam 1, the curve is quasi linear from 86 to 94 m and has a very slightly variation which is compensated by the phase advance variation.

Table 5.6: Evolution of the optics parameters by changing the initial condition on β^*.

β^* (m)	β_{A7R1} (m)	μ_{A7R1} (°)	$M_{12} = L_{eff,y}$ (m)
85	907.952	0.24953	277.804
86	897.394	0.249524	277.804
87	887.079	0.249519	277.804
88	876.999	0.249513	277.804
89	867.145	0.249508	277.804
90	857.511	0.249502	277.804
91	848.088	0.249497	277.804
92	838.869	0.249492	277.804
93	829.849	0.249486	277.804
94	821.022	0.24948	277.804
95	812.379	0.249475	277.804

All the parameters of the lever arm term vary and compensate which gives the same result at the end. The only way, then, to modify the optics and impact on the lever arm is to change the quadrupoles strengths. This is another study shown in chapter 6.
The measurement of the total cross section depends on the simulation and on the lever arm value. The errors coming from a longitudinal misalignment of the RPs could be checked before the experimental run. It was also planned to combined the ALFA run with ATLAS measurements. It was then necessary to check if the ATLAS solenoid could disturb the measurement. These two items were studied in § 5.3.3 and § 5.3.4.

5.3.3 Longitudinal RPs position

RPs detectors position is of interest as a longitudinal shift can give different sets of optics parameters and impact the lever arm. A small study has been performed in order to quantify the impact of RPs position change taking into account ± 5 cm longitudinal position range.

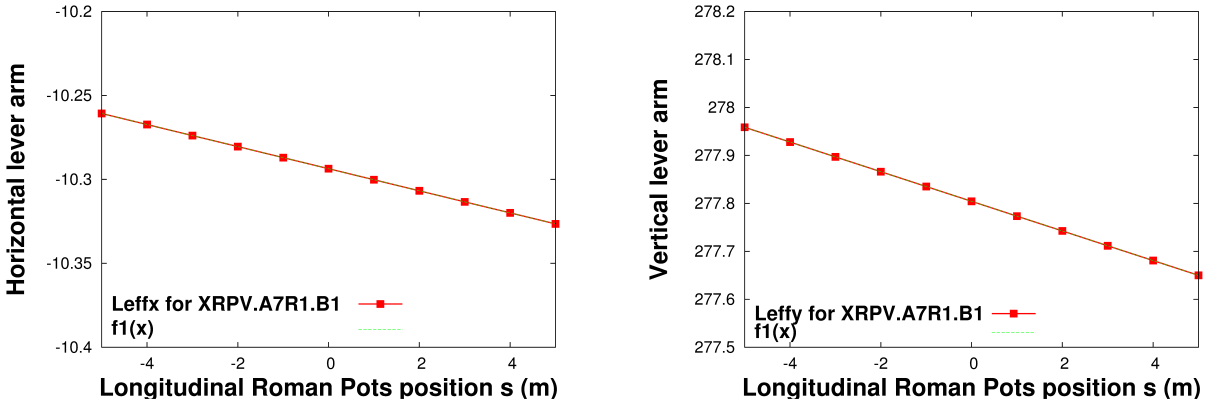

Figure 5.11: Impact of a longitudinal displacement of the A7R1 RP on the horizontal (left) and vertical (right) lever arm.

As can be seen on Fig. 5.11, for A7R1 Roman Pots on beam 1, the slope for L_{effx} is -0.0065 and for L_{effy} is -0.0031. The same result for both lever arms has been found for B7R1. This gives a relative difference on the vertical lever arm of about 0.3 %.

Due to the impact of the longitudinal RPs positions, it was re-measured in the LHC tunnel. Precise location of the RPs are now: 237.389 m for A7R1, 241.538 m for B7R1, 237.395 m for A7L1 and 241.539 m for B7L1 instead of the previous ones 237.398 m and 241.538 m for both pots for both beams. It has then been demonstrated that the detectors positions could be shifted only by 1 mm. This allows us to exclude a possible error from RPs position.

5.3.4 Impact of the ATLAS solenoid

As detailed in § 1.4, ATLAS inner detector is included in a solenoid. This solenoid has been modeled for LHC in the MAD – X sequence [63]. One can add or not the ATLAS solenoid in beam tracking and simulations. In our case, the idea was to know if the solenoid will affect the particle tracking. Tracking was performed including or not the ATLAS solenoid.

At the Roman Pots, it was shown that the impact of the solenoid is negligible. Indeed, the acceptance remains the same and looking at the position (x, y) or the angle (p_x, p_y) difference, the RMS values for A7R1 are for x: 7.472×10^{-8}, for y: 2.039×10^{-6}, for p_x: 3.744×10^{-9} and for p_y: 2.249×10^{-8} as shown on Fig. 5.12 and Fig. 5.13. As these values are much smaller than the detector position resolution ($\approx 40\,\mu$m) [64], the tracking can be

performed without taking care of the ATLAS solenoid. This conclusion can be extended to the three other RPs.

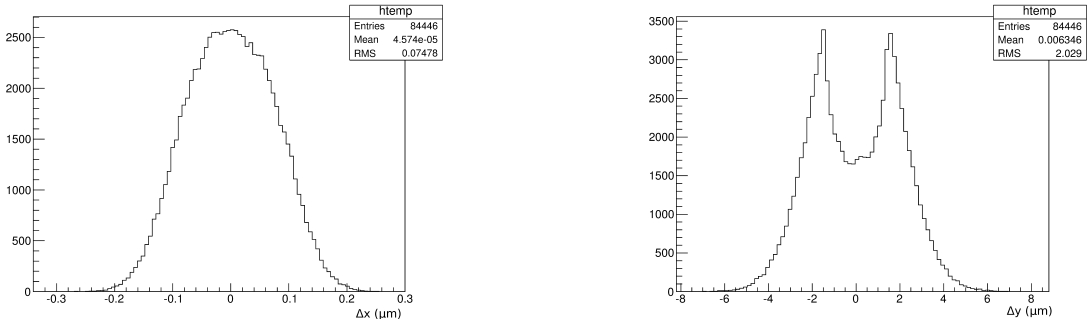

Figure 5.12: Difference in x and y at A7R1 after tracking with and without the ATLAS solenoid simulation.

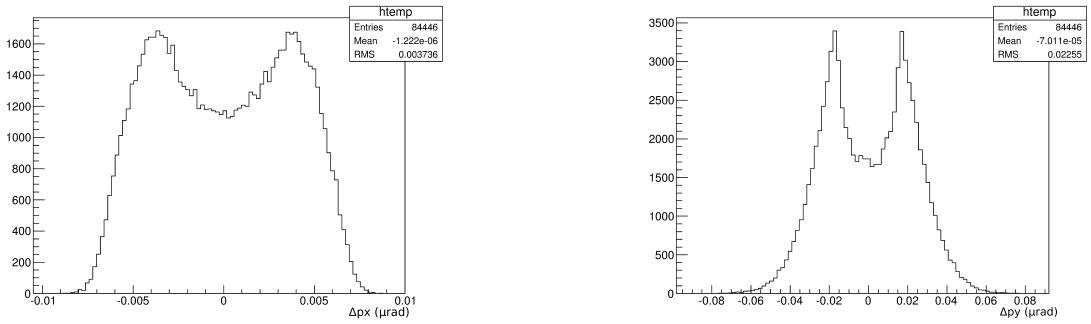

Figure 5.13: Difference for p_x and p_y at A7R1 after tracking with and without the ATLAS solenoid simulation.

Conclusion

We've shown here that the lever arm is a robust quantity. One needs large errors to impact on it. It has also been shown that to calculate the lever arm, we can consider a beam line. The $\beta^* = 90$ m optics developped in this chapter has been implemented in LHC. This will be the topic of the next chapter.

Chapter 6

Experimental study of 90 m β^* optics

Contents

To improve the LHC performances, slots of beam time called MD for **M**achine **D**evelopment are dedicated for accelerator physics to test any improvement method for LHC. MDs are distributed along the year in periods of 5 days usually followed by technical stops. To test new optics, as the intermediate 90 m β^* optics for ALFA, one need to ask for beam time during these MD sessions. Then, when the MD periods are successfull, the data taking period with ALFA Roman Pots can take place. These periods were performed in 2011 and 2012 during few weeks distributed along the year. The experimental results are extracted from both periods in order to evaluate the uncertainties and compare simulation to data. The MDs will be given in chronological order as at each MD, step by step, the understanding of the optics was improved.

6.1 90 m β^* commissioning and optics measurements

The 90 m high β^* optics was commissioned in several studies and operation periods in 2011. The 2011 commissioning periods are listed in table 6.1.

Table 6.1: Summary of the MDs fills for 2011 for 90 m β^* optics.

Fill	Date	Action
1760	05/05/11	De–squeeze tests
1902	28/06/11	First data with Roman Pots
2047	23/08/11	Dump due to power glitch
2172 - 2173	30/09/11	Beam lost before data taking
2174 - 2175	30/09/11	Beam lost before optics measurements
2227	18/10/11	Beam dumped
2228	10/11	Loss maps and optics measurements
2229	10/11	Self triggered beam dump
2230	10/11	Beam dumped : rqt13.l4b2 tripped : access required
2231	10/11	For VdM, dumped during de – squeeze
2232	10/11	Data taking

This gives a total of 13 fills corresponding to 4.2 days of running time [65]. The fill number corresponds usually in a complete scheme: cycle, injection, ramp, de – squeeze, optics measurements or data taking and dump. To simplify, we could say that each de – squeeze attempt corresponds to one fill. The de – squeeze from $\beta^* = 11$ m injection optics to $\beta^* = 90$ m was successfully achieved from the first try using the main quadrupoles of the LHC arcs for the external tune compensation. A second run was more dedicated for the 90 m β^* optics with parallel separation bumps. Beams were brought into collisions at the end of this second run. Then, the other runs were used to re – measure the optics, adjust collimators and Roman Pots for, finally, performing data taking for both experiments ALFA and TOTEM.

The beam intensity in 90 m β^* optics is much reduced compared to standard high luminosity operation. Furthermore, there's no crossing angle at IP1 and IP5 for high β^* operation. To avoid parasitic collisions, the maximum number of bunches is then limited to 156. A list of the filling scheme used during special 90 m β^* operation is given in table 6.2. Typically, for the runs described here, 15 bunches are used. Two with 7×10^{10} protons and thirteen considered as probe bunches with very low intensity ($\sim 1 \times 10^{10}$ protons), close to the instrumentation lower limit. Another reason, from which low intensity is required, is due to machine protection during the β beating measurements using the AC dipole. Collisions were not happening in all the fills, only protons in the same buckets from left and right can collide. When the buckets are different, this means that the bunch location makes that there's no collisions.

Table 6.2: Filling schemes for 90 m β^* optics MDs during 2011.

Collisions	Bunch number	Intensities (protons per bunch)	Buckets
28/06/11	Fill 1902		
Beam 1	1	1×10^{10}	3001
Beam 2	1	1×10^{10}	3001
Beam 1	1	2×10^{10}	1
Beam 2	1	2×10^{10}	1
23/08/11	Fill 2047		
Beam 1	3	7×10^{10}	1–17851–18851
Beam 2	3	7×10^{10}	1–8911–18851
30/09/11	Fills 2172-2173		
Beam 1	2	7×10^{10}	1–17851
Beam 2	2	7×10^{10}	1–8911
Beam 1	13	1×10^{10}	all colliding
Beam 2	13	1×10^{10}	all colliding
18/10/11	Fills 2227–2228–2229–2230–2231–2232		
Beam 1	2	7×10^{10}	1–17851
Beam 2	2	7×10^{10}	1–8911
Beam 1	13	1×10^{10}	all colliding
Beam 2	13	1×10^{10}	all colliding

6.1.1 90 m β^* commissioning in 2011 at 3.5 TeV

Before commissioning the 90 m β^* optics, first hardware commissionings on IP1 and IP5 quadrupoles have been performed [62] which means inserting the quadrupoles currents without beam to check the settings. They are called dry – runs. The one that has been performed for IR5 is shown on Fig. 6.1. A first test of the de – squeeze without beam was performed successfully on the 15th February in the LHC sector 5 – 6. This complete dry – run was performed few days before the actual MD, and revealed, that the RQ4.B1 ramp down was slightly slower than requested, resulting in a trip between $\beta^* = 25$ and $\beta^* = 30$ m. This was fixed by stretching the function length in the critical segments by 70 s, bringing the total time needed for the simultaneous de – squeeze in IP1 and 5 from 1772 s to 1842 s (without stops).

De – squeeze

The simultaneous de – squeeze in IP1 and IP5 from the injection $\beta^* = 11$ m to $\beta^* = 90$ m results in a significant tune reduction of up to 0.45. It is compensated by an increase of the strength of the main LHC quadrupoles (QD, QF). The validity of this approach was demonstrated in a first test performed in May 2011. As illustrated in Fig. 6.2 and

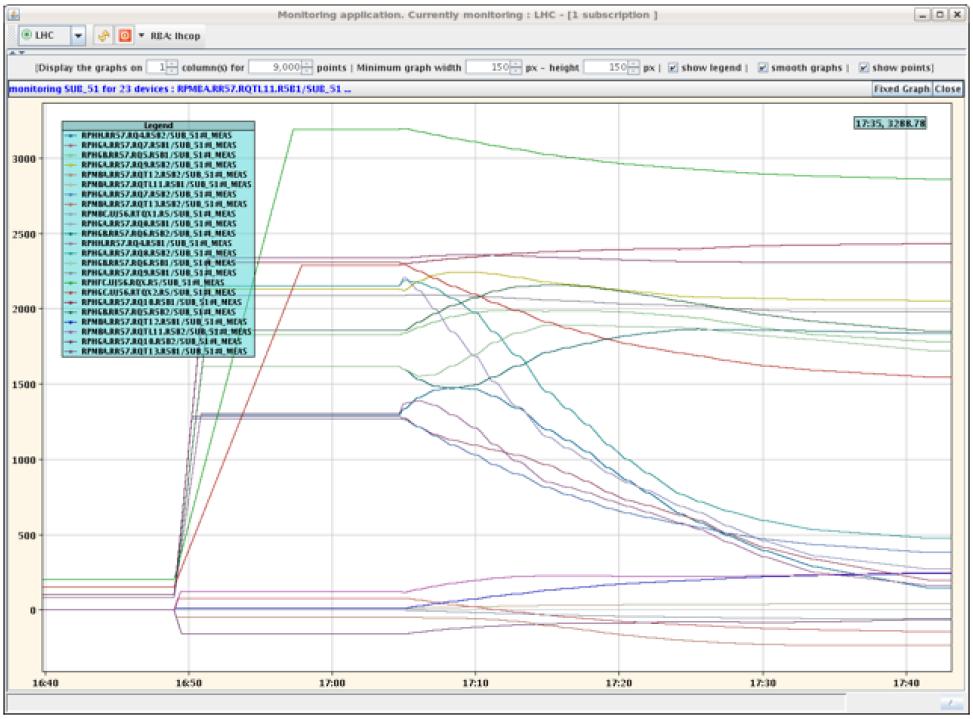

Figure 6.1: Screenshot from the Control Room of the quadrupoles first hardware commissioning on IP5 for both beams performed the 15th february 2011 (overall horizontal scale spread is 1 hour).

Fig. 6.3, it was possible to reach $\beta^* = 90$ m without any significant beam losses.
To keep matters simple and minimize the risk of damage in case of uncontrolled beam loss, the first study was performed using single bunches of rather low intensity in each of the LHC proton rings, located such that they would not collide in the interaction regions. This worked very well. The beam intensity was close to 1.2×10^{10} protons for each beam. Feedbacks were used to automatically correct orbits and tunes. Linear interpolation is used for the magnet strengths between the steps. The tune distortions introduced by the linear interpolation were calculated. The calculated corrections reach values up to 0.006 between the steps and can be corrected using the LHC trim quadrupoles. To test the procedure, the calculated corrections were only applied for beam 1.

The time evolution of the tune trims during the first de – squeeze study are shown in Fig. 6.4. The tune evolution for beam 1 is rather flat which shows, that the tune excursion between the de – squeeze steps was well predicted and corrected while these excursions are visible for beam 2 and compensated by tune feedback. The orbit and tune corrections found in the first de – squeeze were incorporated as correction for the second de – squeeze.
In the second study, beams were injected in the same buckets in beam 1 and beam 2 of the LHC to allow for collisions. This requires beam separation at the interaction points to avoid collisions during the injection and de – squeeze. The separation is provided by closed orbit bumps in the interactions regions which keep the beams transversely separated by at least $\pm 5\,\sigma$. The intensity in the second study was increased to 3×10^{10} protons.

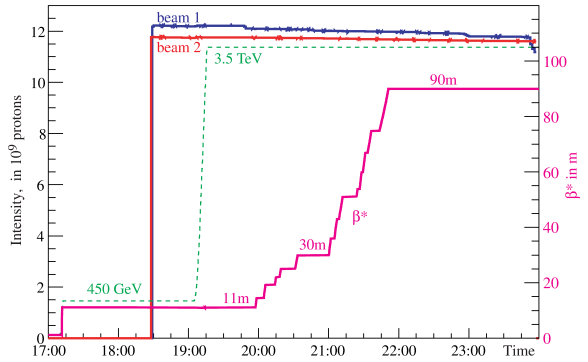

Figure 6.2: Beam intensities up to about 11×10^{12} protons (blue, red), energy (green) and β^* (pink) as a function of time during the first de – squeeze.

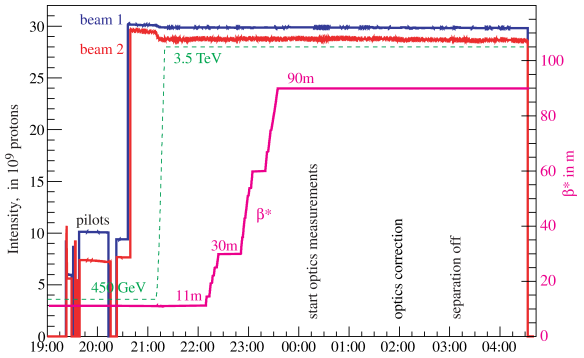

Figure 6.3: Beam intensities, energy and β^* as a function of time during the second de – squeeze.

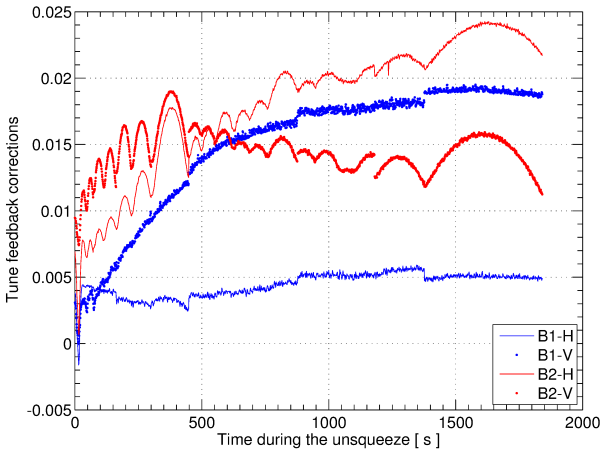

Figure 6.4: Time evolution of tune trims during the first de-squeeze study.

A summary of all the de – squeeze during 2011 is shown in Fig. 6.5. The values have been extracted from the TIMBER database after runs for each different fills for the 90 m β^* optics. It shows that all the de – squeeze are very similar for each fill. The time steps in abscissa have been equalized and put in hour unit in order to be able to compare each fill. We can also see that one of them has stopped before reaching $\beta^* = 90$ m due to a beam dump. The first de – squeeze had taken 85 minutes as optics was checked at each step whereas, at the end, only 35 minutes were needed.

Optics measurements

Optics measurements are an important part of the commissioning for two different reasons: the first is to make sure the optics is overall sufficiently well known and corrected and the second to obtain a good knowledge of β^* and the optics parameters between the

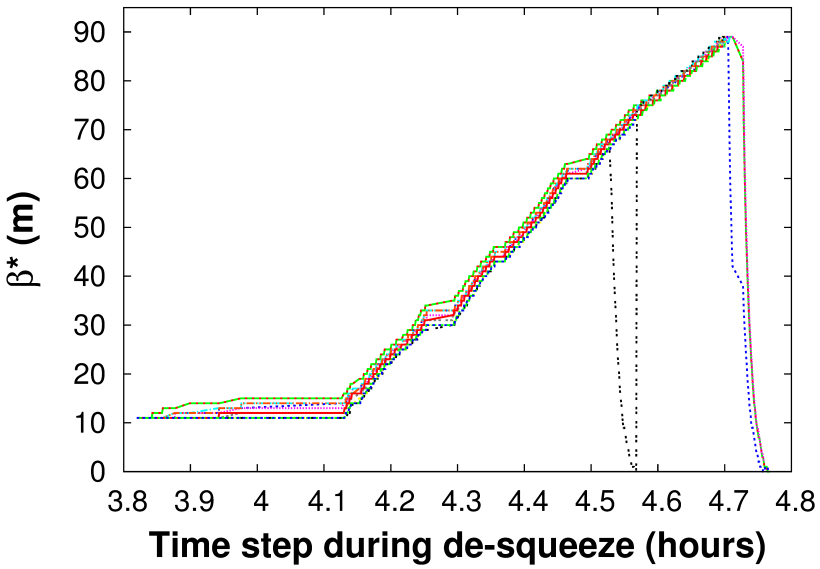

Figure 6.5: Superimposition of all 90 m β^* de – squeeze during 2011.

interaction point and the Roman Pot detectors.

β beating

This was measured at three steps: 11 m, 30 m and 90 m. The evolution of the β beating is shown in Fig. 6.6.

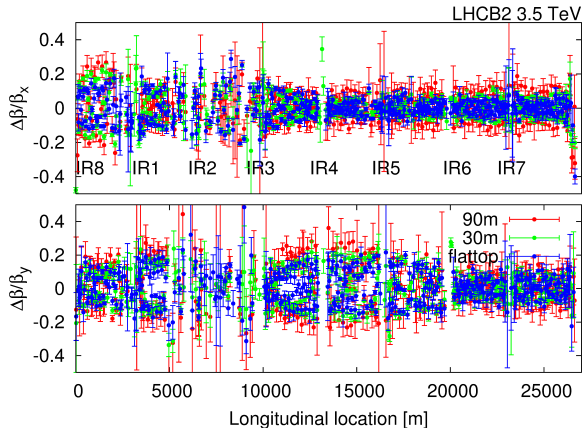

Figure 6.6: Evolution of the β beating during the de – squeeze for beam 2.

It shows that there is no major anomaly and that the de – squeeze behaves basically as expected. The peak value for β beating is 25 % for beam 1 in the horizontal plane and 20 % in vertical plane. For beam 2 the peak value is close to 30 %.

Coupling

The standard LHC tunes which are also used here are $Q_x = 64.31$ and $Q_y = 59.32$ which is close to the coupling resonance and requires a good tune and coupling control. The technique used to calculate the local corrections at IP1, IP2, IP5 and IP8 is called segment by segment technique and described in [15]. The local corrections applied on the quadrupoles are summarized in table 6.3.

Table 6.3: Summary of local corrections for coupling during 90 m β^* MDs.

Corrector	Strength(m)	Corrector	Strength(m)
kqsx3.l1	0.0008	kqsx3.l5	0.0006
kqsx3.r1	0.0008	kqsx3.r5	0.0006
kqsx3.l2	-0.0009	kqsx3.l8	-0.0007
kqsx3.r2	-0.0009	kqsx3.r8	-0.0007

Fig. 6.7 shows the coupling measurement at $\beta^* = 90$ m after correction. Small remaining effects can still be seen at IP6 for beam 1 and at IP1 for beam 2.

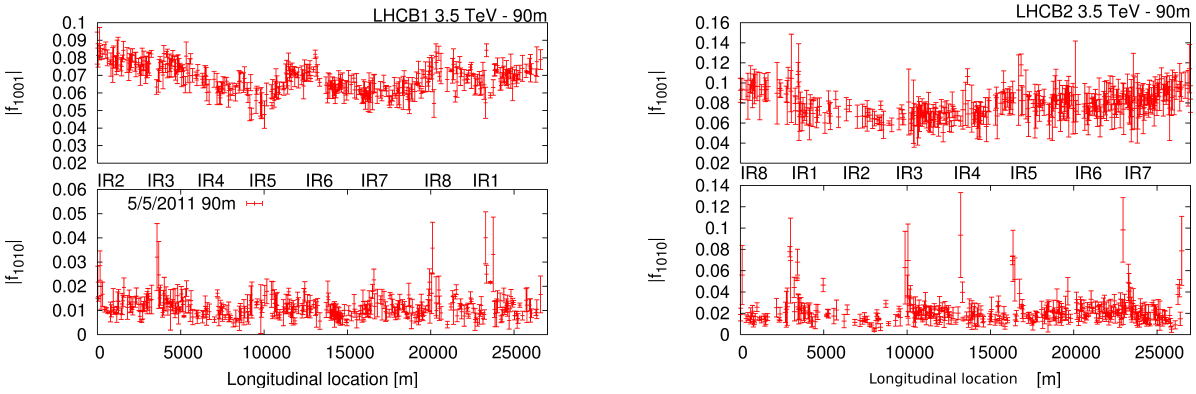

Figure 6.7: Measured coupling for beam 1 (left) and beam 2 (right) for $\beta^* = 90$ m. The method uses the resonant driving terms, $|f_{1001}|$ being the difference resonance and $|f_{1010}|$ being the sum resonance [66].

Dispersion and β^* measurement

The technique to measure dispersion is to use a turn – by – turn data acquisition with an energy offset $\frac{\Delta p}{p}(b_1) = -0.4076$ and $\frac{\Delta p}{p}(b_2) = -0.394$. Fig. 6.8 shows the difference between the measured and predicted dispersion for beam 1 and beam 2. Then K–modulation (§ 1.3.3) was used to calculate the β^* and the waist for both IPs. The β^* values found are listed in table 6.4.

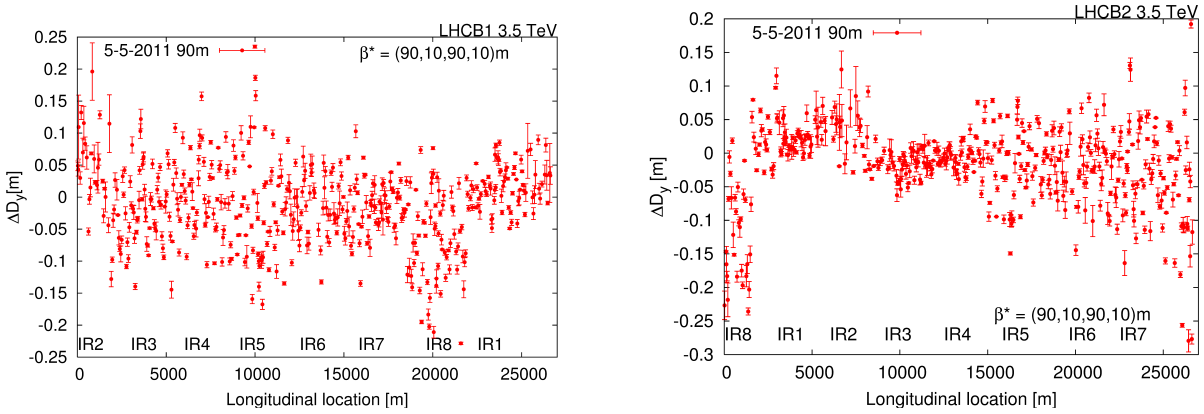

Figure 6.8: Difference between predicted and measured vertical dispersion for beam 1 (left) and beam 2 (right).

Table 6.4: Summary of the β^* measurements at IP1 during the 90 m β^* MD.

IP1	β_x (m)	β_y (m)
Beam 1	83.4 ± 0.5	89.7 ± 0.3
Beam 2	97 ± 5	87.7 ± 1.6

Emittance Measurement

The measured emittances for beam 1 and beam 2 are summarized in table 6.5.

Table 6.5: Measured normalized emittances for beam 1 and beam 2.

	Beam 1	Beam 2
$\epsilon_{N,x}$ (μm.rad)	2.6 ± 0.2	3.0 ± 0.05
$\epsilon_{N,y}$ (μm.rad)	2.0 ± 0.2	2.4 ± 0.05

The conclusion that can be drawn here is that, on average, the emittance was much closer to 2 μm.rad than the 3.75 μm.rad foreseen at the beginning which is important for ALFA RPs detectors measurement.

Separation bumps

To separate the two LHC beams, three types of corrector magnets are used: MCBC, MCBY and MCBX. The shape of these bumps is shown in Fig. 6.9.
The separation bumps were calculate to provide a constant parallel separation of ± 2 mm between beam 1 and beam 2 at IP1 and IP5. Since the optics changes during the de – squeeze and since IP1 and IP5 generally use separation in opposite planes, this required the separated calculation of separation bumps for every step separately for IP1 and IP5.

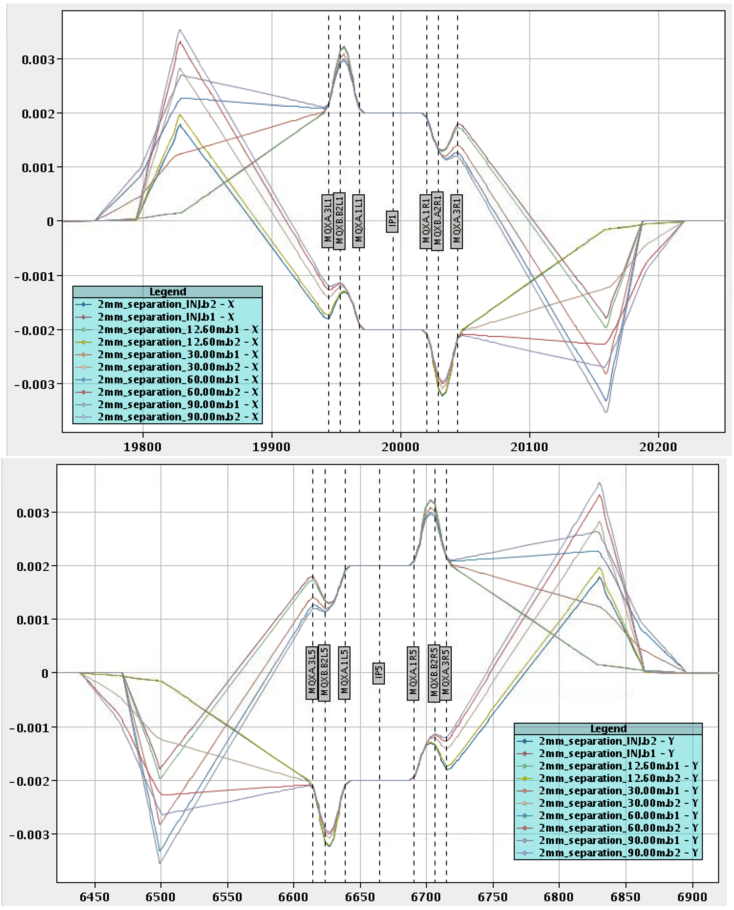

Figure 6.9: Screenshot from the Control Room of the calculated parallel separation bumps from $\beta^* = 11$ m to 90 m. The horizontal separation in IP1 is shown in the upper figure and the vertical separation in IP5 in the lower figure.

6.1.2 90 m β^* re – commissioning in 2012 at 4 TeV

In 2012, LHC has increased its energy up to 4 TeV instead of 3.5 TeV in 2011. The main program was to go up to $\beta^* = 1$ km going through the 90 m β^* optics [67]. But we'll focus here on the first part corresponding to the 90 m β^* optics and let the other optics be described in chapter 7. For this purpose, the 90 m β^* optics need to be re – commissioned with and without separation. Two fills (2740 and 2751) were used to test both configurations. But firstly, the 5th May, new dry – runs were performed, as in 2011, to test the quadrupoles settings for $\beta^* = 90$ m. This is shown in Figs. 6.10 and 6.11.
The first 90 m β^* re – commissioning has been performed the 18th June. The filling scheme was to use three non colliding probes and no separation in IP1 and IP5. The β^* evolution from the re – commissioning as seen in the Control Room by the operation team is shown in Fig. 6.12.
During the re–commissioning MD, optics measurements were performed at $\beta^* = 90$ m using the same knobs as in 2011. The results compared with 2011 are shown in Fig. 6.13.

As it can be seen, for beam 1 and beam 2, the correction is similar from 2011 and even

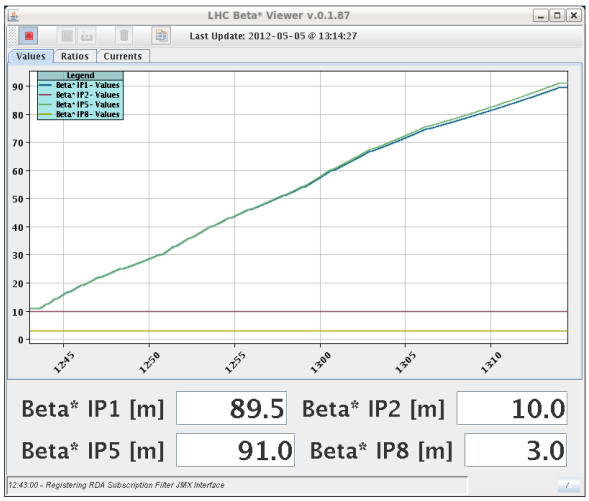

Figure 6.10: β^* increase during the dry run performed the 5th May 2012 (Screenshot from the Control Room).

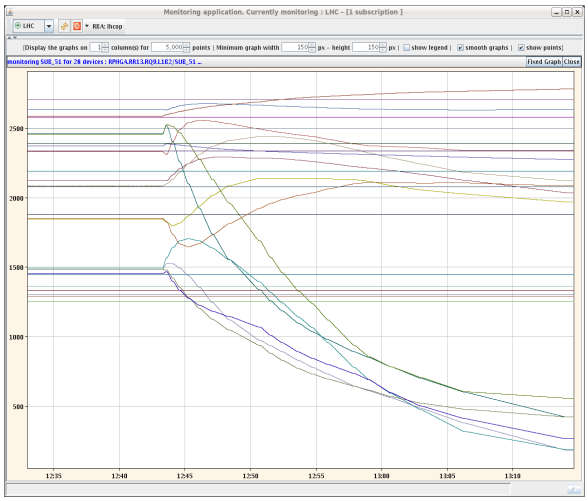

Figure 6.11: Quadrupoles currents evolution during the dry run performed the 5th may 2012 (Screenshot from the Control Room).

better. The β beating was about 10 %. For this measurement the quadrupoles between IP1 and the RPs have been left untouched. The other optics parameters re – measured was the coupling. The results are shown in Fig. 6.14. It can be seen that the coupling has been better corrected than in 2011. We can then deduce that the impact of the coupling on ALFA measurements will be weak.

The 21th June, the high β^* optics have been tested, this time with separation, with a stop of about 3 hours at $\beta^* = 90$ m before going to higher β^*. In the latter case, the filling scheme has consisted on three probes bunches per beam (1.2×10 protons per bunch). The de – squeeze up to $\beta^* = 90$ m goes well and the test was successfull.

6.2 Data at the Roman Pots and results

6.2.1 RPs first data taking at 3.5 TeV in 2011

Data taking at 3.5 TeV in 2011

After the optics tests, on october 2011, first data taking with the RPs has been done. The summary of the different fills used during the october period to allow for data taking is shown in Fig. 6.15. The first fills failed for different reasons. For instance, either the beam dumped because of a power supply tripped or because a self triggered beam dump happened. The intensities were at about 2.1×10^{11} protons per beam corresponding to two bunches at 7×10^{10} protons and 12 probe bunches at 1×10^{10} protons. The RPs were set at a distance of $6.5\,\sigma$. This distance n lower than 12 has been possible due to the background much smaller than expected and the fact that the collimators could be approached closer to the beam. As soon as the RPs have approached the beams, a view

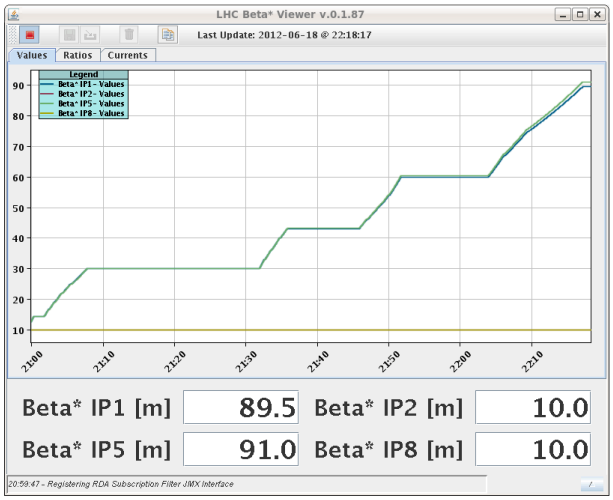

Figure 6.12: Screenshot from the Control Room of the β^* evolution during 90 m β^* optics re–commissioning.

of the RPs position is shown in Fig. 6.16 and the elastic rate has been visible as shown in Fig. 6.17. In the figure, we can also see that during the run, the RPs are beam centered. That's why relatively to the beam pipe center, the beam is shifted by 5.8 mm for A7R1 for instance. Finally, data taking has been performed during at least 5 hours with quiet beam allowing to collect about 90 k events. The hit map showing the events at one RP position in (x, y) after the background has been cut is shown in Fig. 6.18.
The beam is, as expected, expanded in y in order to catch the maximum number of elastic protons. The higher protons intensity is marked in blue – green.

Data taking at 4 TeV in 2012

The re – commissioning of the 90 m β^* optics in 2012 has again been a success. This has allowed, the 7th of July, to put the beams into collision for a data taking period with ALFA RPs (fill 2815). This data taking was performed at low intensity 90 m β^* of 2.1×10^{11} protons for beam 1 and 2.1×10^{12} protons for beam 2 with RPs at $6.5\,\sigma$, $8\,\sigma$ and $9.5\,\sigma$. The way the RPs are approached to the beam from the control room is shown in Fig. 6.19 with the example of the bottom pot from A7R1. The optimized luminosity for this run as seen on the lumiscan application from the control room is shown in Fig. 6.20.

A second data taking period has been performed the 11th and 12th July (fill 2830 and 2836). This run was at higher intensities about 8.9×10^{12} for both beams during the 8 hours of stable beams duration. This is illustrated in Figs. 6.21 and 6.22.

6.2.2 Physics Analysis and Results at the RPs

From the first significant data taking run the 20th of october 2011 from about 14h to 18h, a final plot approved by ATLAS collaboration has been produced and is shown in Fig. 6.23. This shows the reconstructed scattering angle correlation after cutting the background

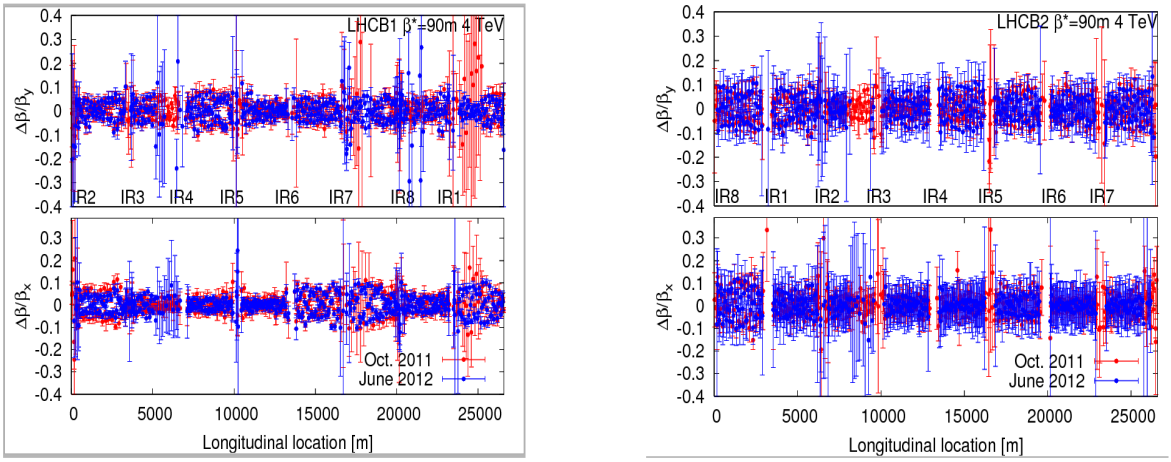

Figure 6.13: β beating measurements the 19th June for beam 1 (left) and beam 2 (right). The 2011 curve (in red) is compared the the 2012 measurements (in blue).

and using the combination of the left and right arm from ALFA. These data are used to compare with the simulation. In the t – reconstruction, there was some difference between the simulation and the data.

6.2.3 Ratios errors found between data and simulation

The first part of the study has been made by the analysis team to evaluate the difference between the matrix terms issued from simulation and the one extracted from the data [68]. The ratios on the matrix elements extracted from this study were mainly the matrix ratios from beam 1 and beam 2 (two different Roman Pots) as seen in table 6.6 and the scale factors for M_{12} and M_{34} (for Roman Pots on beam 1) as shown in table 6.7.

Table 6.6: Ratios constraints on the beam matrix elements coming from the data analysis of the 20th october 2011 run.

Ratios	Scale factor	Ratios from simulation
M_{12} (A7L1/A7R1) B2/B1	1.0065 ± 0.0062	1.0002
M_{12} (B7L1/B7R1) B2/B1	1.0031 ± 0.0042	0.9999
M_{34} (A7L1/A7R1) B2/B1	0.9978 ± 0.0041	1.0001
M_{34} (B7L1/B7R1) B2/B1	0.9981 ± 0.0037	1.0002
M_{34} (A7R1/B7R1) B1	1.0475 ± 0.0014	1.0483
M_{34} (A7L1/B7L1) B2	1.0476 ± 0.0021	1.0482

These ratios come from the different t –reconstruction method which were giving different results on the total cross section. The results are that the M_{12}/M_{22} ratios for one RP has to be larger from about 6.77 % which is a huge value. To understand the difference on the matrix term by this amount, a complete study has been performed. The search of

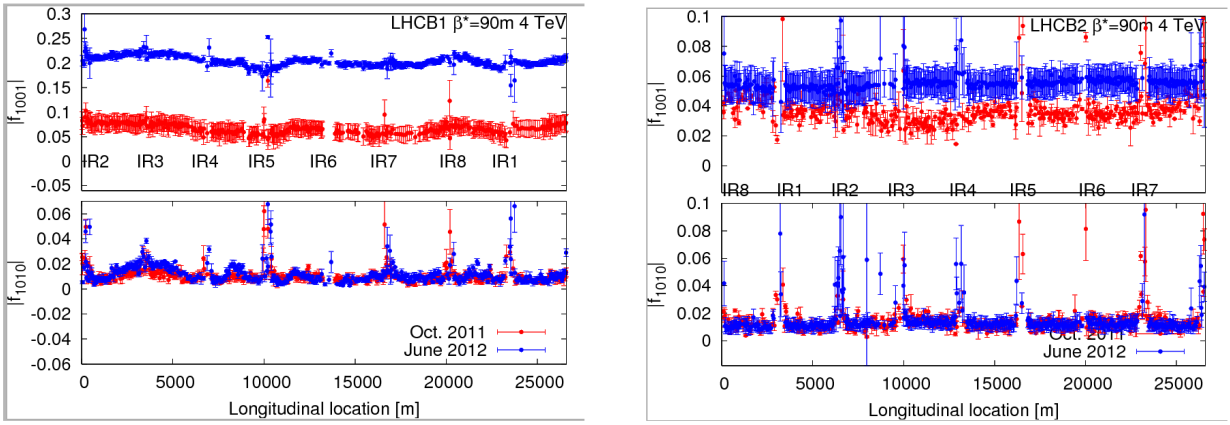

Figure 6.14: Coupling measurements the 19th June for beam 1 (left) and beam 2 (right). The 2011 curve (in red) is compared the the 2012 measurements (in blue).

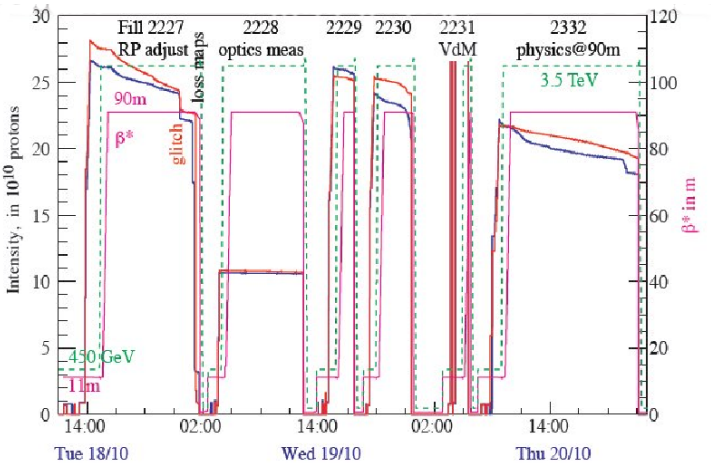

Figure 6.15: Summary of LHC fills for the 90 m β^* optics from the 18th of october to the 20th of october 2011

optics parameters or errors that could be responsible of the difference in the matrix terms between data and simulations are described in § 6.3.

6.3 Systematic uncertainties on the lever arm

The errors and effects on the 90 m β^* optics could affect the measurement as it was analysed. These first MDs have been used to evaluate the possible uncertainties given by the new values obtained with the experimental measurements. A study of errors on the beam matrix parameter called here the lever arm L_{eff} has been done [69] in order to determine what could lead to the biggest impact i.e. the maximum matrix error found in the complete ALFA simulation. Different problems have been identified and studied. The main ones are listed below.

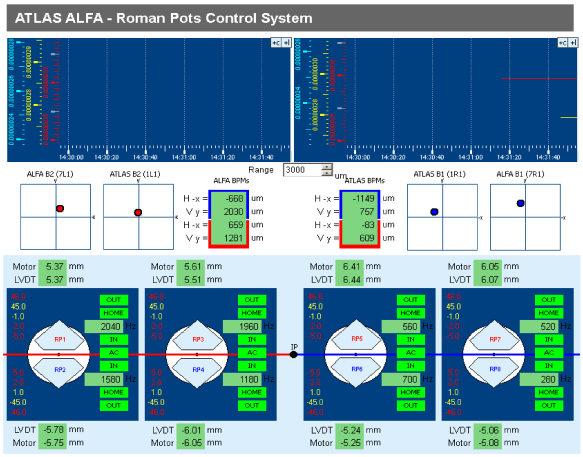

Figure 6.16: View of the Roman Pot control system from the ATLAS Control Room during 20th october 2011 data taking period.

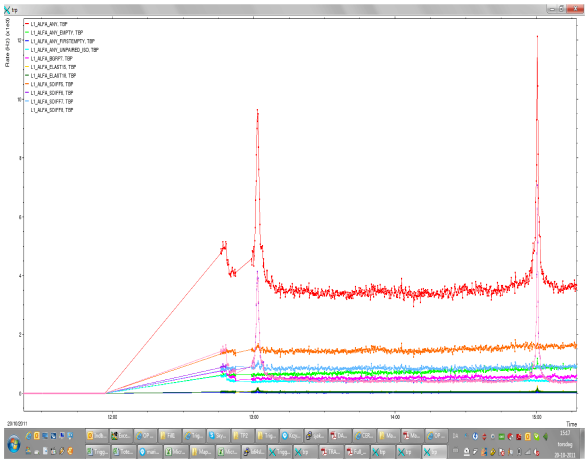

Figure 6.17: Elastic rates for all the RPs from the 20th october 2011 data taking period.

Table 6.7: Scale factors for the M_{12}/M_{22} and M_{34}/M_{44} ratios.

Ratios	Scale factor
M_{12}/M_{22} A7R1	1.0677 ± 0.0082
M_{12}/M_{22} B7R1	1.0575 ± 0.0060
M_{34}/M_{44} A7R1	1.0098 ± 0.0018
M_{34}/M_{44} B7R1	1.0104 ± 0.0016

6.3.1 Beam – beam effect

An effect that could impact on the lever arm value is the beam – beam effect. Beam – beam effect is quantified by the tune shift induced by a linear kick:

$$\Delta Q_x = \frac{-\beta_x}{4\pi}\frac{\Delta x'}{x} \tag{6.1}$$

For round beams, the linear beam – beam parameter ξ defined in (6.2) is equal to the tune shift.

$$\xi = -\frac{N r_0}{4\pi\epsilon_N} \tag{6.2}$$

N is the bunch population and r_0 the classical proton radius. Table 6.8 summarized the linear tune shift parameter for the emittance of $2\,\mu$m.rad used during the runs.

The beam – beam effect can be simulated by adding an equivalent quadrupole in the beam line. The L_{eff} is recalculated taking into account the new optics parameters. The results obtained, shown in table 6.9, consider a bunch population of 7×10^{10}. One can see that the beam – beam effect on $L_{eff,y}$ is of about 0.3 %. It seems to be the dominant

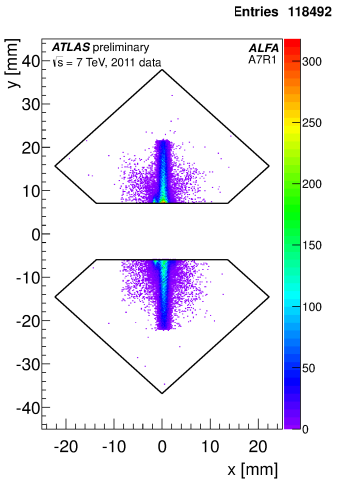

Figure 6.18: Hit maps for the A7R1 RPs detector [64] during the 2011 data taking period after background cut.

Table 6.8: Linear tune shift parameter for different bunch population and a normalized emittance of 2 μm.rad.

N	ξ
4×10^{10}	-0.00246
7×10^{10}	-0.00432
1.5×10^{11}	-0.00926

effect for the time being. Nevertheless, this effect can be corrected during a run, as the global tune is corrected, such as it won't impact the measurement.

6.3.2 Off momentum

The lever arm is completely correlated to the twiss parameters. A change in energy leads also in twiss parameters change. The lever arm has been computed for two different values of $\Delta p/p_0$. They are summarized in table 6.10. The impact of $\Delta p/p_0 = 0.001$ on the lever arm is non – negligible. But the off momentum energy at the LHC has been estimated close to 10^{-4} which means that we won't allow to reach this value. Anyway, 10^{-4} leads to a negligible difference in the lever arm.

6.3.3 Gradient field differences

Quadrupoles are defined by their magnetic fields and more over their strengths k (6.3). A modification of the strengths is directly linked to a modification of optics parameters ie a modification on the lever arm. The interest here concerns the quadrupoles located in IR1 around the Roman Pots.

$$k = \frac{1}{B\rho}\frac{\partial B_y}{\partial x} \tag{6.3}$$

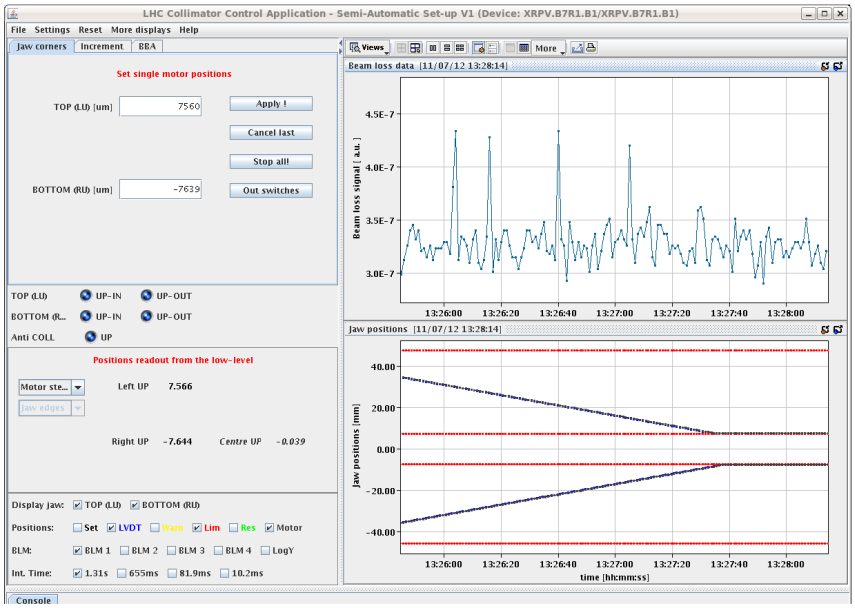

Figure 6.19: Roman Pots application showing the motion of B7R1 top and bottom during the 2^{nd} data taking 90 m β^* period in July 2012.

Table 6.9: L_{eff} uncertainty at each roman pots taking beam – beam effect into account.

Roman Pots	$\left\lvert\frac{\Delta L_{eff,x}}{L_{eff,x}}\right\rvert$ (%)	$\left\lvert\frac{\Delta L_{eff,y}}{L_{eff,y}}\right\rvert$ (%)
A7R1	0.1198	0.3015
B7R1	0.1664	0.3016
A7L1	0.1198	0.3015
B7L1	0.1664	0.3016

As already shown in Fig. 4.2, six quadrupoles are located before the RPs: the triplet Q1, Q2, Q3 and three more Q4, Q5, Q6. Quadrupoles up to Q13 are included to match the whole insertion to the rest of the LHC ring.

In order to estimate the errors on the k value for quadrupoles from Q1 to Q13, a JAVA interface has been provided [71]. The JAVA interface allows to find the strengths k values for each quadrupoles taking into account the real magnet currents used during the run coming from the TIMBER database [72]. On TIMBER, one can find all the parameters used during the run like intensities, β^* and a lot more. These values are then compared with the ones used in MAD – X to obtain the optics parameters listed in table 5.1. The gradient difference $\Delta k/k$ found are listed in table 6.11.

The largest error is close to 0.7×10^{-4} and located in the triplet. These new values have

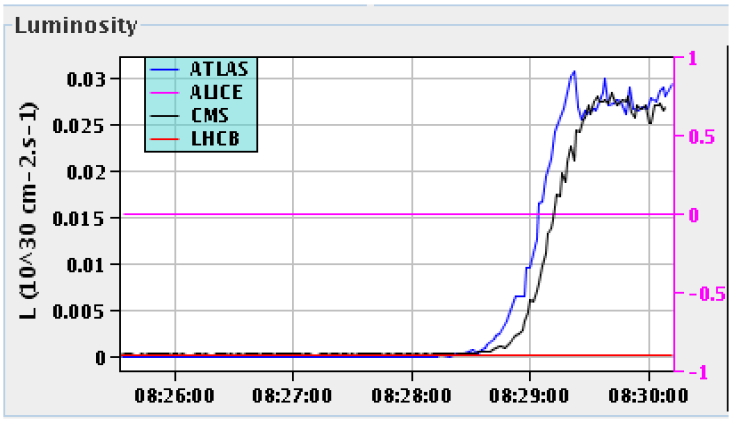

Figure 6.20: Luminosity for ATLAS (in blue) and CMS (in black) during the 90 m β^* data taking run the 7th July.

Figure 6.21: Intensities configuration as captured from the LHC op vistar during the 90 m β^* ALFA data taking.

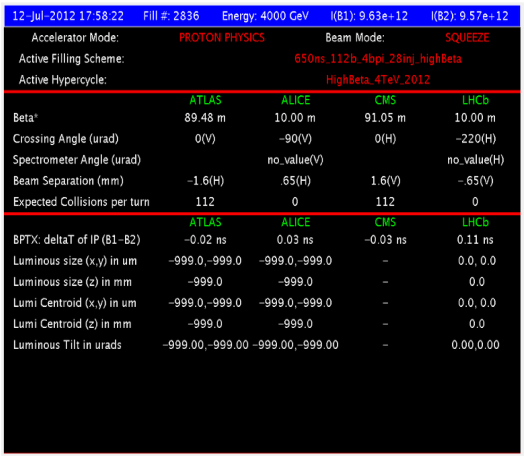

Figure 6.22: β^* configuration as captured from the LHC op vistar during the 90 m β^* ALFA data taking.

been implemented in MAD – X. Firstly, only quadrupoles in front of the Roman Pots ie quadrupoles Q1 to Q6 have been modified with the new k values and the impact on $L_{eff,y}$ estimated.

The uncertainty goes from 0.2×10^{-4} and 0.9×10^{-4}. Then, the same has been done with quadrupoles Q11 to Q13, have a larger gradient error than previous quadrupoles. But nevertheless, the ratio on the lever arm uncertainty stays between 0.2×10^{-4} and 0.9×10^{-4}. This allows to conclude that in this case, the impact of gradient errors on $L_{eff,y}$ is negligible.

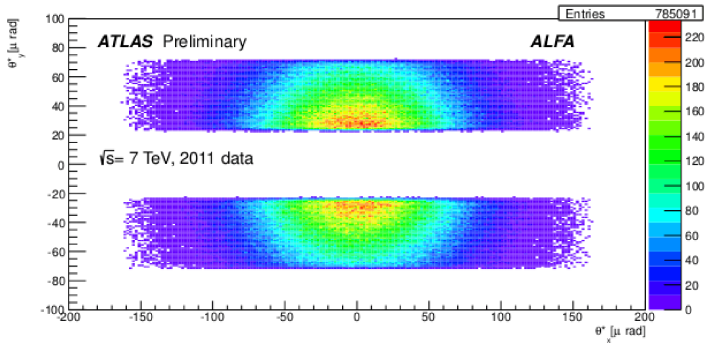

Figure 6.23: Reconstructed scattering angle correlation after background cut combining the left and right arm from ALFA [70].

Table 6.10: Table summarizing L_{eff} variations as a function of $\Delta p/p_0$.

$\Delta p/p_0$	$\Delta L_{effx}/L_{effx}$	$\Delta L_{effy}/L_{effy}$
0.0	0	0
0.001	0.8	0.12
0.0001	0.08	0.012

6.3.4 Misalignments

Misalignments or orbit distortions can affect the β – functions used to calculate the lever arm. The orbit is being corrected using orbit correctors so as the effect on magnet misalignments on the beam. But still, the orbit correction is not completely perfect. As we can see on Fig. 6.24 for beam 2, the RMS orbit is about 0.053 mm in horizontal and 0.061 mm in vertical.

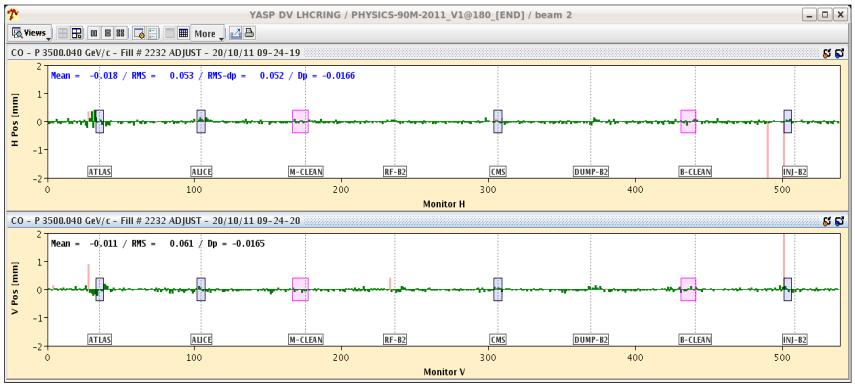

Figure 6.24: Orbit RMS from LHC elogbook during $\beta^* = 90$ m run for beam 2.

To ensure that orbit errors won't affect the lever arm and leads to systematic uncertainties, an arbitrary value has been chosen, higher than the RMS value. Quadrupoles will have a

Table 6.11: Gradient values used during the MD run for the 90 m β^* optics.

MadX strengths names	$\frac{\Delta k}{k}$
kqx.l1	-0.11×10^{-4}
ktqx.l1	-0.66×10^{-4}
ktqx2.l1	-0.1×10^{-4}
kqx.r1	-0.12×10^{-4}
ktqx1.r1	-0.67×10^{-4}
ktqx2.r1	-0.12×10^{-4}
kq4.r1b1	-0.11×10^{-4}
kq5.r1b1	-0.11×10^{-4}
kq6.r1b1	-0.11×10^{-4}
kqtl11.r1b1	0.06
kqt12.r1b1	-0.02
kqt13.r1b1	-0.17
kq4.l1b2	-0.15×10^{-4}
kq5.l1b2	-0.11×10^{-4}
kq6.l1b2	-0.11×10^{-4}
kqtl11.l1b2	0.14
kqt12.l1b2	-0.01
kqt13.l1b2	-0.01

misalignment of 1 mm. This misalignement is not really achievable but if this quite high misalignment value doesn't give significant errors, no realistic misalignments will give significant errors. Misalignements have been firstly applied on several quadrupoles from Q1 to Q6 and then, for more precise results with all quadrupoles in IR1, from Q1 to Q13. The results are summarized in table 6.12. Even for the high quadrupole misalignements value of 1 mm, the impact on the $L_{eff,y}$ value is still negligible.

6.3.5 Tracking and Acceptance results

A key parameter for the measurement is the experimental acceptance. This acceptance is determined by the complete simulation as described in chapter 4. The parameters identified as a source of errors for the acceptance are the crossing angle and emittances.

Crossing angle

Collisions for the measurement with the Roman Pots are head – on. But if an unexpected crossing – angle is added, the beam is shifted at Roman Pots location which can provide alignement considerations problems. The values for 10 μrad crossing angle (value measured by BPMs during the run) are listed in table 6.13. The mean offset found at the Roman Pots for a 1 μrad crossing angle in vertical y position is close to 0.3 mm whereas for 10 μrad the offset is close to 3 mm.

Table 6.12: Impact of quadrupoles misalignements on $L_{eff,y}$.

	$L_{eff,y}$
Without misalignements	277.804266
Q1 to Q6	277.804265
$\frac{\Delta L_{\mathrm{eff,y}}}{L_{\mathrm{eff,y}}}$	$< 10^{-4}$ negligible
Q1 to Q13	277.8042614
$\frac{\Delta L_{\mathrm{eff,y}}}{L_{\mathrm{eff,y}}}$	$< 10^{-4}$ negligible

Table 6.13: Unexpected crossing angle effect at IP1 on the beam position.

	10 μrad crossing angle in y	
Roman Pots	$\Delta x(\mu\mathrm{m})$	$\Delta y(\mathrm{mm})$
A7R1	2.4	2.7
B7R1	3.5	2.6
B7L1	-5.9	-2.7
B7L1	-6.9	-2.6

Emittances

During the run, the emittances have been measured using Wire Scanners. The emittances values measured for colliding bunches with 7×10^{10} protons are shown in table 6.14. To take into account the emittances errors, proton elastic generation used for acceptance calculation has been changed applying an error of $\pm$ 0.2 μm.rad. Then protons are tracked and the acceptance is computed. The final acceptance has been compared to the acceptance result without any emittance errors. Both acceptance are shown in Fig. 6.25 and numerical acceptance parameters are summarized in table 6.15.

Table 6.14: Emittance measurements and errors during fill 2232 for bunch intensity of 7×10^{10} protons.

	$\epsilon_{x,N}$	$\epsilon_{y,N}$
Beam 1	2.302 $\pm$ 0.220	1.748 $\pm$ 0.064
Beam 2	2.362 $\pm$ 0.236	1.999 $\pm$ 0.022

If the emittance increases of about 0.2 μm.rad, looking only at the elastic protons that

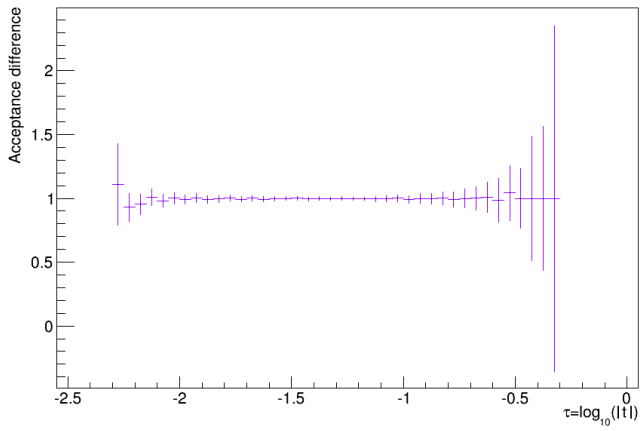

Figure 6.25: Acceptance difference with and without emittances errors.

Table 6.15: Emittances measurements and errors during fill 2232 for bunch population of 7×10^{10} protons.

	$\left\lvert\frac{\Delta Acc}{Acc}(total)\right\rvert$ (%)	$\left\lvert\frac{\Delta Acc}{Acc}(8\sigma)\right\rvert$ (%)
Beam 1	0.002	0.20
Beam 2	0.001	0.20

have hitten the sensitive area of the detectors and when the detectors are located at $8\,\sigma$, the error generated on the acceptance is about 0.2 %. As the error is non negligible, the exact emittance values will be taken into account in the complete simulation i.e. in the elastic protons generation.

6.3.6 Longitudinal misalignements and corrected magnetic lengths

The two ideas that came in then were the longitudinal misalignements impact and magnetic lengths exact values. Longitudinal misalignements appear to change quite a lot the matrix terms and after some investigations, it also appear that the magnetic length could change, as the energy was not the 7 TeV planned at the beginning but 3.5 TeV. Then, the current won't be the same, and the magnetic lengths could vary slightly. A survey study has been performed [73] to measure both longitudinal misalignements and magnetic lengths. Both studies are described below:

Longitudinal misalignments

A first study was performed with different longitudinal misalignements (s location), to evaluate what kind of misalignement would be necessary to reach the 6.7 % increase for M_{12}/M_{22}. Different configurations have been studied and compared with different softwares (MAD – X, Mathematica). Table 6.16 summarizes the longitudinal misalignements

for A7R1.

Table 6.16: Impact of longitudinal quadrupoles misalignements on the different matrix terms for A7R1.

Longitudinal misalignments applied	$\Delta M_{11}/M_{11}$	$\Delta M_{12}/M_{12}$	$\Delta M_{21}/M_{21}$	$\Delta M_{22}/M_{22}$
Q1, Q2 and Q3 by 5 cm	-0.0048	0.6	-0.13	-0.1
Q4, Q5 and Q6 by 5 cm	0.077	-0.31	0.13	-0.036
All quadrupoles by 5 cm	0.072	0.28	0	-0.14
Q1 and Q3 by 5 cm	0.0037	2.89	-0.59	-0.52
Longitudinal misalignments applied	$\Delta M_{33}/M_{33}$	$\Delta M_{34}/M_{34}$	$\Delta M_{43}/M_{43}$	$\Delta M_{44}/M_{44}$
Q1, Q2 and Q3 by 5 cm	4.34	-0.023	0.15	-0.021
Q4, Q5 and Q6 by 5 cm	-2.42	0.078	-0.15	0.027
All quadrupoles by 5 cm	1.92	0.056	$-4,3 \times 10^{-06}$	0.006
Q1 and Q3 by 5 cm	-49.7	0.24	-1.67	0.21

The 5 cm misalignments were applied in order to check what could happen in a pretty bad situation. In the table, all matrix elements are shown for different misalignements configuration. The maximum reached for M_{12} is 2.88 %. Still, even 5 cm seems to be not enough. The same has been done for the other Roman Pots B7R1, giving approximately the same results on the $\Delta M/M$.
The second step was to use the measurements on the longitudinal position mentioned above. The following results were extracted and are shown in table 6.17. This shows

Table 6.17: Longitudinal position difference between MAD–X simulated values and measurements for Q1 to Q6 quadrupoles for beam 1.

Quadrupoles	Nominal longitudinal position	Corrected longitudinal position	Difference (mm)
MQXA.1R1	26.15	26.156	5.7
MQXB.A2R1	34.8	34.797	-3.4
MQXB.B2R1	41.3	41.297	-3.4
MQXA.3R1	50.15	50.156	6.0
MQY.4R1.B1	169.553	169.549	-3.8
MQML.5R1.B1	196.49	196.492	2.1
MQML.6R1.B1	228.39	228.390	0.0

that the longitudinal misalignments should not reach more than 6 mm difference which is much lower than the 5 cm used before.

Corrected magnetic lengths L_{mag}

The initial MAD – X sequence has been established with the magnetic lengths determined for nominal LHC configuration for 7 TeV energy per beam. But these values are not completely exact for the LHC at 3.5 TeV beam energy. The magnetic lengths have been then corrected and included in the MAD – X setup simulation as listed in table 6.18. These corrected magnetic lengths have an impact not only on the lever arm results but on

Table 6.18: Magnetic lengths differences between nominal LHC values and corrected values for 3.5 TeV beam energy.

Quadrupoles	Corrected L_{mag}	Nominal L_{mag}
MQXA.1R1	6.364	6.37
MQXB.A(B)2R1	5.497	5.5
MQXA.3R1	6.364	6.37
MQY.4R1.B1	3.4	3.4
MQML.5R1.B1	4.8	4.8
MQML.6R1.B1	4.8	4.8

all the matrix elements. From the measurements, one can see that the magnetic lengths are reduced. We'll call R_x the ratio M_{12}/M_{22} and R_y the ratio M_{34}/M_{44}. Comparing the matrix term ratios from ALFA data, we found $\Delta R_x/R_x$ = -1.2 % and $\Delta R_y/R_y$ = 0.01 % for A7R1. For B7R1, this gave $\Delta R_x/R_x$ = -0.9 % and $\Delta R_y/R_y$ = 0.02 %. This was done for both beams. The R_x ratio is negative which is in the opposite direction than the one expected for this ratio. The R_y ratio goes to the right direction but is still far away from the expected result. The modified magnetic lengths is not an answer to the ratios difference.

Summary

Both corrected longitudinal position and corrected magnetic lengths have been simulate with MAD–X to check the matrix terms evolution. Including both, the results on the R_x and R_y ratios are the following:

- M_{12}/M_{22} (A7R1) = 0.9888 and M_{12}/M_{22} (B7R1) = 0.9911
- M_{34}/M_{44} (A7R1) = 1.0002 and M_{34}/M_{44} (B7R1) = 1.0002

This is far from the ratios constraints defined at the beginning. Longitudinal misalignements are not enough large to induce the ratio errors expected and the corrected smaller magnetic lengths induce a smaller M_{12}/M_{22}. This leads to the fact that gradients induce larger possible errors in the matrix terms. This is the next study.

6.3.7 Strengths errors up to ± 0.1 %

The k strengths for the triplets (kqx.r1, ktqx1.r1 and ktqx2.r1) have been varied from ± 1/1000 which was the highest possible error foreseen for these magnets. Several com-

binations have been tried with $\pm 1/1000$ for each strengths. The maximum value found in this case for the lever arm was 0.7 % larger than the initial value which is still far away from the 6.7 % (table 6.7). The quadrupoles strengths values having a small but non negligible effect, a mimimization has been started [74] in order to check what kind of strengths set was fulfilling the ALFA contraints. The study at the time this PhD is written, was not finished.

Conclusion

The 90 m β^* optics has been tested on LHC and was a success. Optics measurements were done in addition to data taking. The lever arm has been extensively studied using different possible source of errors (misalignements, strengths errors, magnetic lengths etc....) explaining the difference observed between data and simulation. The main source of errors have been identified and are further investigated in order to calculate the total cross section and cross check the results with the different t –reconstruction methods.
But as already mentioned, the 90 m β^* optics is an intermediate optics which is not enough to reach the coulomb region. For this, new high β^* optics with β^* up to 500 m and 1 km have been made and this is the purpose of the next chapter.

Chapter 7

High β^* 500 m and 1 km optics

Contents

The experience gained with the 90 m β^* optics in 2011 helped to create new high β^* optics up to 500 m [75] and 1 km β^*. These optics are very useful for ALFA as they are needed to reach the coulomb region (§ 5.1.1). This is illustrated on Fig. 7.1. The $-t_{min}$ calculated using (3.17) is equal to 1.14×10^{-4} GeV^2 with 4 TeV beam energy, $\epsilon_N = 1.5$ μm.rad and $n = 4.5\,\sigma$. From previous experience, the RPs distance n was smaller than the one planned for the very high β^* optics (2625 m). This means, one can take smaller values for the calculation than it was done in the ALFA TDR. These new optics will be described here with the main parameters and the commissioning experience gained in 2012.

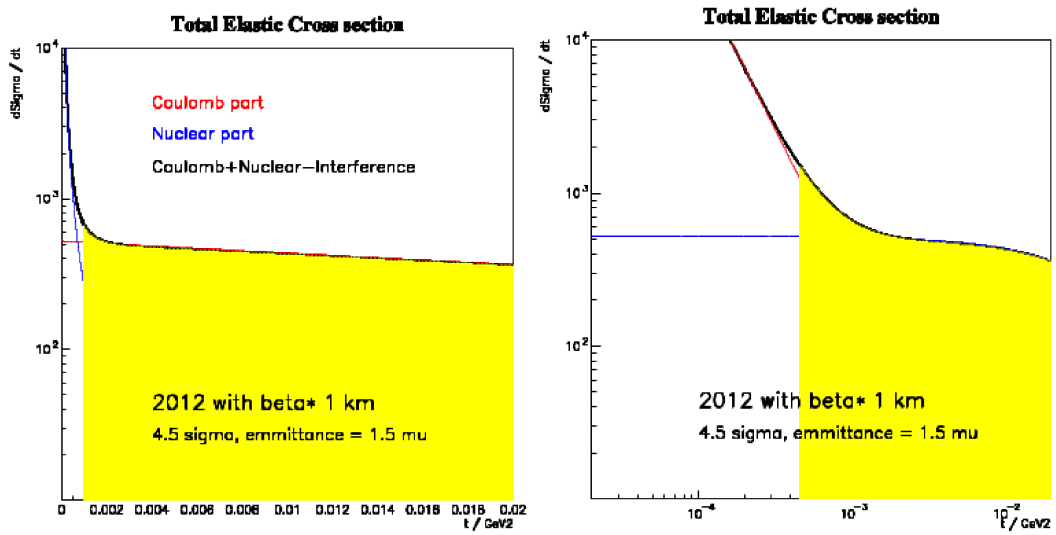

Figure 7.1: Minimun t – value achievable with $\beta^* = 1$ km, $\epsilon_N = 1.5$ μm.rad and $n = 2.5\,\sigma$ [76]. The right part of the figure is a zoom of the left part showing more precisely the achievable region.

7.1 High β^* optics

7.1.1 Main parameters

The de – squeeze for 500 m and 1 km β^* optics starts after the 90 m β^* optics de – squeeze. Both high β^* optics have been matched the same way as the 90 m β^* optics taking the beam 1 over beam 2 ratio strengths into account ($0.5 <$ b2/b1 < 2). The de – squeeze is enough smooth with sufficiently small steps to respect this strengths ratio. The total number of steps is 13 to go up from $\beta^* = 90$ m to $\beta^* = 500$ m and only 5 steps are necessary to go from $\beta^* = 500$ m to 1000 m. The matching has first be done for IP5 using TOTEM RPs at 220 m, only the last step has been adapted for ALFA with a phase advance of $\pi/2$ at 240 m instead of 220 m. The constraint on the x phase advance was relaxed.

A summary of the main parameters for both optics are shown in table 7.1 and table 7.2. The β and dispersion functions around IP1 are shown on Fig. 7.2. The high β^* optics can be achieved up to 1000 m by simulation. Like the 90 m β^* optics, one need to commission them in order to validate their feasibility.

If we compare the 1000 m β^* optics with the 90 m β^* optics, at 1000 m β^* optics, the divergence at IP1 is reduced by a factor 5 and the beam size is increased by a factor 3. At the Roman Pots, for the 1000 m β^* optics on beam 1, β_y is strongly lower by 750 m oppositely to β_x which is larger by 95 m. This reduces the vertical beam size at the A7R1 by a factor 4. The vertical phase advance is equal to 90° in all the optics and the horizontal phase advance gets closer to 180° during the increase in β^* ($\mu_x = 186°$ for $\beta^* = 90$ m and $\mu_x = 180°$ at B7R1).

Table 7.1: 500 m optics parameters for beam 1, at 4 TeV beam energy and for an emittance of $\epsilon_N = 2\,\mu$m.rad (LHC version V6.503).

IP1		**RPs**	
ϵ_n (μm)	2.0	β_x (m)	246.3 – 220.8
β_x^* (m)	500	β_y (m)	184.8 – 175.1
β_y^* (m)	500	σ_x (μm)	340 – 322
α_x^*	0.0	σ_y (μm)	294 – 287
D_y^* (m)	0.0	σ_x' (μrad)	1.38 – 1.46
$D_y^{*\prime}$	0.0	σ_y' (μrad)	1.59 – 1.64
σ^* (mm)	0.484	$\Delta\mu_x$ (2π)	0.496 – 0.499
$\sigma^{*\prime}$ (μrad)	0.97	$\Delta\mu_y$ (2π)	0.248 – 0.251

Table 7.2: 1000 m optics parameters for beam 1, at 4 TeV beam energy and for an emittance of $\epsilon_N = 2\,\mu$m.rad (LHC version V6.503).

IP1		**RPs**	
ϵ_n (μm)	2.0	β_x (m)	289.3 – 259.3
β_x^* (m)	1000	β_y (m)	103.4 – 99.9
β_y^* (m)	1000	σ_x (μm)	368 – 349
α_x^*	0.0	σ_y (μm)	220 – 217
D_y^* (m)	0.0	σ_x' (μrad)	1.27 – 1.34
$D_y^{*\prime}$	0.0	σ_y' (μrad)	2.13 – 2.17
σ^* (mm)	0.985	$\Delta\mu_x$ (2π)	0.498 – 0.500
$\sigma^{*\prime}$ (μrad)	0.69	$\Delta\mu_y$ (2π)	0.246 – 0.252

7.1.2 High β^* optics strategy

The first step for the commissioning for the 500 m and 1000 m β^* optics was to start from the 90 m β^* optics with the new set of optics files. Then with dedicated beam time for optics, the idea was to perform the de – squeeze up to 500 m without crossing bunches and another run this time with separation. Then, if things goes extremely well and with enough beam time, the strategy was to go up to 1000 m. After the optics commissioning, data taking could be performed for ALFA also with dedicated beam time.

7.2 ALFA simulation with High β^* optics

7.2.1 Generation and tracking

The generation has been adapted in the two different cases ie $\beta^* = 500$ m and 1 km. The parameters included in the generation are the same as the 90 m β^* optics except the optics parameters like the beam size and the beam divergence which are different. The t – generation has been performed and is shown in Fig. 7.3.

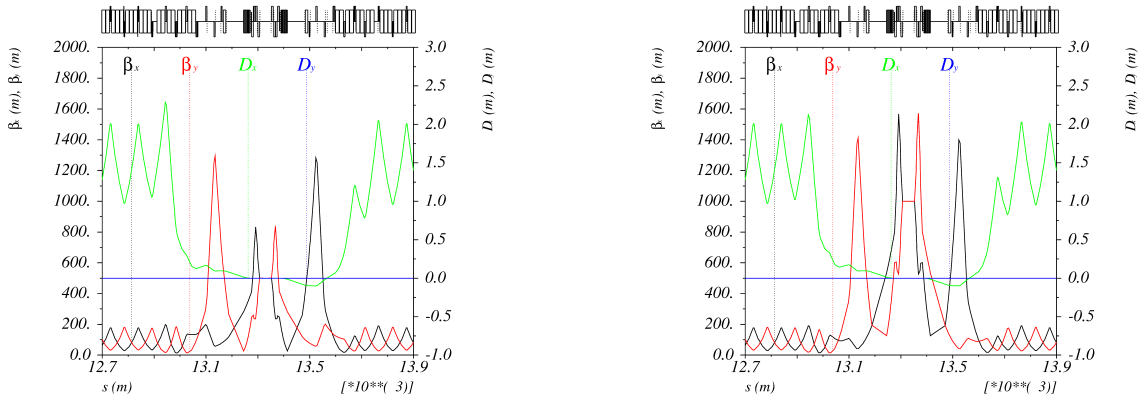

Figure 7.2: β and dispersion functions for beam 1 for the 500 m (left) and 1000 m (right) β^* optics around IP1.

Tracking has then be performed for 100 000 particles for both optics to give the lever arms needed for ALFA analysis and to give an overview on the experimental acceptance in order to be able to compare with previous intermediate optics.

7.2.2 M_{12} and M_{34} lever arms

The lever arms comparison between the three different optics is shown in table 7.3. The

Table 7.3: M_{12} and M_{34} lever arms comparison for 90 m, 500 m and 1000 m β^* optics with A7R1 and B7R1 on beam 1.

	Roman Pots	$M_{12} = L_{eff,x}$	$M_{34} = L_{eff,y}$
90 m β^* optics	A7R1	-10.288	277.831
	B7R1	-13.018	265.021
500 m β^* optics	A7R1	8.97	303.996
	B7R1	2.582	295.841
1000 m β^* optics	A7R1	7.721	321.418
	B7R1	-0.404	316.075

high β^* optics have been optimized for the vertical direction y. $L_{eff,y}$ increases with β^* whereas on the contrary $L_{eff,x}$ is strongly reduced despite the increase in β^* due to phase advance approaching the 180° value in the 1000 m β^* optics case. The lever arms in table 7.3 have been calculated taking into account the measured longitudinal position of the Roman Pots as stated in § 5.3.3.

7.2.3 Acceptance

The complete ALFA simulation described in chapter 4 has been performed for the 500 m and the 1000 m β^* optics. The result in terms of acceptance is shown on Fig. 7.4. As

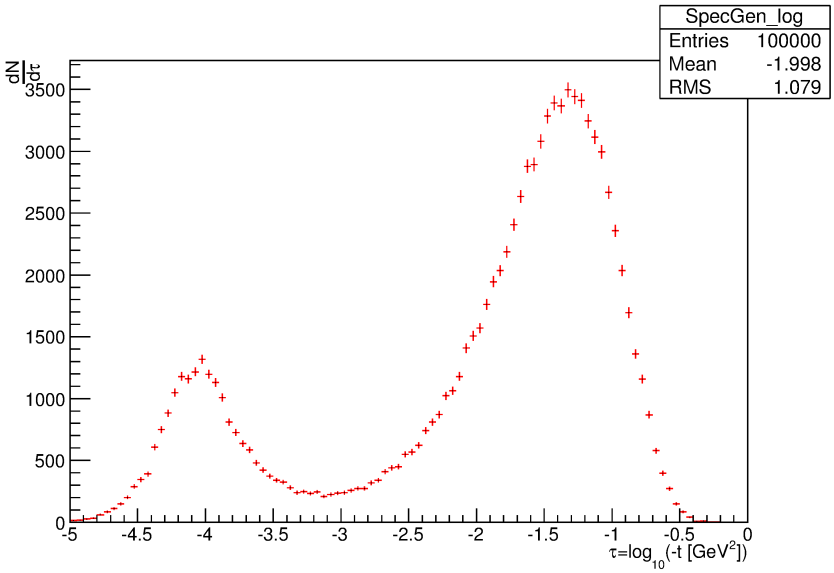

Figure 7.3: Generated spectrum for 1 km β^* optics with $b = 20$, $\rho = 0.14$, $\sigma = 985$ μm and σ' = 0.69 μrad and a minimum limit for t: $t_{min} = 4.0 \times 10^{-5}$ GeV^2.

shown on the acceptance plot, to get an acceptance of at least 50%, the t – value will be higher than the minimum one calculated. If we perform a t_{min} calculation for the three high β^* optics, we find the result in table 7.4. The t_{min} values are comparable to the

Table 7.4: t_{min} values as calculated from (3.17) with $\epsilon_N = 2\mu$m.rad and 4 TeV beam energy.

Optics	$-t_{min}$ (GeV^2) (n = 8)	$-t_{min}$ (GeV^2) (n = 4.5)
90 m β^* optics	$\log_{10}(5.34 \times 10^{-3})$ = -2.27	$\log_{10}(1.7 \times 10^{-3})$ = -2.77
500 m β^* optics	$\log_{10}(9.61 \times 10^{-4})$ = -3.02	$\log_{10}(3.04 \times 10^{-4})$ = -3.52
1000 m β^* optics	$\log_{10}(4.8 \times 10^{-4})$ = -3.32	$\log_{10}(1.5 \times 10^{-4})$ = -3.82

one found in the acceptance plot for each optics. If we consider now a closer approach to the beam reacheable during the run, we can see that the used values take into account the reacheable optics parameters (like ϵ_N) coming from the commissioning of the 90 m β^* optics. The t_{min} value reaches the coulomb region ($t < 10^{-3}$) with 1000 m β^* optics but we have to take into account the acceptance values above 50% and in this case, the coulomb region is nearly reached ($\log(t) \sim -3$) but one need to go to higher β^* to really reach the coulomb region.

7.3 Optics commissioning

In 2012, some MDs time was dedicated to high β^* optics in order to able data taking for TOTEM and ALFA with higher β^* optics than in 2011. The same strategy has been applied for 500 m and 1000 m β^* optics as for the 90 m β^* optics. A summary of the

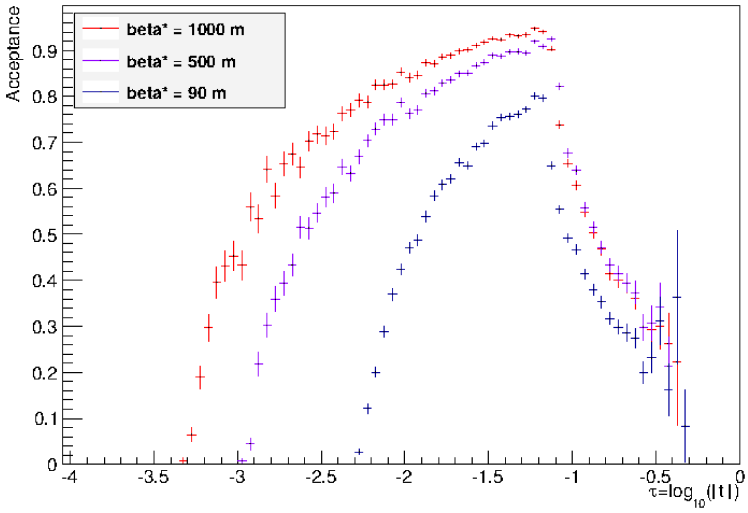

Figure 7.4: Acceptance comparison for the three high β^* optics: 90 m, 500 m and 1000 m at 4 TeV, $n = 8$ and with $\epsilon_N = 2$ μm.rad.

different successfull fills performed in 2012 for both optics studies and data taking with Roman Pots for 500 m and 1000 m β^* optics is shown in table 7.5.

Table 7.5: Summary of some of the successfull MDs fill for 2012 for 500 m and 1000 m β^* optics.

Fill	Date	Action
2740	05/05/11	500 m β^* optics commissioning without collisions
2751	28/06/11	500 m β^* optics commissioning with separation
2769	23/08/11	1000 m β^* optics commissioning with separation
3060	30/09/11	MDs for optics measurements
3216	24 – 25/10/12	Data taking period with RPs at 4.5 and then $3\,\sigma$

The 500 m β^* optics has been reached with success, first without collisions and without separation. Then the 500 m β^* optics has been tested with the separation of the two beams at IP1 and IP5. And for the first MD with $\beta^* = 1000$ m, it was successfully achieved with the separation.
This has allowed the final goal which is data taking with ALFA Roman Pots with these higher β^* optics. During the run, the Roman Pots were approached down to $3\,\sigma$. Now, the commissioning of these optics will be described briefly.

7.3.1 Dry runs

As for the 90 m β^* optics, dry runs have been performed to check the settings for hardware commissioning. The plots representing these dry runs where no major problems were found are shown in Fig. 7.5.

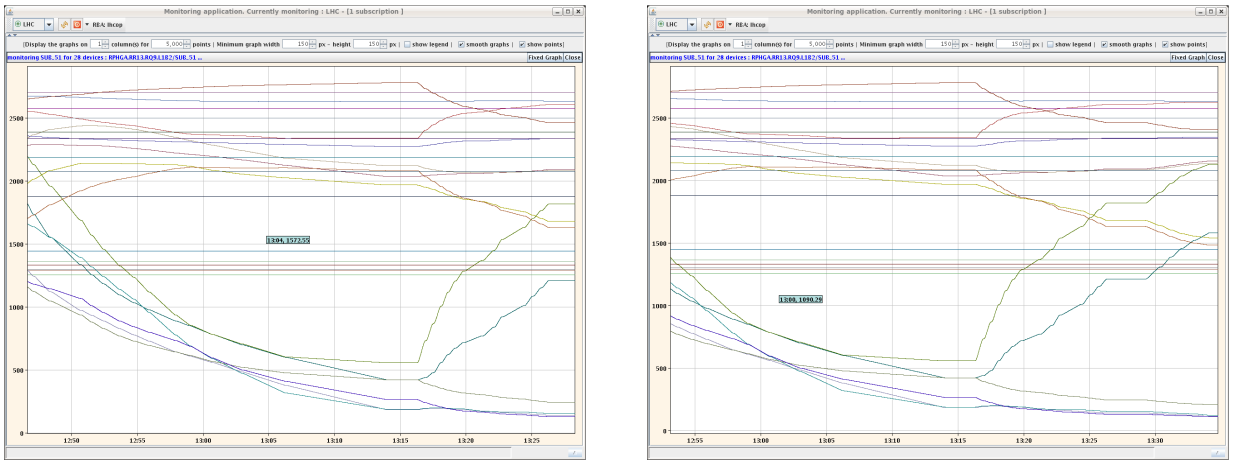

Figure 7.5: Screenshot from the Control Room of the quadrupoles first hardware commissioning on IP1 for the 500 m (left) and the 1000 m (right) β^* optics corresponding to driving magnets without beam.

The dry run has been successfully performed and has allowed to start the 500 m and 1000 m β^* optics commissioning.

7.3.2 De – squeeze

All the de – squeeze starts from 11 m injection to go up to 90 m and then, 500 m and if everything goes well up to 1000 m. As a reminder, a minimum of 35 minutes were necessary to reach the $\beta^* = 90$ m at 3.5 TeV beam energy. The de – squeeze up to 500 m is shown in Fig. 7.6. The values for the 500 m de – squeeze are taken from the TIMBER

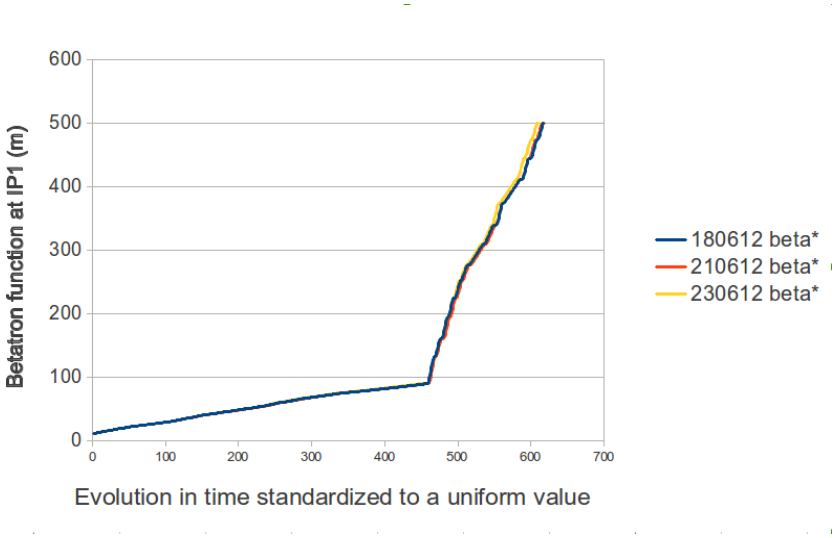

Figure 7.6: 500 m desqueeze during 3 different fills in 2012.

database and illustrates the global behaviour during several fills. And the de – squeeze up

to 1000 m is shown in Fig. 7.7. When $\beta^* = 90$ m is achieved, increasing up to 500 m takes

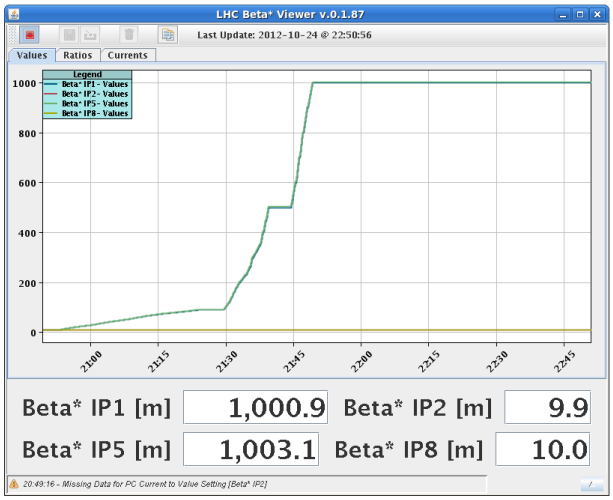

Figure 7.7: 1000 m desqueeze during the data taking period with Roman Pots the 24th october 2012.

approximately 10 minutes and increasing again from 500 m to 1000 m takes at minimum 5 minutes. The de – squeeze up to 1000 m has been a success and has allowed a data taking period for ALFA Roman Pots.

7.3.3 β beating

The β beating has been measured for 500 m and 1000 m. The results are shown on Fig. 7.8. The results have also been captured after measurements with AC dipole [15] in the LHC elogbook. In general, β beating went well and has been corrected for both beams

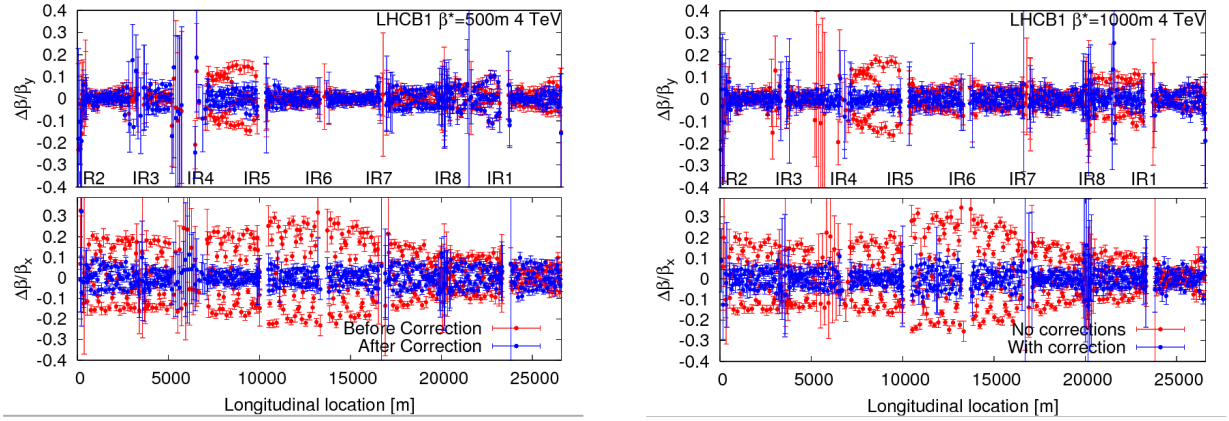

Figure 7.8: Evolution of the beta beating during the de – squeeze up to 500 m (left) and 1000 m (right) for beam 1.

for both 500 m and 1000 m β^* optics. During the optics measurements on the 1000 m run, the beta beating was less than 10 % after corrections have been applied.

7.3.4 Emittances measurements

Table 7.6: Emittance measurements performed the 24th october 2012 before data taking for the three optics steps: 90 m, 500 m and 1000 m.

Emittances	90 m optics	500 m optics	1000 m optics
Horizontal beam 1	1.71 ± 0.25	1.71 ± 0.25	1.83 ± 0.25
Vertical beam 1	1.29 ± 0.3	1.33 ± 0.3	1.3 ± 0.3
Horizontal beam 2	3.54 ± 0.4	3.64 ± 0.3	3.31 ± 0.3
Vertical beam 2	1.52 ± 0.4	1.57 ± 0.4	2.24 ± 0.4

The emittances were measured as shown in table 7.6 for both beams during high β^* runs with the Wire Scanners [13] by the operation team. The measured values shown in table 7.6 can also be found on the LHC elogbook. We can see that during the de – squeeze that occured the 24th october 2012 for ALFA data taking period, from 90 m to 1000 m, the emittances were about the same for both beams. These values are of great interest for ALFA proton generation and simulation.

7.4 Data taking period at the Roman Pots

The Roman Pots have taken data only for the 1000 m β^* optics. During the run, the RPs have been closed down to $n = 4.5\,\sigma$ and $3\,\sigma$ which correspond to beam sizes of respectively 3 mm and 2 mm with 4 TeV beam energy and $\epsilon_N = 2$ μm.rad. This gives a reacheable $t_{min} = 1.5 \times 10^{-4}$ in the case of n = $4.5\,\sigma$. The way the pots were approached during the run is shown in Fig. 7.9.
The data analysis has started for the 1000 m β^* optics and it has pointed out the problem on the low t – resolution found due to the value of the horizontal phase advance. Indeed, this parameter induces a very low lever arm for B7R1 (± -0.40 m) as it has been seen in table 7.3 and this has a direct impact on the t – resolution when using the substraction method. One idea that has been given to improve this was to move the B7R1 station further by 6 cm in order to increase the horizontal lever arm. It increases the t – resolution by 80 %. The feasibility for this is in study.

Conclusion

The 1000 m high β^* optics is a successfull achievement. Everything went quite well during the commissioning. Optics corrections were applied and data taking was possible after the dedicated optics MDs. But this optics is not enough to reach the coulomb region or the very small scattering angles as it has been seen on the acceptance plots. But the possibility to remove the beam 1 over beam 2 ratio by adding additional cables to the quadrupoles would give more flexibility for the matching. It will help to avoid the 180° horizontal phase advance and the necessity of Q4 inversion. Furthermore, the normalized

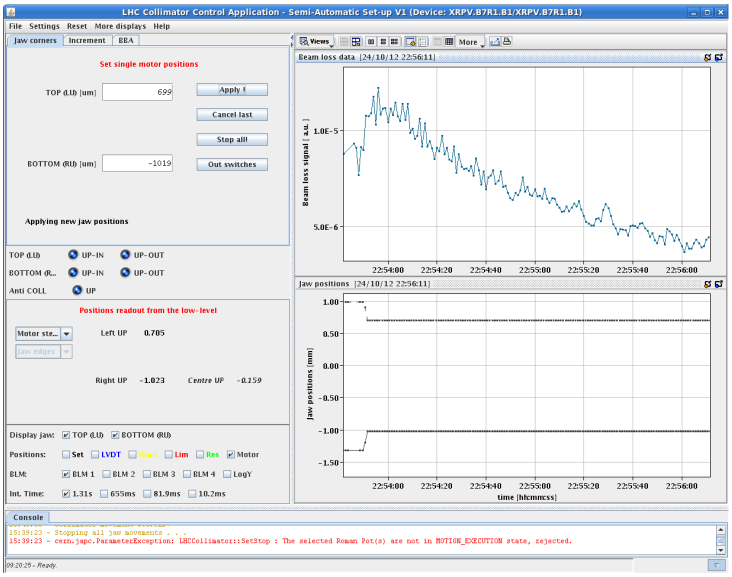

Figure 7.9: Roman Pot B7R1 at $3\,\sigma$ during the data taking period the 24th October 2012.

emittance is smaller and the distance n is smaller. There is a high possibility that to reach the coulomb regime, a β^* equals to 2625 m won't be needed.

Conclusion

The main purpose of this PhD was to study the intermediate optics ($\beta^* = 90$ m) and to use them, including errors, in order to understand the impact on the ALFA simulation. The 2625 m high β^* optics has been studied in order to understand the key parameters. Then, the work has first concerned the use of this optics parameters for the ALFA simulation package where after misalignements errors were included. Different twiss files have been produced on demand in order to feed the ForwardPackage code implemented in ATLAS simulation by the soft-sim ALFA group. This was true for all the high β^* optics.

Then, the work has focussed on the 90 m high β^* optics, after having implemented the last step to reach the 90° phase advance at 240 m where the RPs are located, a first acceptance study was done and the minimum scattering angle that could be achieved was checked. Even if the coulomb regime is not reached with the $\beta^* = 90$ m optics, it has allowed to evaluate the impact of longitudinal RPs misalignement on the lever arm and to justify the more precise measurement of the RP position. The impact of the ATLAS solenoid was also checked and has no effect on the lever arm.

During the commissionning of the 90 m β^* optics at 3.5 and 4 TeV, by extracting the LHC data from TIMBER, the de-squeezes have been studied in more details and compared. Optics measurements were performed and could be used for ALFA simulation and acceptance calculation. Also, during the commissionning, the emittance appears to be smaller than the one previously planned which was also implemented in ALFA simulation. Then, data at the Roman Pots have been performed. But the three different t – reconstruction method were not converging on the total cross section measurement. Ratios coming from the analysis were showing a difference on the matrix elements at the RPs between data and simulations. A more extensive study on the lever arm ($= M_{12}$) which is the key parameter in the t – reconstruction, has been performed in order to check its robustness. Different kind of errors (quadrupoles strengths k, beam-beam effect, misalignments) have been studied. The optics parameters incriminated are the longitudinal misalignments of the magnets and the quadrupoles strengths.

The last step was to study the experimental acceptance results on the 500 m and 1000 m high β^* optics and to attend the first commissionning part concerning the de – squeeze. The results are encouraging and higher β^* will be welcome in the future.

Indeed, the main goal of ALFA is to reach the coulomb region which means reaching

higher β^* values up to 2625 m with a phase advance in x different from 180°. This goal is challenging as this very high β^* optics needs to fulfil the beam 1 over beam 2 ratio even if some actions have been taken to get rid of it and new features have not been tested yet like the injection with Q4 polarity change, no separation and a 1μm.rad normalized emittance. And also all this needs time during LHC runs which can be difficult to get.

Nevertheless, the good experimental results reached on optics parameters like the smallest normalized emittance and the smallest distance n of the Roman Pots detectors, may allow to reach the coulomb regime with a $\beta^* < 2625$ m. This is promising for the future of ALFA after the LHC longshutdown LS1.

Bibliography

[1] O. S. Brüning, P. Collier, P. Lebrun, S. Myers, R. Ostojic, J. Poole, and P. Proudlock *LHC Design Report*, CERN, Geneva, 2004.

[2] *LEP Design Report*, CERN-LEP/84-01, CERN, Geneva, 1984.

[3] The ATLAS collaboration, *The ATLAS experiment at the CERN LHC*, JINST, 3:S08003, 2008.

[4] The CMS collaboration, *The CMS experiment at the LHC*, JINST, 3:S08004, 2008.

[5] ATLAS Collaboration, *ATLAS Forward detectors for Measurement of Elastic Scattering and Luminosity*, Technical Design Report, CERN/LHCC/2008-004, 2008.

[6] M. Bozzo et al., *Measurement of the Proton-Antiproton Total and Elastic Cross Sections at the CERN SPS Collider*, Phys. Lett. B147, 1984.

[7] G. Anelli et al., *The TOTEM experiment at the CERN LHC*, JINST, 3:S08007, 2008.

Chapitre 1

[8] The LHCb collaboration, *The LHCb detector at the LHC*, JINST, 3:S08005, 2008.

[9] The ALICE collaboration, *The ALICE experiment at the CERN LHC*, JINST, 3:S08002, 2008.

[10] O. Adriani et al., *The LHCf detector at the CERN LHC*, JINST, 3:S08006, 2008.

[11] J. Wenninger, *The LHC machine*, GIF2012, Orsay, France, 2012.

[12] J. P. Koutchouk, *Measurement of the Beam Position in the LHC Main Rings*, LHC-BPM-ES-004, 2002.

[13] F. Roncarolo, *Accuracy of the transverse Emittance Measurements of the CERN Large Hadron Collider*, Thèse de doctorat, Ecole Polytechnique Fédérale de Lausanne, 2005.

[14] P. Castro, *Luminosity and beta function measurement at the electron-positron collider ring LEP*, Doctoral Thesis, CERN, Geneva, 1996.

[15] R. Tomàs et al., *the LHC optics in practice*, 2nd Evian 2010 Workshop on LHC Beam Operation, Evian-les-bains, France, 2010.

[16] J. Serrano and M. Cattin, *The LHC AC dipole system: an introduction*, CERN BE Note 2010-14-CO, 2010.

[17] R. Calaga et al., β^* *measurement in the LHC based on K-modulation*, IPAC11, San sebastian, Spain, 2011.

[18] A. Marsili, *Identification of LHC beam loss mechanism: A deterministic treatment of loss patterns*, Université Paris Sud, Thèse de doctorat, 2012.

[19] G. Aad et al., *The ATLAS Experiment at the CERN Large Hadron Collider*, JINST, 3:S08003, 2008.

[20] *ATLAS detector and physics performance : Technical Design Report, 1*, Technical Design Report ATLAS, CERN, Geneva, 1999.

[21] A. Yamamoto et al., *The ATLAS Central Solenoid*, Nucl. Instrum. and Meth., A 584, 53-74, 2008.

[22] A. Dudaref et al., *Construction of the ATLAS toroid magnet system*, submitted to JINST.

Chapitre 2

[23] A. Tkatchenko, *Mouvement d'une particule chargée dans un champ magnétique (courbure et focalisation transverse)*, DEA Physique et Technologie des Grands Instruments, Université Paris Sud 11.

[24] A.W. Chao,M. Tigner, *Handbook of accelerator physics and engineering*, World Scientific, 2009.

[25] H. Wiedemann, *Particle Accelerator Physics*, volume I, II. Springer, 1999.

[26] A. Chancé, *Etude et conception de l'anneau de désintégration d'une usine à neutrinos utilisant les décroissances β des noyaux Hélium 6 et Néon 18 produits par un faisceau intense de protons frappant diverses cibles*, Université Paris Sud 11, Thèse de doctorat, 2007.

[27] H. Grote and F. Schmidt et al. http://mad.web.cern.ch.

[28] W. Herr, *Beam-Beam Interaction*. Yellow Report, (CERN 2006-002), 2006.

[29] A. Chancé, *Détermination de la matrice sigma du faisceau dans l'espace 5D*, Note interne, IRFU, CEA-Saclay, 2010.

Chapitre 3

[30] V. Cindro et al., *The ATLAS Beam Conditions Monitor*, JINST, 3:P02004, 2008.

[31] S. Jakobsen, *Performance evaluation and optimization of the luminosity detector ALFA*, Master Thesis, University of Copenhagen, 2010.

[32] D. Berge et al., *Luminosity measurement using the ATLAS Minimum Bias Trigger Scintillator System*, ATL-LUM-INT-2010-004, 2010.

[33] P. Jenni, M. Nessi, and M. Nordberg, *Zero Degree Calorimeters for ATLAS*, Technical Report LHCC-I-016. CERN-LHCC-2007-001, CERN, Geneva, 2007.

[34] H. Schmickler and S. White, *On the Potential Use of Zero Degree Calorimeters for LHC Luminosity Monitoring*, Technical Report, AB-Note-2005-030. CERN-AB-Note-2005-030, CERN, Geneva, 2005.

[35] P. Jenni and M. Nessi, *ATLAS Forward Detectors for Luminosity Measurement and Monitoring*, Technical Report, CERN-LHCC-2004-010. LHCC-I-014, CERN, Geneva, 2004.

[36] H. Burkhardt and P. Grafström, *Absolute Luminosity from Machine Parameters*, Technical Report, LHC-PROJECT-Report-1019. CERN-LHC-PROJECT-Report-1019, 2007.

[37] S. Van der Meer, *Calibration of the effective beam height in the ISR*, CERN-ISR-PO-68-31, 1968.

[38] S. White, *Determination of the absolute luminosity at the LHC*, Thèse de doctorat, Universié Paris Sud 11, 2010.

[39] S.M. White, *Luminosity calibration*, Proceedings of Chamonix 2011 workshop on LHC performance, Geneva, 2011.

[40] R. G. Newton, *Optical theorem and beyond*, American Journal of Physics, 44(7):639-642, 1976.

[41] V. Berardi et al., *Total cross-section, elastic scattering and diffraction dissociation at the Large Hadron Collider at CERN : TOTEM Technical Design Report*, Technical Design Report TOTEM. CERN, Geneva, 2004.

[42] M. Heller, *Mesure de la luminosité absolue et de la section efficace totale proton-proton dans l'expérience ATLAS au LHC*, Thèse de doctorat, Universié Paris Sud 11, 2010.

[43] A. Faus-Golfe, M. Haguenauer and J. Velasco, *Luminosity determination using Coulomb scattering at the LHC*, EPAC, Paris, 2002.

[44] A. Faus-Golfe, *Optimized β^* insertion optics for the TOTEM experiment in IR1 and IR5 for Ring1 and Ring2 of the LHC version 6.0*, LHC-Project-Note-207, 1999.

[45] A. Faus-Golfe and A. Verdier, *Optics studies for diffractive physics at the LHC*, EPAC, Paris, 2002.

[46] A. Faus-Golfe and A. Verdier, *High β and very high β optics studies for LHC*, EPAC, Lucerne, 2004.

[47] A. Faus-Golfe et al., *A very high β optics for an abolute luminosity determination with forward detectors with ATLAS*, EPAC, Lucerne, 2004.

[48] H. Burkhardt and S. White, *High-β^* optics for the LHC*, LHC Project note 431, 2010.

[49] S. Jakobsen, private communication.

[50] D. Bernard et al., *The real part of the proton-antiproton elastic scattering amplitude at the centre of mass energy of 546 GeV*, Phys. Lett. B, 198 (CERN-EP-87-147), 1987.

[51] C. Augier, *Mesure de la partie réelle de l'amplitude de diffusion élastique proton-antiproton vers l'avant, à l'énergie dans le référentiel du centre de masse de 541 GeV*, Université Paris 11, Thèse de doctorat, 1993.

Chapitre 4

[52] PYTHIA web page, http://home.thep.lu.se/torbjorn/Pythia.html.

[53] MADX web page, http://mad.web.cern.ch.

[54] J. Cudell et al.,*Benchmarks for the Forward Observables at RHIC, the Tevatron-run II and the LHC*, Phys. Rev. Lett., 89(hep-ph/0206172) 2018011-2018014, 2002.

[55] F. Schmidt, E. Forest, and E. McIntosh, *Introduction to the polymorphic tracking code : Fibre bundles, polymorphic Taylor types and Exact tracking*, Technical Report CERN-SL-2002-044-AP. KEK-REPORT-2002-3, CERN, Geneva, 2002.

[56] F. Schmidt et al., *MAD-X PTC Integration*, CERN-AB-2005-036, 2005.

[57] https://atlas-france.in2p3.fr/cgi-bin/twiki/bin/view/Atlas/GuideAthena.

[58] S. Cavalier et al., *Tracking and tolerances study for the ATLAS high β optics*, Vancouver, IPAC, 2009.

[59] H. Stenzel, *Luminosity calibration from elastic scattering*, ATL-LUM-PUB-2007-001, Geneva, CERN, 2006.

Chapitre 5

[60] H. Burkhardt and S. Cavalier, *Intermediate 90 m optics for ATLAS-ALFA*, CERN-ATS-Note-2011-027 PERF, 2011.

[61] H. Burkhardt, *High-beta optics*, LHC Lumidays, Geneva, CERN, 2011.

[62] S. Cavalier et al., *90 m Optics Commissioning*, San Sebastian, IPAC, 2011.

[63] A. Koschik et al., *On the implementation of experimental solenoids in MADX and their effect of coupling in the LHC*, Edinburgh, IPAC06, 2006.

[64] S. Abdel Khalek, *Mesure de la section efficace totale proton - proton et de la luminosité absolue dans l'expérience ATLAS au CERN*, Thèse de doctorat, Université Paris Sud, 2013.

Chapitre 6

[65] A. Macpherson, *LHC availability and performance in 2011*, Proc. Chamonix 2012.

[66] G. Vanbavinckhove, *Optics measurements and corrections for collider and other storage ring*, University from Amsterdam, 2012.

[67] H. Burkhardt et al., *90 m optics studies and operation in the LHC*, New Orleans, IPAC, 2012.

[68] H. Stenzel, *Update on Ly/Lx*, ALFA Physics meeting, 20 february 2013.

[69] S. Cavalier, *Systematic uncertainties.*, LHC Lumidays, Geneva, CERN, 2012.

[70] The ALFA collaboration, *ALFA performance plots for approval*, ALFA analysis meeting, ATLAS note, 17 february 2012.

[71] http://wikis/display/OnlineModel/K+from+Logging+Current.

[72] http://lhc-logging.web.cern.ch/lhc-logging/software/.

[73] P. Fassnacht and R. Ostojic, Private communications.

[74] R. Staszewski, H. Stenzel and M. Heller, Private communications.

Chapitre 7

[75] H. Burkhardt et al., *Plans for high beta optics in the LHC*, New Orleans, IPAC12, 2012.

[76] K.H. Hiller, *Plans for 2012*, ALFA general meeting, Lisbon, 2012.

List of Figures

List of Tables

Résumé

ALFA (Absolute Luminosity for ATLAS) vise à mesurer la luminosité absolue pour l'expérience ATLAS avec une incertitude de 2 – 3% et la section efficace totale. La luminosité est reliée au nombre d'évènements. Plus la luminosité est élevée, plus le nombre d'évènements est élevé. C'est donc une quantité importante pour les collisionneurs en général et notamment pour le LHC (Large Hadron Collider). LHC est constitué de deux faisceaux circulant dans deux chambres à vide différentes et collisionnant aux quatres points d'intéraction oú les principales expériences de physique sont positionnées (ATLAS, CMS, ALICE et LHCb). Les détecteurs constituant ALFA insérés dans des Pots Romains sont positionnés à 240 m de distance du point d'intéraction d'ATLAS aprés six quadrîpoles et deux dipôles qui constituent la partie de ligne faisceau utile à ALFA et localisée sur le LHC. Les détecteurs sont constitués de fibres scintillantes pour détecter les protons élastiques issus du Point d'Intéraction. Ces protons sont transportés au travers des différents aimants qui constituent la ligne de faisceau considérée et qui nécéssite une optimisation des paramètres optiques pour les besoins de la mesure. Nous appellerons les optiques fort β, les optiques utilisées durant les périodes expérimentales dédiées à ALFA. Les paramètres des optiques fort β ont été simulés afin de remplir le cahier des charges demandé pour ALFA et elles ont été testées sur le LHC en 2011 et 2012 pendant un certain nombre de périodes expérimentales spécifiques aux optiques fort β sur le LHC. Ces périodes expérimentales se sont terminées en 2013 avant l'arrêt du LHC. Les paramètres optiques ont été mesurés et comparés aux simulations. Certains paramètres ayant des valeurs bien meilleures que celles attendues. Cela a aussi permis de regardes quelques incertitudes sur les paramètres optiques et d'évaluer l'impact de certains de ces paramètres sur la mesure de section efficace totale.

Mots-clés: Pots Romains, Optiques fort β, puces, ALFA, LHC.

Abstract

ALFA (Absolute Luminosity For ATLAS) aims at measuring the absolute luminosity for the ATLAS experiment with an incertitude down to 2-3 % and the total elastic cross section. The luminosity is related to the number of events, the highest the luminosity, the highest the number of events. This is, then, an important quantity for colliders like LHC (Large Hadron Collider). LHC is made of two beams circulating in two different beam pipes and colliding at four interaction points where the four physics experiments are located (ATLAS, CMS, ALICE, LHCb). ALFA detectors inserted into Roman Pots (RPs), have been placed around ATLAS at 240 m distance from the collision point (IP1) after six quadrupoles magnets and two dipoles defining the ALFA beam line which is part of the LHC ring. The detectors are made of scintillating optics fibers to catch elastic protons generated at IP1. These protons are tracked through the LHC magnets beam line which

needs to be optimized in terms of optics parameters. We call high β optics, the optics used for special ALFA runs measurements. The high β optics parameters have been simulated to fulfill the ALFA requirements and have been tested on LHC in 2011 and 2012 during a certain number of LHC special runs. It has ended at the end of 2013. The parameters have been measured and compared with simulations. Some of them achieving a better value than expected. It allowed us to calculate systematic uncertainties and to evaluate the impact of some optics parameters on the total elastic cross section measurement.

Keywords: Roman Pots, high β optics, ALFA, LHC.